Analyzing and optimally controlling the Kelvin water dropper

Thijs Knapen

s1008137

Master thesis of Applied Mathematics

Specialization: MASS

Chair: Hybrid Systems

Assessment committee:
prof. dr. H.J. Zwart
dr. ir. G. Meinsma
prof. dr. J.C.T. Eijkel

Date: August 25, 2015

Contents

Chapter 1

Introduction

1.1 The Kelvin Water Dropper

On 19 June 1867, sir W. Thomson (later known as lord Kelvin) presented the paper "On a Self-acting Apparatus for multiplying and maintaining Electric Charges, with applications to illustrate the Voltaic Theory."
Years later his 'apparatus' still seems to intrigue physicists, judging on the wealth of information that can be found about the described setup and the physical 'working principle' it relies on.
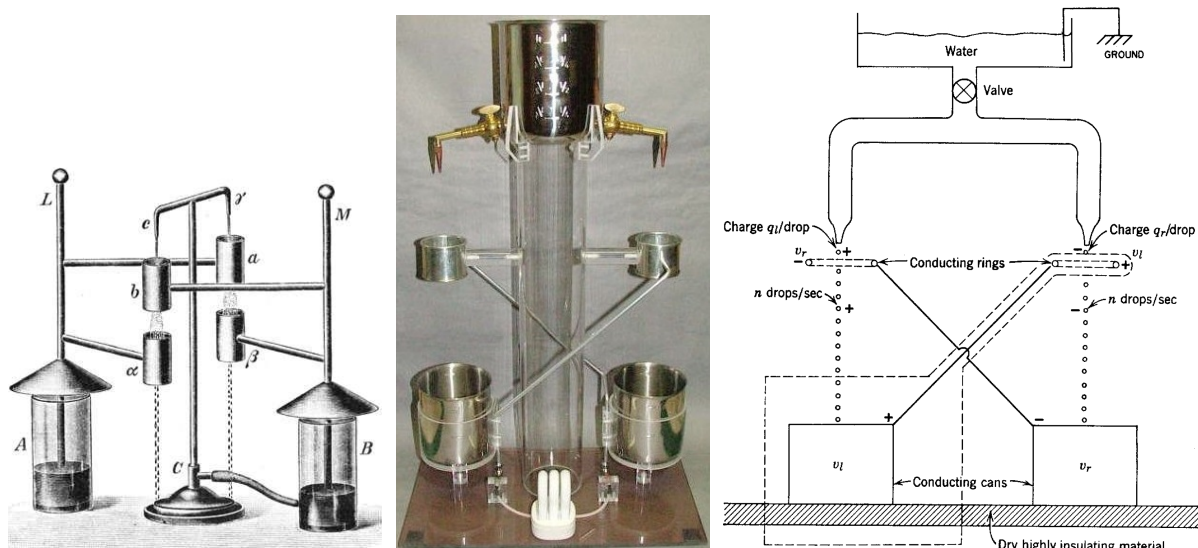
(a) Original Kelvin water dropper with Leyden jars (see [14]) (b) Typical Kelvin experimental setup. (c) A schematization of the Kelvin water dropper (see [15])

Figure 1.1: The Kelvin water dropper

At the same time however, the apparatus is not as popular as it might seem ([11]). Although one can easily find several short inspiring articles on the device, as well as detailed internet links and demonstration videos, the device does not seem to be well known to the vast public. This is a bit of a pity, as the device suits itself perfectly to be used as a standard physics experiment in secondary schools. A point that may be clear from e.g. [6], [20] and [11].
It is therefore nice to see that the curiosity in the device still seeps through in the present, as may be evident from the final question (Question No 17) in the International Young Physicists' Tournament (IYPT) of 2010 in Vienna, Austria. The question at hand was as follows:

> "Construct Kelvin's dropper. Measure the highest voltage it can produce. Investigate its dependence on relevant parameters."

Interesting to note is that over the years Kelvin's original apparatus has endured a slight make-over. This may be observed from the comparison between Figure 1.1a and Figure 1.1b. In Figure 1.1a Kelvin's original setup is depicted, where Figure 1.1b shows an example of a more modern typical setup.

However, the differences between the 'modern' and original Kelvin water dropper are only minor. The physical 'working principle' of the setup is thereby exactly the same. Where Kelvin relied on Leyden jars to store electric charges, nowadays these early capacitors are known to be redundant when the targets are well insulated. Another difference between most modern experimental setups and Kelvin's original setup can be found in the receiving targets. In most modern setups the water from the dripping streams is contained by the targets, whereas in Kelvin's original apparatus the receiving cans contained a funnel through which water could sip through.

1.1.1 The physics behind Kelvin's water dropper

The 'working principle' of Kelvin's setup can be explained by the clever interconnection between the targets and the induction rings. How the sudden voltage build-up between the targets occurs, is illustrated by the 3 steps of Figure 1.2.

(a) random initial imbalance   (b) opposite charge induction   (c) positive feedback loop
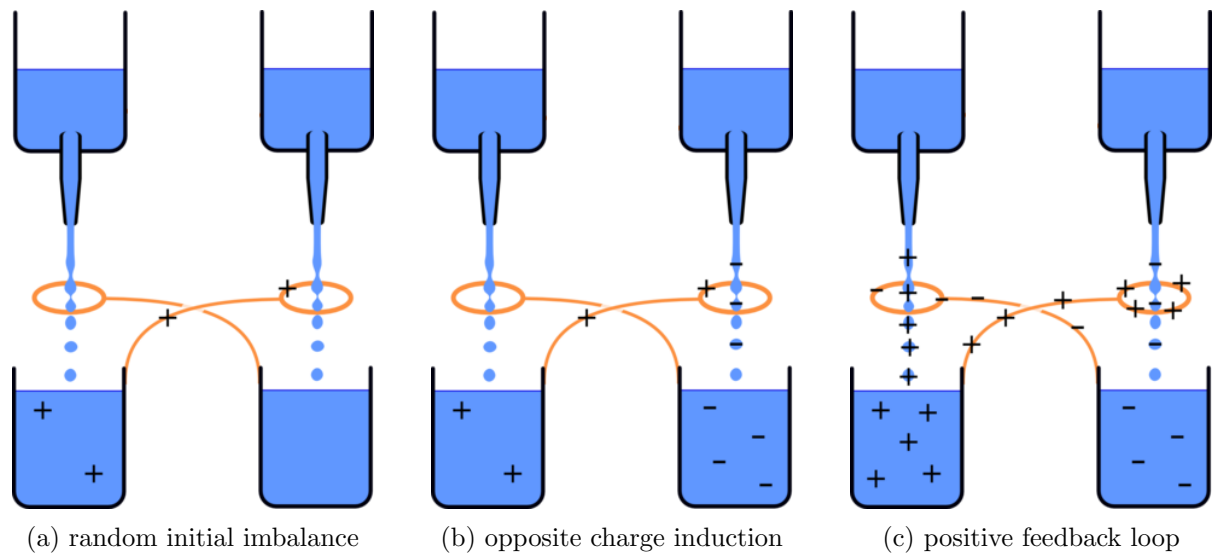
Figure 1.2: Simple illustration of the charge separation process in Kelvin's water dropper

At first glance Kelvin's setup may seem to be nothing more than two dripping streams of water, where each stream of water is collected by downstream targets. However for some reason the setup allows for accumulation of charges. The key to explaining how this can happen can be found in the water itself.

Even though water has no overall electric charge, it is full of movable electric charges; H^+ and OH^- ions. These ions are transported by the droplets, and theoretically each target will thereby collect an equal amount of positive and negative charges. However at some point in time a slight imbalance in the charge distribution may occur. In practice, this imbalance will likely be the cause of random natural fluctuations ([4]). Each target is hereby equally likely to obtain either a slight positive charge or a slight negative charge. However, if one presents a charged object

near one of the induction rings, one can easily force a target to start off with a given charge. A positive object will thereby induce a negative charge and visa versa.

Let us assume that at some moment the left target is slightly positively charged. As the left target is directly connected to the right induction ring, this right induction ring will then also be slightly positively charged (see Figure 1.2a). Since opposite charges attract, this positively charged right induction ring will then attract negative charges in the right dripper. In turn this causes the right target to become negatively charged (see Figure 1.2b). However, the right target is also connected to the left induction ring, analogously causing more positive charges to be induced in the left dripper. This completes a positive feedback loop, creating a self amplifying process (see Figure 1.2c).
It may speak for itself that if we had assumed the left target to start off with a slight negative charge, the exact same principle would still apply. The only difference would now be that the right target obtains a positive potential, where the left target obtains a negative potential. In other words: according to some initial charge imbalance, the sign for each of the targets is determined.

1.1.2 The physics behind the induction process

Although Figure 1.2 can be used to explain the 'working principle' of Kelvin's water dropper, it may not be so clear how the charge induction can take place near the induction rings. As already briefly mentioned this has to do with the existing ions in the water and is figuratively illustrated in Figure 1.3.

(a) The electrical field originating from the induction ring attracts opposite charges as the droplet form

(b) The charge induction proces explained from the ions.

(c) Extremely simplified representation of charge induction in the droplets.
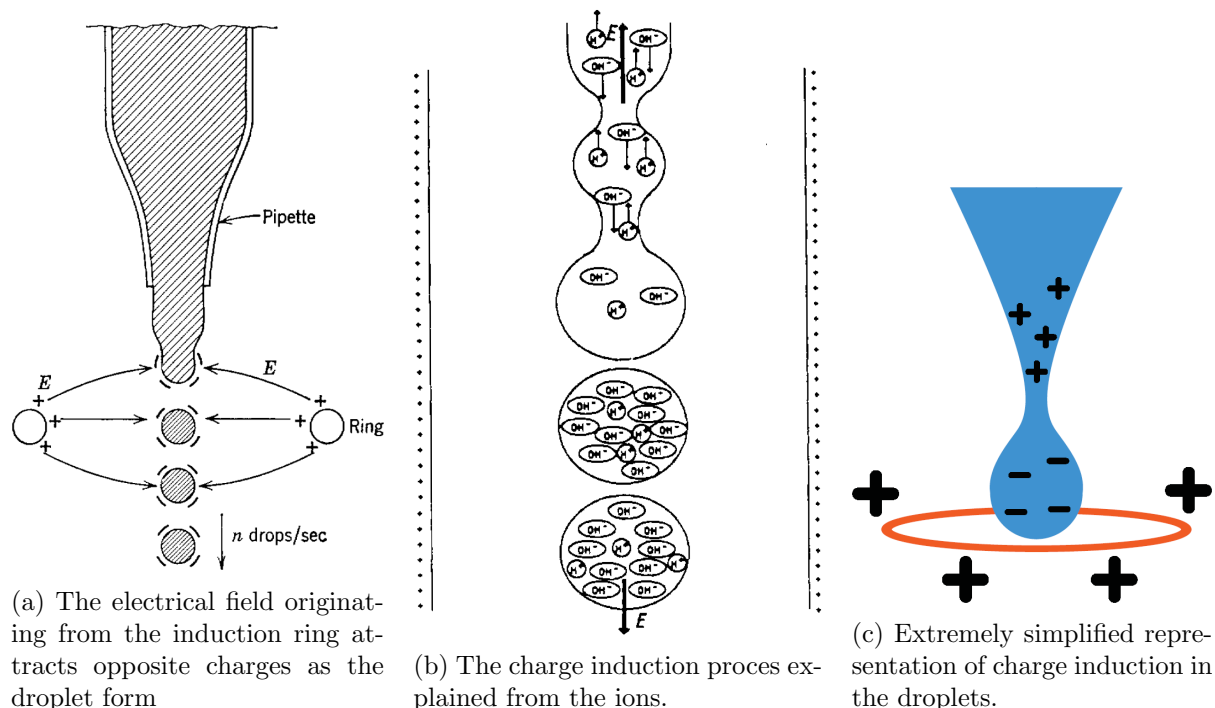
Figure 1.3: An schematization of the charge induction process in the (forming) droplets

As one may know, water is build up of OH^- ions and H^+ ions. Similar to magnets, charged objects posses two characteristic properties: opposite charges attract each other, while alike charges repel each other. These properties are also fundamental to explain the charge induction

process at each of the jet tips in Kelvin's setup.

Let us for the moment only consider the right induction ring and assume that this induction ring is positively charged (similar to the case in Figure 1.2). Due to the electrical field of this induction ring, OH^- ions will be attracted to the boundary of the water stream (see Figure 1.3a). This is the direct result of the attractive force between opposite charges.

However, at the same time opposite charges repel, causing the positive H^+ ions to be 'pushed' further into the water stream. Both these processes ensure that when the droplets break free from the waterjet, an overall negative charge is captured in the droplets (see Figure 1.3b). In summary the charge induction process may thereby be explained from the extremely simplified Figure 1.3c.

As described, after the droplet formation the water stream will be slightly positive at the jet tip. In the case that a single reservoir is used to provide the water stream for both the left and right jet, this net positive charge at one jet tip will be counterbalanced by the net negative charge at the other jet tip, since in an idealized perfect symmetrical system these charges will be the same. Furthermore, any charges that would remain due to some imbalance between left and right subsystem, are allowed to escape as the reservoir is grounded.

In the case that two separate reservoirs are used in the setup, one may ground each reservoir separately. A two reservoir approach was for instance also used in [18] (see also Figure 2.1b). In the same paper ([18]) it was shown that one can 'harvest' the downstream currents in Kelvin's setup, by connecting the targets to ground through large resistors. In the same way however, it may also be possible to 'harvest' some of the upstream currents. To verify whether this can also lead to a larger amount of electrical output power would however require further experimental research. The downside of placing resistors between the reservoir and ground would be that this will also effect the amount of charge that can be induced. Consider for instance the induction case shown by Figure 1.3. When the repelled positive charges are not free to 'escape', also more positive charges will end up encapsulated in the droplets (see 1.3b), reducing the total charge that is induced. Furthermore for a single jet system it was already shown in [17] that the systems efficiency is already close to a theoretically calculated maximum when each of the reservoirs is 'simply' grounded.

1.1.3 Relation to electrical networks

In Kelvin's original paper [14], lord Kelvin already remarked that his apparatus shows an interesting analogy to a self-sustaining electromagnetic system. Using this analogy, Kelvin already proved that if losses are not significant: "ultimately the charges augment in proportion to $e^{\rho t}$ if ρ be the positive root." A result that would later be rediscovered using analogies between Kelvin's setup and electrical circuits. Furthermore the exponential buildup of charge will also be discussed in section 2.2.2 of this thesis.

The analogy between Kelvin's apparatus and an electrical network can be explained from the fact that most physical elements of Kelvin's setup have a more or less equivalent electrical component as a counterpart. In this way Kelvin's setup allows itself to be 'translated' in an electrical circuit.

At first there are the droplets that 'carry' charges from the jet tip to the target. This may be compared to the flow of electrons in electrical wires. Furthermore, charges are induced due to the oppositely charged induction rings. In an electrical network, the creation of charges can

be compared to a current source. Furthermore the induction of charge may be modelled using a field effect transistor (FET) element in the system ([18]). Also it can be observed that the targets gradually 'charge' as droplets are collected, which is somewhat similar to a capacitor and its RC time.

For successful operation of the device, it is important that the receiving targets are sufficiently able to preserve their charge. In order to achieve this they need to be insulated from the ground, but also from each other. The extend by which the targets are insulated from the ground is generally modelled using a (large) resistor. The mutual insulation of the targets may also be described this way. However, as the insulated targets will also store opposite charges, the comparison to a parallel-plate capacitor can also be made.

The above described analogy between Kelvin's water dropper and an electrical network has also made it to more recent literature (e.g. see [15], [19], [1], [18] and [9]).

It is however interesting to see that throughout the literature there seem to be several 'equivalent' electrical networks that can be used to describe the governing physics in Kelvin's water dropper device. 'Equivalent' electrical networks that can clearly be seen to differ from one another, as is illustrated in Figure 1.4.

(a) 'Equivalent' electrical circuit as studied in [15]

(b) 'Equivalent' electrical circuit as studied in [1]

(c) 'Equivalent' circuit (with voltage divider) as studied in [18]
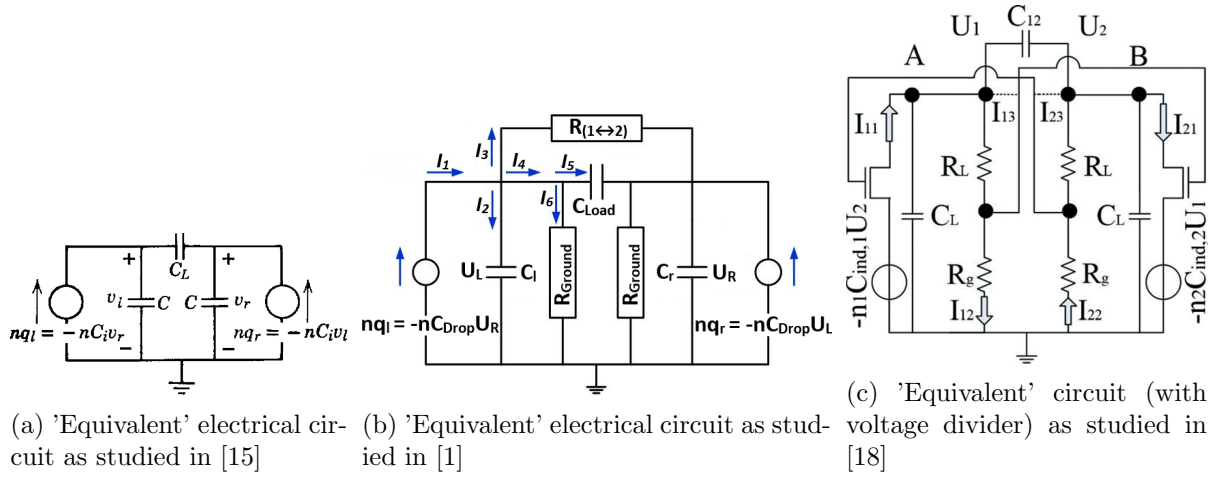
Figure 1.4: Several 'equivalent' circuit representations of the Kelvin water dropper

At first, for some of the circuits shown in Figure 1.4 there are some small eccentric points to note.

In Figure 1.4a one can see from the depicted '+' and '-' signs that in both the right and left 'subsystem' the positive terminal is depicted upstream, while the negative terminal is depicted downstream. During normal operation of the device, opposite charges are induced in the left and right subsystem, and therefore at one side the terminals need to be flipped.

Another observation we make is that in Figure 1.4c it seems that the presence of the voltage dividers has not been accounted for in the current induction equations (as shown at the current sources). In this setup, the two separate resistors R_L and R_g are placed in such a way that only a fraction $m = \frac{R_g}{R_L + R_g}$ of the accumulating voltages U_1 and U_2 are used for the current induction at the induction rings. Because of this we expect that an additional constant m needs to be added at the current induction equations, i.e. we would get $-n_i C_{ind,i} m U_j$, with $(i,j) = (1,2)$ or $(2,1)$.

Furthermore, Figure 1.4c also depicts current losses that occur when droplets deflect to the induction rings. These are indicated by I_{13} and I_{23}. However, when overcharged droplets are

deflected they will deflect to 'their own' induction ring, as is also shown in a similar electrical circuit in the Phd thesis [16] of the same main author (see also Figure 2.1c). It therefore seems that in Figure 1.4c the lines for I_{13} and I_{23} are falsely connected to the opposite induction ring.

Putting these peculiar points aside, one may note that from the 3 circuits shown in Figure 1.4, the electrical circuit representation shown by Figure 1.4b is the most elaborate. Nevertheless, as mentioned in [19], it is important to note that the 'essential ingredients' of self-excitation can be treated by a simpler idealized model with no losses where we have that:

$$C_{Load} = 0$$
$$R_{(1 \leftrightarrow 2)} = \infty$$
$$R_{Ground} = \infty. \qquad (1.1)$$

Under the idealized conditions of (1.1) it may indeed be verified that all 'equivalent' electrical circuits in Figure 1.4 are indeed equivalent.

As a side note, in [19] the circuit representation shown in Figure 1.4b was also used to extend Kelvin's idea to an N dropper setup, as is depicted in Figure 1.5.
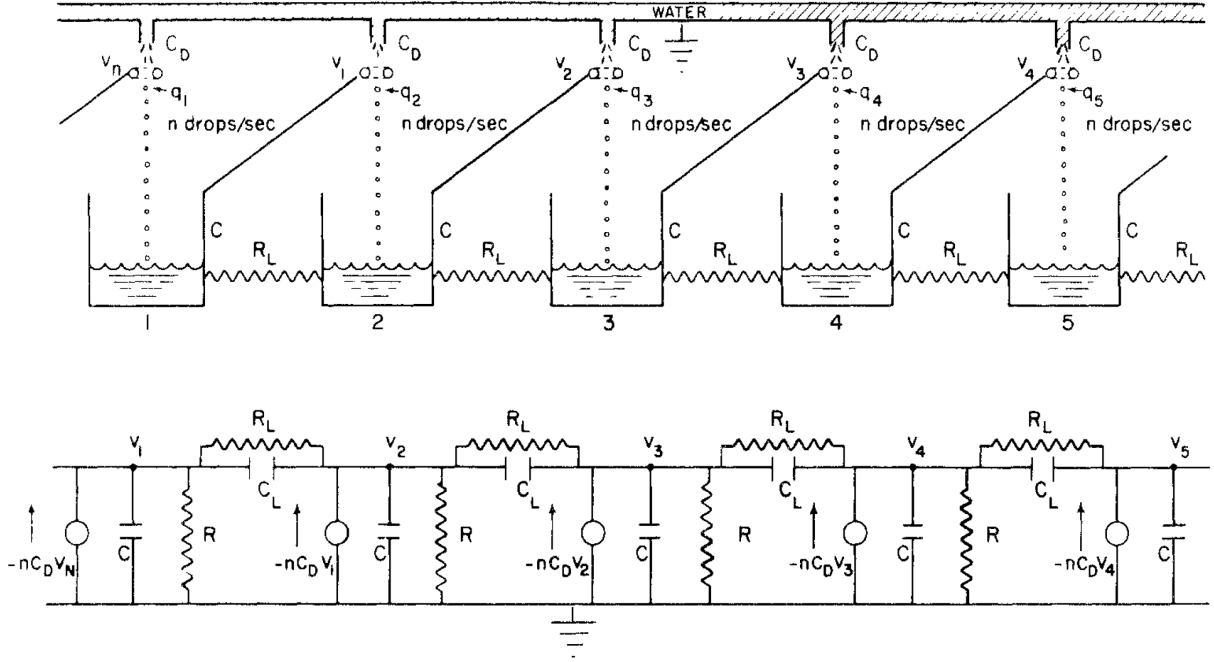
Figure 1.5: Extension of Kelvin's water dropper to N cans. Each of the N identical cans and streams are cross connected to adjacent cans. The Nth can is coupled to the first stream, completing the loop.

Furthermore, in [19] it is described that the potential of any node in the circuit of Figure 1.5 is related to the potentials of the preceding and succeeding nodes according to the equation:

$$V_i = \frac{R}{RCs + 1} \left(-nC_D V_{i-1} + \frac{V_{i-1} - V_i}{R_L}(R_L C_L s + 1) - \frac{V_i - V_{i+1}}{R_L}(R_L C_L s + 1) \right), \qquad (1.2)$$

where 's' represents the domain variable of the Laplace transform.

Note that (1.2) is a combination of a linear difference equation and a linear differential equation. This is due to the fact that V_i is described in terms of V_{i-1}, V_i and V_{i+1}, but the equation also contains the Laplace differentiator 's'. Solving equation (1.2) it can be shown that for $N = 2$ we can generate Direct Current (DC), for $N = 3$ we can generate three-phase Alternating Current (AC) and for $N = 4$ we can generate two-phase AC or DC.

Peculiarly we notice that in [19] the equation describing the largest natural frequency of the Kelvin water dropper setup, is slightly different from the one found in [1] and [9]. In [19] they find:

$$\lambda_{max} = \frac{nC_D - \frac{4}{R_L} - \frac{1}{R}}{C + 4C_L}, \tag{1.3}$$

while in [1] and [9] the same eigenvalue solution (in similar notation) is:

$$\lambda_{max} = \frac{nC_D - \frac{2}{R_L} - \frac{1}{R}}{C + 2C_L}. \tag{1.4}$$

Closer inspection on this slight difference in constants between (1.3) and (1.4) seems to indicate that author of [19] failed to recognize that he could not use $N = 2$ in his solution of (1.2). The reason for this lies in the fact that (1.2) is a three term linear difference equation. Consider for instance that nevertheless we do use $N = 2$ and plug in $i = 2$ into equation (1.2). For the previous and next node we then must have that $i - 1 = i + 1 = 1$. Thereby we obtain:

$$V_2 = \frac{R}{RCs + 1}\left(-nC_D V_1 + \mathbf{2}\frac{V_1 - V_2}{R_L}(R_L C_L s + 1)\right). \tag{1.5}$$

From (1.5) we see that the '$V_1 - V_2$ term' is now weighed twice, where in truth this should only be weighed once. One may verify that this constant '$\mathbf{2}$' indeed explains the difference in (1.3) and (1.4). The nature of the mistake lies in the fact that equation (1.2) requires V_{i-1}, V_i and V_{i+1} to be unique, where for $N = 2$ this can not be the case.

1.1.4 Theory of energy conversion

In the preceding sections the basic physics behind Kelvin's apparatus are explained. What is most intriguing about Kelvin's water dropper device is that it can seemingly spontaneous generate a large potential difference between two targets. Using the device one is even able to 'harvest' currents by allowing some charges to escape to the ground through a large resistor. Note that from equation (1.4) we can see that in an idealized setting, exponential voltage build-up occurs as long as current losses do not have the upper hand. The analogon of this equation for a setup using a voltage divider (see Figure 1.4c) will be treated in section 2.2.

Interestingly we can thus conclude that there can be a small current flow to the ground originating from the target, where the target has a large potential difference relative to the ground. This actually implies that electrical power can be generated by the device according to the equation:

$$P_{electrical}(t) = V(t) \cdot I(t),$$

where $V(t)$ represents the voltage at time t and $I(t)$ represents the current at time t.

This may come to a bit of a surprise, as one may wonder where this power comes from. There is not such a thing as a free lunch in physics right? Furthermore equation (1.4) would lead us to believe that we have exponential voltage build-up in the system. Apart from the finite capacity of the reservoirs this would imply that we have invented a perpetuum mobile.

Unfortunately the 'holy' physics law still stands, which is caused by the fact that charges are gradually lost when the target voltages and induced currents grow. As the droplets induce a greater charge, the repelling forces between the droplets also increases. This in turn causes droplets to 'bend' from their straight path to the targets. Ultimately fewer droplets then make it to the targets causing the current losses to increase. If the device works really well, droplets may even bend upwards in an anti-gravity alike fashion. This can be explained from the attractive force between the induction ring and the droplets, from the repulsive force between the droplets and the targets, and also from the repulsive force between mutual droplets.
Apart from the increase of losses due to larger induced charges, it can be observed from the single jet system in [17] that also the target voltages influence the current losses. This is most likely the result of the repelling force between the charged droplets and receiving targets.
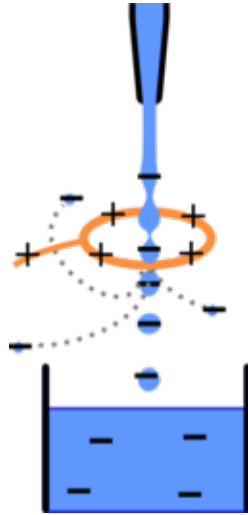
Figure 1.6: Simple illustration of current losses near the induction rings.

Besides the fact that the output power is haltered by current losses, the resulting output power itself is the result of an internal energy conversion process taking place in the Kelvin water dropper. This energy conversion process is illustrated in Figure 1.7 for the 'ballistic pressure-driven' setup used in [18].

Although no energy is fed to the system after it is started, it is important to realize that a mass (in this case the water) at height possesses gravitational potential energy according to the equation:

$$E_{potential} = Mgh,$$

where M represents the mass of the object, $g \approx 9.81$ represents the gravitational constant and h represents the vertical height of the object above the ground. In the same way the pressurized reservoirs used in [18] possess an amount of mechanical potential energy.

When the droplets travel from the induction ring to the targets they pass through the electrical field that accumulates between the induction rings and the targets. In Kelvin's water
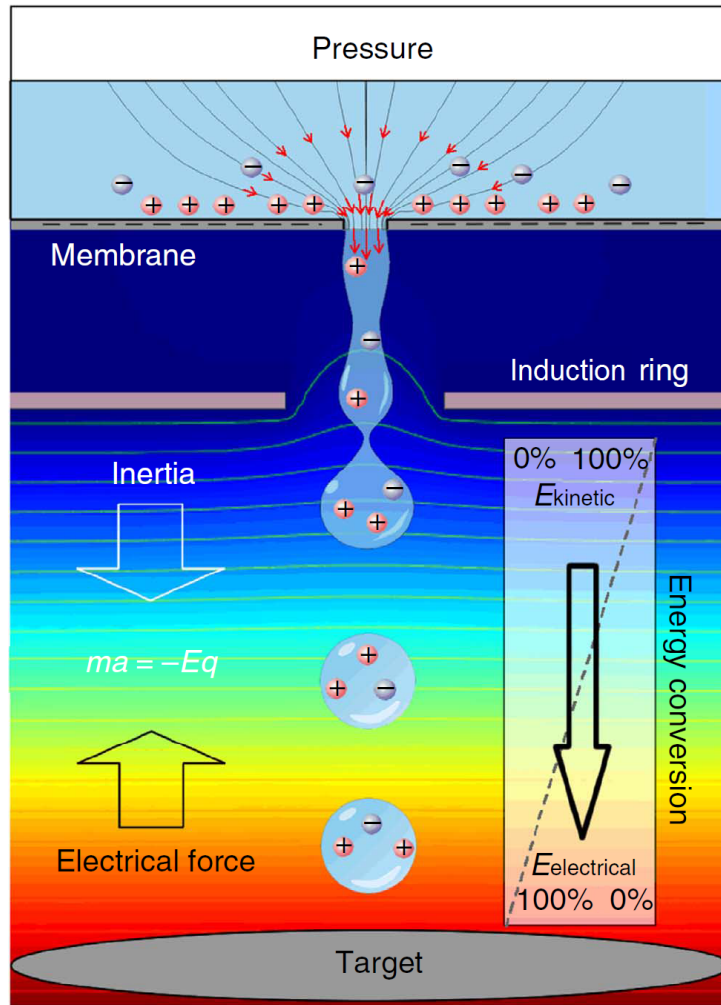
Figure 1.7: Illustration of energy conversion at each jet

dropper, the action of gravity opposes the electrical force ($\sum \vec{F} = m\vec{g} - q\vec{E}$), whereas in the ballistic system inertia opposes the electrical force ($\sum \vec{F} = m\vec{a} - q\vec{E}$, ([17]). Thereby electrical energy is being created due to the work that gravity does in pulling the charged droplet away from the grounded dripper, and away against the electrical field (`http://amasci.com/emotor/kelvin.html`).

Interestingly the opposite phenomenon; the acceleration of charges in an electrical field, is already used in many practical applications ([17]).

1.2 Research goals

Our aim for this thesis is twofold. At first we will analyze the (ballistic) Kelvin water dropper from a mathematical point of view. Thereby we use the mathematical theory of systems and control, and apply this on the equivalent network representation of Figure 1.4c. In particular we will focus on the stabilizing role of current losses, equilibrium points and stability, and for the last part we investigate whether we may distinguish inputs in the system, as the original Kelvin dropper is from itself an autonomous system.

Provided that we can identify specific system inputs will imply that we have a certain amount of control over the system. This brings us to our next aim of our thesis; how could we put this control to good use? Or even stronger, is there an optimal way in controlling the Kelvin system?

To answer this second question we first need to define what we consider to be an optimal control, i.e. we need to specify our optimization goal. Building on the observation that we are dealing with an energy conversion device, as we discussed in the previous subsection 1.1.4, we aim to maximize the energy conversion in the (ballistic) Kelvin setup. From this perspective this thesis can be interpreted as a follow-up to [18], which is based on the Phd work of [16].

Specifically, we aim to optimally convert the mechanical input power of the system into electric output power. In this way, similar to the project aim described in [16], we seek to maximize the systems (energy conversion) efficiency:

$$\text{Eff}(t) = \frac{P_{out}(t)}{P_{in}(t)}.$$

For the pressure-driven ballistic Kelvin system from [18] the above equation can be continued to:

$$\begin{aligned}
\text{Eff}(t) &= \frac{P_{electric}(t)}{P_{pressure}(t)} \\
&= \frac{V(t) \cdot I(t)}{(\Delta p)(t) \cdot Q(t)},
\end{aligned} \tag{1.6}$$

where the voltage function $V(t)$ is given in Volts (V), the current function $I(t)$ is given in Ampere (A), the pressure difference function $(\Delta p)(t)$ is given in Pascals (Pa, SI units: Nm^{-2}) and the volumetric flow rate function is given in cubic meters per second (m^3s^{-1}).

For the regular Kelvin setup, i.e. when the droplets are only 'powered' by gravity, equation (1.6) is be slightly different. The input power $P_{in}(t)$ is then given by the dripping water stream, which is constant by the assumption of drops falling with a constant frequency n.

In fact, also in the pressure driven system from [18] the input power remains fairly constant over time, due to the constant applied pressure and flow rate.

At a constant input power, it is easy to see from (1.6) that a maximal efficiency is achieved when the electrical input power is maximized. Thereby we will focus on the following equivalent maximization problem:

$$\max \int_0^T P_{electric}(t) \, dt, \tag{1.7}$$

where the time window is defined as $t \in [0, T]$.

In the (ballistic) Kelvin setup, the maximum time T may be given from a rather natural constraint; the (pressurized) containers can only contain a finite amount of aqueous solution. Provided some constant pressure and flow rate, the reservoirs will eventually become empty, by which the system comes to a halt.

1.3   Outline of thesis

Having introduced the main system of interest in this thesis; the Kelvin water dropper setup, in the rest of this thesis we will pursue to analyze and optimally control this system. Thereby, in chapter 2 we first have a brief look at some of the work from [16]. The reason for this lies in the fact that this work, in particular the part on the Self-excited ballistic energy harvesting device, also discussed in the paper [18], is the motivating pillar behind this thesis. Of particular importance here is the induction model from [18], which is based on an equivalent circuit representation for the setup, see also Figure 1.4c. This induction model will be treated in more detail in section 2.2 and 2.2.2. After this we will show how the imperfect diodes used in [18] can provide some valuable insights in the design of a controller later on in this thesis. At last, in section 2.4 we will show that the induction model can indeed be used to explain the measurements from [16], thereby demonstrating that this model may serve as a solid basis for further study.

In chapter 3 we will start to extend this induction model by incorporating current loss into the system equations. Thereby we will first look for the differential equations describing the new manifest behaviour. This is done by introducing additional latent variables, which are then elemination using elemination procedure from [13], but we will also directly eliminate the latent variables by hand.
It will turn out that the extended model introduces additional equilibrium points, which are studied by means of linearization in subsection 3.1.2. Furthermore, under symmetry assumptions, the differential equations describing the new manifest behaviour are also solved in subsection 3.1.4.
Next, in section 3.2 we investigate whether more equilibrium points can be found than the ones studied in subsection 3.1.2. Also here we pursue this goal in two ways, in subsection 3.2.1 we try to find these directly from the differential equations, whereas in subsection 3.2.2 we investigate the behaviour of the implicit solution curves.
At last, in section 3.3 we investigate input-output approaches for the system. Inspired the external voltage sources used in [17], in subsection 3.3.1 we first consider the induction ring voltages as an input. Then, in subsection 3.3.2 we investigate variable resistors as input, which is inspired on the different resistors used in [18] for the pursuit of proper charge induction.

Based on the case that the resistors serve as an input for the system, optimal control for the system is discussed in chapter 4. In this chapter we begin with a minimalistic version of our aimed optimal control problem, starting with the regular Pontryagin minimum principle and a single input. This result is then also used as a basis for optimal control with two inputs. At last, in section 4.2, we discuss our most elaborate optimal control problem, where we also incorporate state variable inequality constraints. These constraints are included to make sure that current losses remain small, which on its turn, when small, make the systems differential equations linear.

Finally, in chapter 5 we will discuss our conclusions and recommendations. Which is followed by some appendices that were included as additional material for some of the previous chapters.

Chapter 2

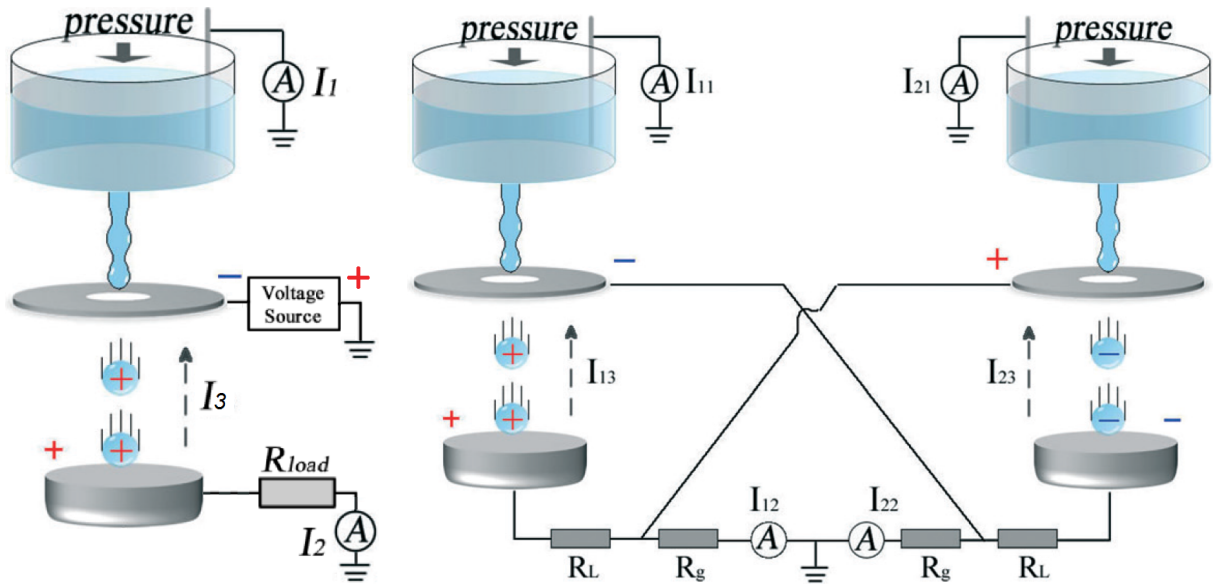# Pressure-driven ballistic Kelvin's water dropper

As mentioned in our research goals (section 1.2), to some extent this thesis can be seen as a follow up on [18], which is based on the Phd work of [16]. Therefore, in the following sections we will first briefly go over some of the essential concepts of this earlier work. In the next section we thereby start by discussing an older, more general research interest: creating power from microjets.

2.1   Power from microjets

A central goal of current energy research is to efficiently produce electricity from renewable sources ([5]). This goal may clearly be pursued in several ways. A relative new method that is explored for this purpose is the use of liquid water microjets for direct conversion of electrokinetic energy to electrical power. This approach has recently been followed in [5] and [17]. In [17] an efficiency of 48% was obtained when using an external voltage source to control the induction ring voltage (see Figure 2.1a).

However, for an electrical energy conversion device, an external voltage source is cumbersome to implement. Instead, a self-excited energy conversion system will be much more convenient for applications, as it is in many other self-excited energy devices that have been studied ([18]). Thereby a pressure driven version of the Kelvin dropper may be used, which setup is shown in Figure 2.1b. However, one of the disadvantages of (a pressure driven) Kelvin's water dropper is that it uses a positive feedback system that is inherently unstable since the droplet charge keeps increasing until the droplets are deflected ([18]). To overcome this issue the induction ring voltages need to be properly controlled, which is one of the main goals of this masters thesis.

In Figure 2.1 a schematic comparison is made between the single jet energy conversion device from [17], and the self-excited energy conversion device from [18], which is inspired on Kelvin's water dropper device. It is important to note that the pressure driven Kelvin system is formed from two intertwined single jet systems. The external voltage source from the single jet system is thereby replaced by a voltage divider in the downstream circuit. In this intertwined connection, the voltage used for the charge induction is now autonomously regulated by the system. By the voltage divider in this setup, a fraction $m = \frac{R_g}{R_L + R_g}$ of the target voltages will be 'submitted' to the induction rings.

(a) Schematic of the single jet system as studied in [17].

(b) Schematic of the pressure driven ballistic Kelvin dropper as studied in [18].
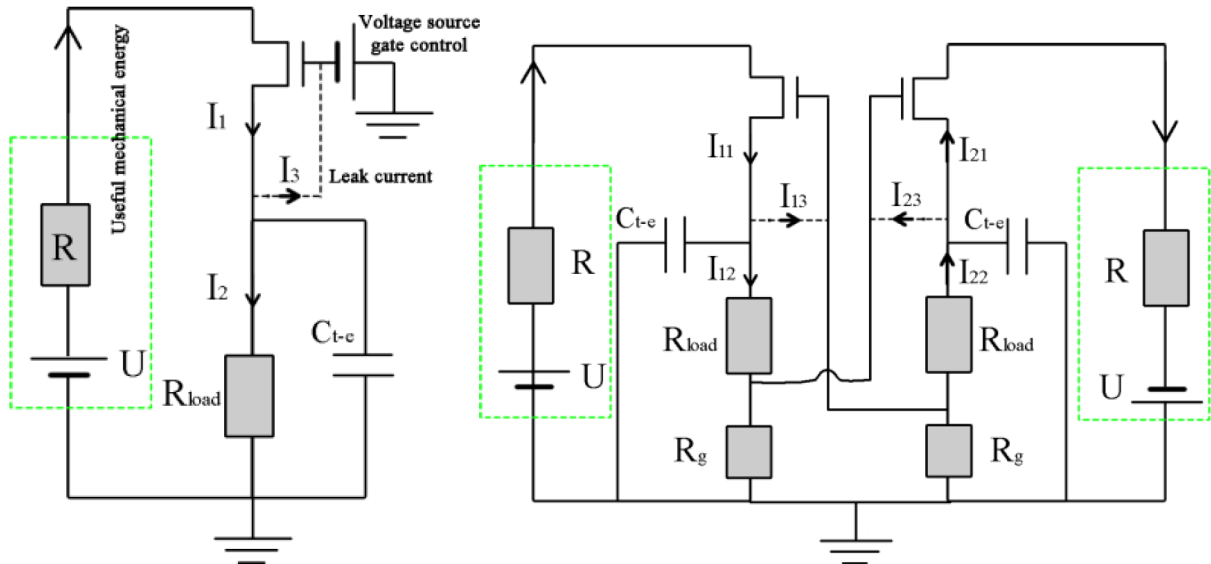
(c) The equivalent electrical networks for the single and dual jet systems shown above. ([16])

Figure 2.1: Comparison between single jetting system as studied in [17] and the pressure driven ballistic Kelvin dropper as studied in [18].

A comparison between the electrical network representation of both the single and dual jet system is shown in Figure 2.1c. The green rectangle represents a current source, which resembles the charges that are induced when droplets separate at the jet tip. When comparing these two electrical networks one may again notice that in essence the ballistic Kelvin dropper setup contains two single jet subsystems. This observation is especially useful, as it partly allows for the incorporation of results from [17], in the design of an optimal controller for the ballistic Kelvin setup.

2.2 Induction model

In this section the induction model from [18] is studied. This model describes the physics of the Kelvin water dropper on the basis of an equivalent electrical network. As described in subsection 1.1.3 from the Introduction, several electrical networks can be used to analyze the behaviour of Kelvin's water dropper, and the one that is used in [18] is depicted by Figure 1.4c and the right of Figure 2.1c. A special property of this setup is that two resistors are used at each target, which we shall refer to as a load resistor R_L and a gate resistor R_g. Using such a voltage divider in the setup makes it possible to use only a fraction of the target voltage for the induction process at the induction/gate rings.

To simplify calculations, taking the electrical network representation from Figure 1.4c as a starting point, we will initially neglect current losses (I_{13} and I_{23}), the constants are chosen to be symmetrical (i.e. $n_1 = n_2$, $C_{ind,1} = C_{ind,2}$, etc.), and furthermore a perfect capacitance between the two targets is assumed (i.e. $C_{12} = 0$).

Later on, in chapter 3, we will drop the assumption of zero current losses, and analyze the influence these losses have on the system. For now, these simplicity assumptions turn our focus to the following electrical network:
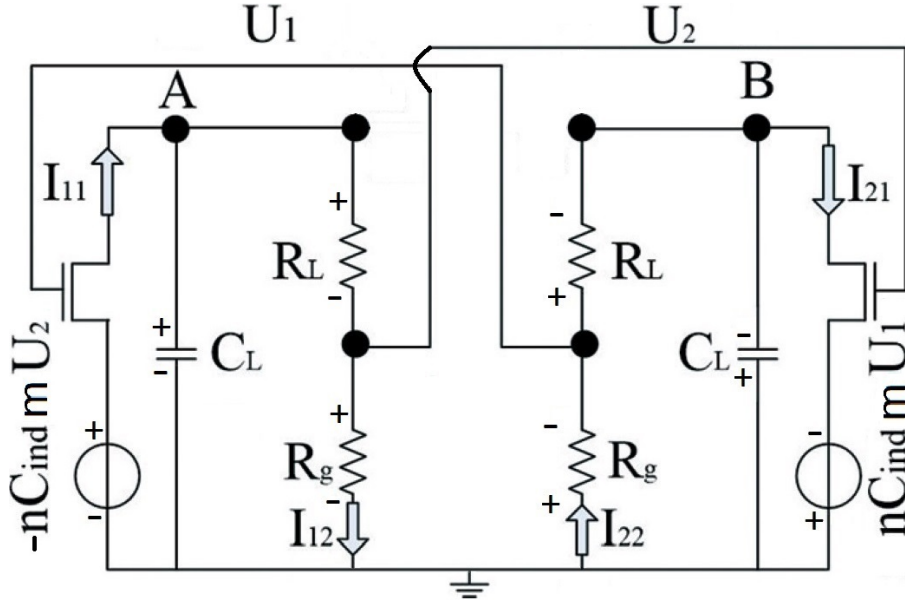
Figure 2.2: An equivalent circuit to model the induction mechanism in Kelvin's water dropper. For convenience, latent variables I_{ij}, with $i, j \in \{1, 2\}$ are introduced, each depicted in the positive direction. The voltages of the left and right target are denoted by U_1 and U_2. Here U_1 is described by the voltage from node A to the ground, whereas U_2 is described by the voltage from node B to the ground. This may be compared to the schematic model representation shown by Figure 2.1b. The constant m in the current source equation represents the fractional voltage division in the system, and is given by $m = \frac{R_g}{R_L + R_g}$.

The current from the two current sources of the system (I_{11} and I_{21}) is induced from the system itself, similar to the charge induction process in the Kelvin water dropper. The amount of current that is hereby induced is proportional to the voltage of the opposite induction rings, i.e. the voltages over the two resistors R_g. Due to the voltage dividers in the system, the voltage on the induction rings can be described by mU_i, where m is a constant that defines the

fractional voltage division in the system. It is easy to verify that we have that

$$m = \frac{R_g}{R_L + R_g},$$

as this result follows directly from, $U_1 = I_{12}(R_L + R_g)$ and $U_{R_g} = I_{12}R_g$. Here we take the left subsystem as an example, but clearly a similar result can be obtained when we consider the right subsystem.

At last the proportionality constant for the current induction is given by the charge per droplet (C_{ind}) and frequency by which the droplets fall (n). Combining the above, we find that the amount of current that is induced can be described by

$$I_{i1} = \mp nC_{ind}mU_i, \quad i = 1, 2. \tag{2.1}$$

There is only a small catch; in the Kelvin system the targets will become oppositely charged due to the opposite charge induction, e.g. see Figure 1.2. In this self-excited induction process each of the targets is equally likely to start with either a positive or a negative charge. We will assume throughout that the left target will become positively charged ($U_1 \geq 0$) and that the right target will become negatively charged ($U_2 \leq 0$). This convention is also adopted in Figure 2.2, as is also exemplified by indicating the '+' and '-' terminal of each component. Doing so may also clarify that all indicated currents I_{ij}, with $i, j \in \{1, 2\}$ are all depicted in the positive direction. In particular this shows that the voltage from node A to the earth, i.e. target voltage U_1, is indeed depicted positive, whereas target voltage U_2 is indeed depicted to be negative. This explains why we need an extra minus sign for I_{11} in (2.1).

The reason that we have an opposite direction of the current flow in the left subsystem (clockwise) and right subsystem (counter-clockwise) may become extra apparent when we compare Figure 2.2 to the schematic system from Figure 2.1b. Here the accumulation of positive charges in the left target, leads to a positive current flow from this target to the earth. On the other hand the accumulation of negative charges in the right target, leads to the flow of 'negative' current from this target to the ground, i.e. a positive current flow from ground to target.

2.2.1 Systems differential equation and the corresponding solution

From the Kirchhof current laws (KCL) we know that the inflow of current at a node must equal the outflow. If we apply this rule at the nodes A and B from Figure 2.2, it can be concluded that the induced current by the gates must equal the sum of the current flow through the resistors and the current through the capacitor. Thereby we find that:

$$-mnC_{ind}U_2 = \frac{1}{R_L + R_g}U_1 + C_L\frac{dU_1}{dt}$$

$$-mnC_{ind}U_1 = \frac{1}{R_L + R_g}U_2 + C_L\frac{dU_2}{dt},$$

which can be rewritten to:

$$\begin{bmatrix} \dot{U}_1 \\ \dot{U}_2 \end{bmatrix} = \begin{bmatrix} -\frac{1}{C_L(R_L+R_g)} & -\frac{mnC_{ind}}{C_L} \\ -\frac{mnC_{ind}}{C_L} & -\frac{1}{C_L(R_L+R_g)} \end{bmatrix} \begin{bmatrix} U_1 \\ U_2 \end{bmatrix}$$

$$\dot{x} = Ax. \tag{2.2}$$

From equation (2.2) we see that voltage build-up in the Kelvin water dropper can be described by an linear differential equation, for which solutions are given by $x = e^{At}x_0$.

To solve the system we first need to find the matrix exponential e^{At}, which is derived in Appendix section A.4.1. For convenience in writing we introduce the notation

$$a = \frac{1}{C_L(R_L + R_g)}$$
$$b = \frac{mnC_{ind}}{C_L}. \tag{2.3}$$

From there on we find that the solution to the systems differential equation is given by:

$$x(t) = e^{At}x_0$$
$$\begin{bmatrix} U_1(t) \\ U_2(t) \end{bmatrix} = \frac{1}{2} \begin{bmatrix} e^{(-a-b)t} + e^{(-a+b)t} & e^{(-a-b)t} - e^{(-a+b)t} \\ e^{(-a-b)t} - e^{(-a+b)t} & e^{(-a-b)t} + e^{(-a+b)t} \end{bmatrix} \begin{bmatrix} x_{0,1} \\ x_{0,2} \end{bmatrix}$$
$$= \frac{1}{2} \begin{bmatrix} [x_{0,1} + x_{0,2}] e^{(-a-b)t} + [x_{0,1} - x_{0,2}] e^{(-a+b)t} \\ [x_{0,1} + x_{0,2}] e^{(-a-b)t} + [x_{0,2} - x_{0,1}] e^{(-a+b)t} \end{bmatrix}$$
$$= \begin{bmatrix} c_1 e^{(-a-b)t} + c_2 e^{(-a+b)t} \\ c_1 e^{(-a-b)t} - c_2 e^{(-a+b)t} \end{bmatrix}. \tag{2.4}$$

where $c_1 := \frac{1}{2}(x_{0,1} + x_{0,2})$ and $c_2 := \frac{1}{2}(x_{0,1} - x_{0,2})$.

It may be verified that, when $x_{0,2} = -x_{0,1}$, then equation (2.4) is identical to equation (3) and (4) of the paper [18].

2.2.2 System behaviour

When looking back at equation (2.4), we can see that the eigenvalues of system matrix A, which are given by $\lambda_{1,2} = -a \pm b$, directly describe the behaviour of the system. In particular one can find that the eigenvalue λ_2 is a stable eigenvalue, while stability of the larger eigenvalue λ_1 depends on the underlying constants. If we have that $\lambda_1 < 0$, both eigenvalues are negative, so that we have a stable system. In this case solutions will tend to the equilibrium solution $(U_1, U_2) = (0,0)$. If on the other hand we have that $\lambda_1 > 0$ the system will be unstable, and the target voltages will grow exponentially. From (2.3) one can find that this is the case when

$$\lambda_1 > 0 \qquad \Longleftrightarrow$$
$$R_g > \frac{1}{nC_{ind}}. \tag{2.5}$$

Another way of looking at inequality (2.5) is to say that charge accumulation can only occur when the 'outflow' of charge is less then the 'inflow' of charge. In the electrical circuit of Figure 2.2, this is equivalent to stating that $I_{11} > I_{12}$. One can easily check that this condition indeed leads us to the same conclusion as we found in (2.5).

From equation (2.5) we observe that when the gate resistor R_g is sufficiently large, the system will be unstable. Furthermore, this is also reflected by (2.4), as one can see that solutions 'blow up' when $\lambda_1 > 0$. Since λ_1 is the largest eigenvalue, the limiting behaviour is thereby described by the corresponding eigenvector

$$v_1 = \begin{bmatrix} 1 \\ -1 \end{bmatrix},$$

so that we have that $U_1(t) \approx -U_2(t)$ as $t \to \infty$.

In conclusion we thus find that the Kelvin system will either result in a stable, non-charging system, or an unstable, over-charging system. Which of these cases will occur is directly given by the value of R_g, as is shown in (2.5). We thus see that if we use ohmic, constant resistors in the system, the induction current will undergo either positive feedback (leading to overcharging) or negative feedback (leading to non-charging).

In the traditional Kelvin setup, i.e. without a voltage divider and with well insulated targets, we have that $R_L = 0$ and $R_g \approx \infty$, which by (2.5) will indeed result in an unstable, over-charging system.

Although we have shown that theoretically, when $\lambda_1 > 0$ the voltages U_1 and U_2 will tend to infinity, this is physically impossible. This is where the, so far neglected, current losses play a role. As the voltages build up in the system, significantly more current losses will occur, eventually stabilizing the system.

When the target voltages U_1 and U_2 build-up in the Kelvin system, droplets will induce more and more charge. As explained in subsection 1.1.4 from the Introduction, this will result in charge losses, as droplets will be deflected to the environment and the induction rings. Clearly these losses will reduce the systems efficiency (see (1.6)), as the electrical output power is reduced.

In particular droplets landing on the induction rings have a double negative effect on the efficiency of the system. At first these deflected droplets, do not transfer their charge to the lower targets, which is also the case for the droplets that are lost to the environment. However, droplets landing on the induction rings also negatively interfere with the charges from the opposite target, since opposite charges are brought into contact with each other. These double losses are illustrated in Figure 2.3.
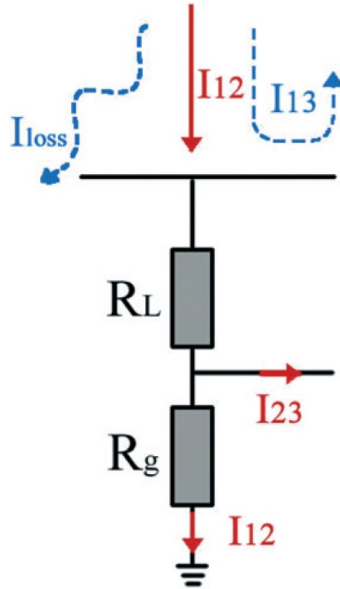
Figure 2.3: Schematic picture of the current losses in the downstream circuit, taking the left jet as an example. This may be compared to Figure 1.6

Please note that the current I_{23} in Figure 2.3 is due to the deflected droplets to the gate ring at the opposite, right jet (similarly to I_{13} at the displayed, left jet).

2.3 Using inverted Diodes

In this section we will first have a closer look at the working of the inverted diodes from [18]. In the Electronic Supplementary Information (ESI) of [18], the 'I-V curve' of this component is given, as is also shown in the figure below.
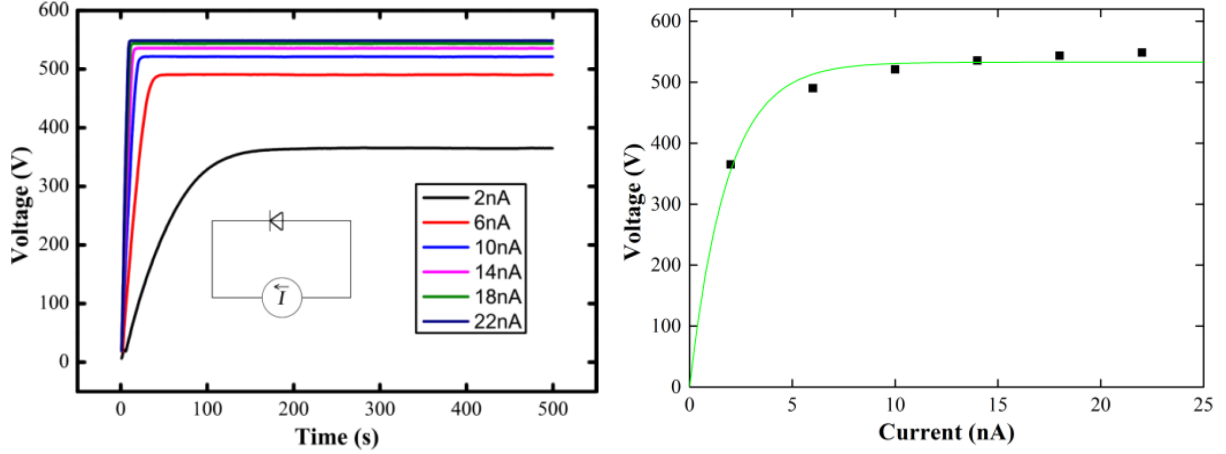
Figure 2.4: Characteristics of the inverted diode used in [18]. The green curve is described by the equation $U_{diode} = 533 \left(1 - e^{-0.55I}\right)$, with U_{diode} in Volts and I in nA.

From Figure 2.4, it can be seen that the (imperfect) inverted diodes can be used to create a more or less constant voltage over a range of (induced) small currents. For the ballistic Kelvin setup this seems to be a very useful characteristic, as a constant voltage will prevent 'overcharging' the droplets in the system.

With this in mind, the (imperfect) inverted diodes were used as voltage dividers in [18] and the measurements that were obtained with this setup are shown in Figure 2.5.
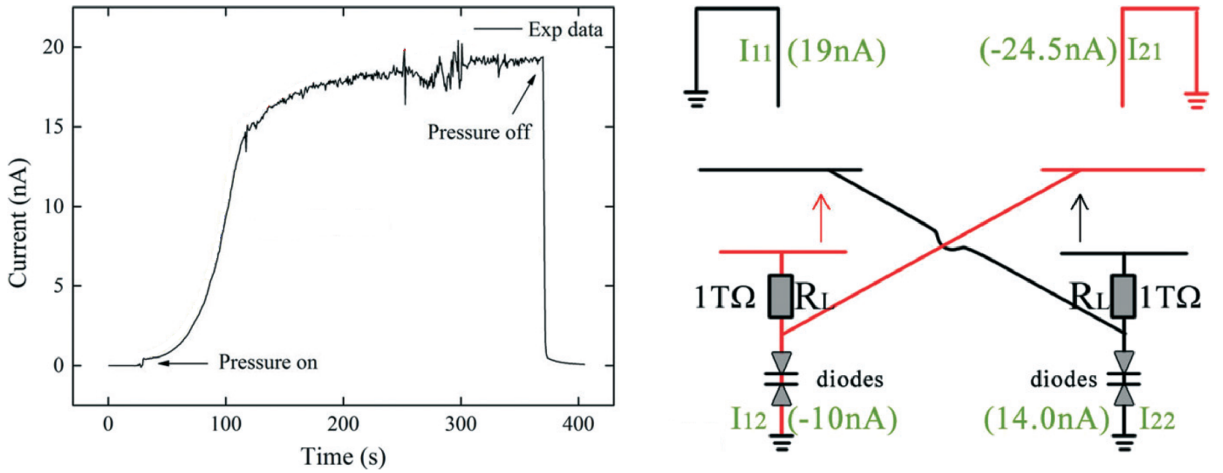
Figure 2.5: Measurements from the (imperfect) inverted diode voltage divider setup. Left: the measured (buildup of) induced current as a function of time. Right: Scheme of the electrical circuit and values of the (steady state) measured currents.

We can see in Figure 2.5 that, compared to a resistor voltage divider, significantly higher downstream currents could be obtained while using the (imperfect) inverted diode as a voltage

divider, as opposed to the use of a resistor voltage divider (e.g. see also Figure 2.7).

From Figure 2.5, we can see that on average (in absolute value) 21.75 nA is induced. The somewhat large difference in up- and downstream currents of the left and right jetting system is expected to be caused by differences in the characteristics of the 4 used (imperfect) diodes. It is hereby important to remember that, by the 'definition' of a diode, they are not designed to allow current to pass in the wrong direction.

Using the I-V curve shown in the right of Figure 2.4, we find that the voltage on the rings was on average (in absolute value) equal to 531.8 V. From these two values we calculate the experimental induction constant: $nC_{ind} = \frac{21.75}{531.8} = 0.0409$ nA/V.

We know from section 2.2.2 that theoretically, when $R_g > \frac{1}{nC_{ind}}$ we have a charging system and when $R_g < \frac{1}{nC_{ind}}$ the setup will be non-charging. On the basis of the (steady state) 'U-I curve' from Figure 2.4, we have therefore also plotted the corresponding 'R-I curve' for this diode, as is shown in Figure 2.6.

Resistance-Current curves
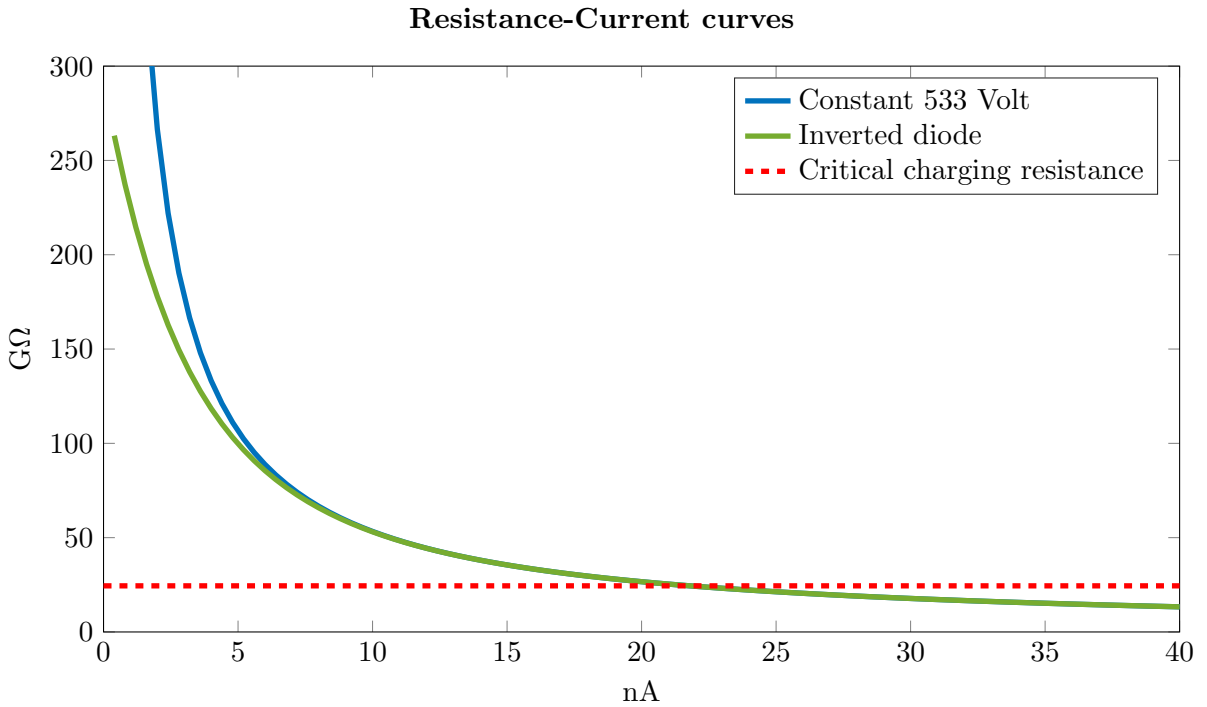
Figure 2.6: Resistant-Current curves for a constant voltage and the used (imperfect) inverted diodes.

In Figure 2.6, the critical charging resistance was determined from the measurements with the experimental setup and equals: $R_g = \frac{1}{nC_{ind}} = 24.45$ $G\Omega$. Further inspection of Figure 2.6 reveals that this figure can help to describe the systems behaviour.

At the start of the system, no current is yet induced. Then, after some initial imbalance, the current will be (greatly) induced, as the resistance of the diodes is now (a lot) higher than the critical value of the gate resistance. However, as more current is induced, the value for the gate resistance is reduced, and when about 15 nA is induced, the resistance is just above the critical value. Because of this, the rate at which the induction current increases will be reduced. In the end, the induction current will increase slowly to the point where it equals the critical resistance, and at this value the induction current will stabilize. This is also exactly the

behaviour of the induction current that we found in the left of Figure 2.5.

For the R-I curve of the diodes we can calculate that this intersection is given at 21.8 nA, which also happens to equal the average (in absolute value) of the induced current of the diode voltage divider experiments.

However, this induction current is still too high, as from the right of Figure 2.5 we can clearly see that current losses are still present. For a better efficiency, we would like to steer the system to a lower equilibrium for the induction current. In this way droplets will not become 'overcharged', reducing the amount of current loss. Which induction current is optimal at the equilibrium, will depend on the nature of the current losses. A large amount of current losses will clearly result in a low efficiency, but if we do not want any current losses to occur we may be too restricted in the extent to which the system can be charged. In [17] we find that typically about 20% of the droplet charge is lost at maximal efficiency.

As discussed, a R-I curve as shown in Figure 2.6 for the diodes, can help to explain the charging behaviour of the Kelvin water dropper. For instance, from section 2.2.2 and [18] we can draw the conclusion that for a symmetric system, the use of constant resistors will either result in a non-charging system, or an overcharging system, directly depending on the value of R_g.

The problem we face is that we need a charging system in order to harvest downstream currents, but at the same time we do not want the system to overcharge, as this will induce current losses which drastically reduce the efficiency of the energy conversion. However, from the R-I curve of the diodes (see Figure 2.6), we may just infer a way to achieve this.

When we allow for variable resistors instead of constant resistors, we may for instance control the induction ring voltages by some continuous function for the resistors (i.e. $R_g = g(I)$) described by:

$$g(I) = \begin{cases} g_1(I) \text{ where } g_1(I) > \frac{1}{nC_{ind}} & \text{if } I < I^* \\ g_2(I) \text{ where } g_2(I) \leq \frac{1}{nC_{ind}} & \text{if } I \geq I^*, \end{cases} \tag{2.6}$$

where I^*, represents the optimal equilibrium solution for the induction currents.

In layman's terms we propose to charge the system until some optimal equilibrium solution is reached. The pursuit of an optimal way in doing so will be treated in chapter 4.

However, from the systems differential (2.2), where $m = \frac{R_g}{R_L + R_g}$ is the voltage divider constant, we may already perform some preliminary analysis. When we substitute this constant m back to its resistor expression and look at a completely symmetrical system, i.e. when $U_1(t) = -U_2(t)$, we have that the system is determined by

$$\dot{U}_1 = \frac{1}{C_L} \frac{nC_{ind}R_g - 1}{R_L + R_g} U_1, \qquad U_1(0) \geq 0. \tag{2.7}$$

Note that from (2.4) we see that the assumption $U_1(t) = -U_2(t)$ is only correct when $U_1(0) = -U_2(0)$. However, since $\lambda_1 = \frac{1}{C_L} \frac{nC_{ind}R_g - 1}{R_L + R_g}$ is the largest eigenvalue of the system, other initial conditions will eventually also converge to this symmetrical system description. This can for instance be verified from the discussion in section 2.2.2 or also directly from (2.4).

From equation (2.7) we can see that the derivative $\dot{U}_1$ increases when R_g increases and/or when R_L decreases. Because of this we expect that the fastest way to charge the system is to use a large gate resistor R_g and a small load resistor R_L. To prevent overcharging the opposite of

this observation may be explored, i.e. one may reduce the gate resistor R_g and/or increase the load resistor R_L.

2.4 Explaining the measurements

In [18] and [16] several measurements have been recorded using the ballistic version of Kelvins water dropper. From these measurements we may be able to validate some of the established theory from the previous section. Let us for instance return to the results from the voltage divider setup studied in [18]. From the paper we can obtain the following measurements of the setup:
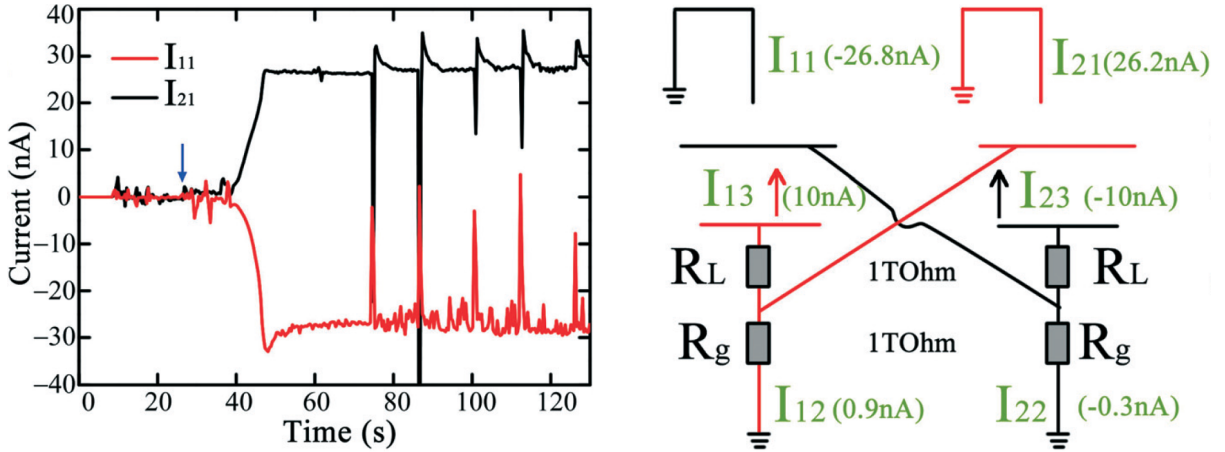
Figure 2.7: Measurements from the dual 1 TΩ voltage divider setup. Left: the measured (buildup of) induced current as a function of time. Right: Scheme of the electrical circuit and values of the (steady state) measured currents.

Comparing the diode voltage divider setup (see Figure 2.5) to the above resistor voltage divider setup, we may note that the same load resistors are used, but for the gate resistors we have a difference between a constant and a non-linear resistor. From the measurements we can furthermore note that for the resistor voltage divider an equilibrium solution is reached a lot faster. From the moment the pressure is turned on, it takes approximately 20 seconds to reach an equilibrium. For the diode setup on the other hand, it takes approximately 90-95 seconds to reach 15 out of the final 19 nA, and from here on the system charges only gradually.
This strong difference in charge time may now be explained from the different values of the gate resistors. In the resistor voltage divider setup, the gate resistor has a constant value of 1 TΩ, allowing for a quick increase in induced current, but unfortunately at the same time causes the system to overcharge. From Figure 2.6 we can see that in the diode voltage divider setup, the gate resistor initially has a resistance of approximately 290 GΩ, which explains the relative quick increase of induction currents for the first 90-95 seconds. However, the resistance can be seen to decrease quite fast when more current is induced, which also explains the gradual charging in the end.

Let us at last have a look at two additional experiments where (constant) resistors were used as a voltage divider:

When we look at the left of Figure 2.8, we can see that this setup resulted in a a non-charging system. This can be explained from the low value for the gate resistance, i.e. assuming an induction constant nC_{ind} of 0.04-0.05 nA/V, we can calculate from (2.5) that the critical gate
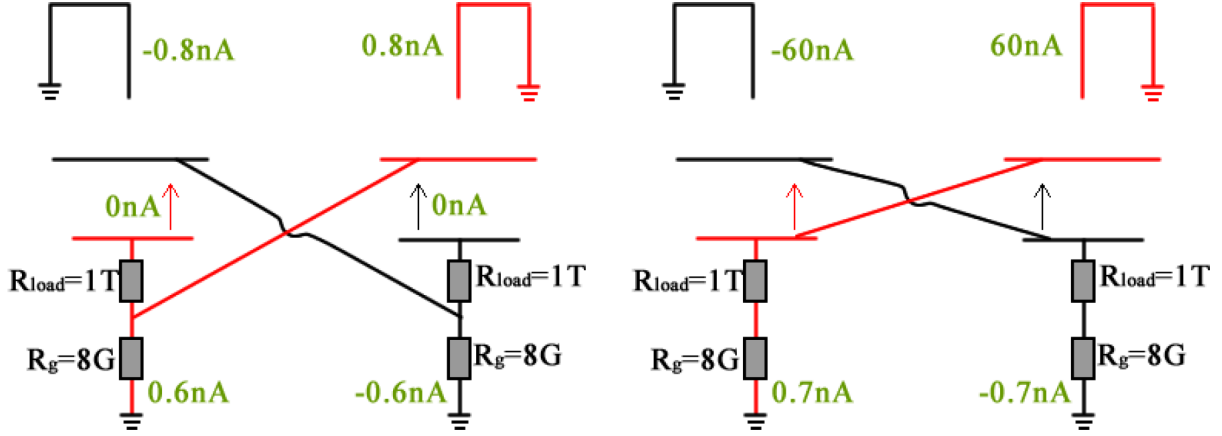
Figure 2.8: Steady state measurements from two additional resistor voltage divider experiments. Left: $R_L = 1$ TΩ, $R_g = 8$ GΩ. Right: Effectively we have $R_L = 0$ Ω, $R_g = 1.008$ TΩ.

resistance equals 20-25 GΩ. As this gate resistance is clearly below this value, the system will be non-charging. Looking at the right of Figure 2.8, similar to the case of Figure 2.7, we can see that a very large value of approximately 1 TΩ is used for the gate resistor. Herby note that the load resistor and gate resistor are connected in series, effectively resulting in just one nett gate resistor of 1.008 TΩ (i.e. without a load resistor).

As this gate resistor is again (much) larger than the critical gate resistance, we will indeed have an overcharging system. This can also be observed from the large steady state induction currents (of $\pm$ 60 nA). What is somewhat strange however, is that the induction currents are this large. Considering the downstream currents of $\pm$ 0.7 nA, we can calculate that the induction constant nC_{ind} in this setup equals: $nC_{ind} = \frac{60}{0.7 \cdot 10^{-9} \cdot 1.008 \cdot 10^{12}} = \frac{60}{705.6} = 0.085$ nA/V. This value is about twice as high as we found in the dual 1 TΩ resistor voltage divider setup (Figure 2.7) or the diode voltage divider setup (Figure 2.5). We expect that this can be explained from a rather sensitive charge induction process (see also Figure 1.3). For instance, from measurements with a similar single jet system in [17], also shown in Figure 3.7, it seems that an induction constant of over 0.1 nA/V should also be achievable.

Chapter 3

Analyzing the Kelvin water dropper

In the setup of the ballistic Kelvin water dropper, at high target voltages droplets are deflected from the target to the induction rings. Furthermore droplets are also lost to the environment. These losses will become severe when the droplets and/or the targets are highly charged. In this chapter we will investigate how these losses can be incorporated in the induction model from the previous chapter, and investigate how these will influence the systems characteristics.

3.1 Extended system with current losses

In this section current losses I_{13} and I_{23} will be incorporated in the system, which were omitted in section 2.2. In order to do so systematically, some latent variables are introduced, as indicated in Figure 3.1.

Figure 3.1: The electrical circuit of Figure 2.2, with the addition of latent variables.

For the electrical circuit shown in Figure 3.1, a list of equations can be formulated. These equations are listed in table 3.1.

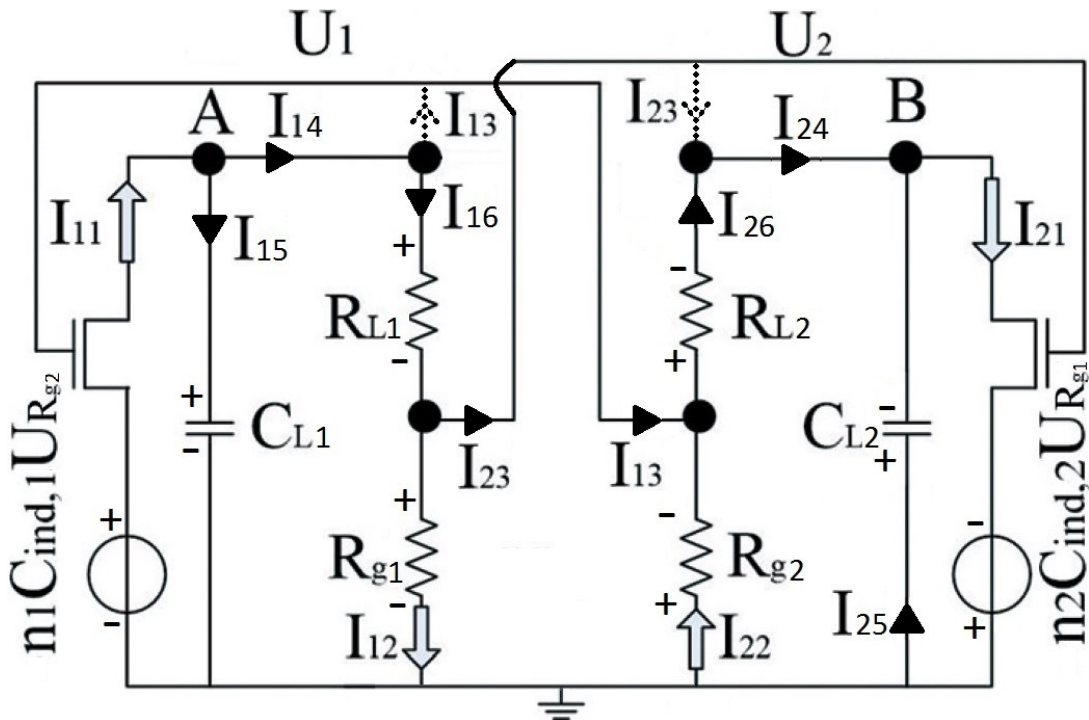| Left jet	Right jet
Kirchhof current laws	Kirchhof current laws
$I_{11} = I_{14} + I_{15}$	$I_{21} = I_{24} + I_{25}$
$I_{14} = I_{13} + I_{16}$	$I_{24} = I_{23} + I_{26}$
$I_{16} = I_{12} + I_{23}$	$I_{26} = I_{13} + I_{22}$
$I_{11} + I_{22} + I_{25} = I_{12} + I_{15} + I_{21}$	
Kirchhof voltage laws	Kirchhof voltage laws
$U_1 = U_{C_{L_1}}$	$U_2 = -U_{C_{L_2}}$
$= U_{CurrSource_1}$	$= -U_{CurrSource_2}$
$= U_{R_{L_1}} + U_{R_{g_1}}$	$= U_{R_{L_2}} + U_{R_{g_2}}$
Component laws	Component laws
$I_{15} = C_{L_1}\frac{dU_1}{dt}$	$I_{25} = -C_{L_2}\frac{dU_2}{dt}$
$(= I_{C_{L_1}})$	$(= I_{C_{L_2}})$
$I_{11} = -n_1 C_{ind_1} U_{R_{g_2}}$	$I_{21} = n_2 C_{ind_2} U_{R_{g_1}}$
$U_{R_{L_1}} = I_{16} R_{L_1}$	$U_{R_{L_2}} = -I_{26} R_{L_2}$
$U_{R_{g_1}} = I_{12} R_{g_1}$	$U_{R_{g_2}} = -I_{22} R_{g_2}$
Current losses	Current losses
$I_{13} = \alpha_1 U_1{}^{\beta_1}$	$I_{23} = \alpha_2(-U_2)^{\beta_2}$

Table 3.1: List of equations corresponding to Figure 3.1

Note that all indicated currents are shown in the positive direction. Furthermore, the voltages U_1 and U_2 are defined to be the voltage drops from the targets to the ground. In the circuit of Figure 3.1, these are the voltages measured from the potential level at node A or B to the ground. As, for the right jet, the 'direction' of this potential drop is opposite to the current flow, one may note that the voltage U_2 is defined to be negative, whereas voltage U_1 is defined to be positive.

The reason for the negative voltage U_2 lies in the fact that, for the right jet, negative charges are being transported by the water. By definition however, (positive) current flow is opposite to the flow of negative charges. This might also lead to a seemingly counter-intuitive current flow at the junction of I_{23}, I_{24} and I_{26}, as well as the junction between I_{13}, I_{22} and I_{26}. It is thus important, especially at these two nodes, to realize that for the right jet the flow of water (and for this right jet thus also the flow of negative charges) is opposite to the current flow.

Finally the nodes connecting the loss currents I_{13} and I_{23} to the gates may need some additional explanation. These loss currents represent deflected droplets contacting the gates (so the dashed line may actually be visualised better when drawn directly to the gates). However, in the ballistic Kelvin dropper, current flowing through the gates is not in contact with the droplets that carry induced charges. Therefore the loss currents I_{13} and I_{23} can only flow to the (opposite) voltage dividers. This will however have a secondary effect on the induced currents I_{11} and I_{21}, as loss currents can be seen to reduce the current flow through resistors R_{g_1} and R_{g_2}, thereby reducing the voltage over these resistors. Finally a reduced voltage $U_{R_{g_1}}$ and $U_{R_{g_2}}$ will lead to smaller induced charges/current at the gates (Since the gates are modelled similar to a field effect transistor ([18])).

3.1.1 Deriving the manifest behaviour

In this subsection we will derive the differential equations that describe the manifest behaviour of the extended system. With the term manifest behaviour we mean that we are interested in the behaviour of the target voltages U_1 and U_2. To do so we need to eliminate the latent variables that were introduced in Figure 3.1. A structured way of doing so is shown in Appendix section A.1.

Unlike we did in section 2.2 on the induction model, for now we will not assume that all constants are symmetrical. In this way the resistor voltage divider of the left subsystem can be different than the one in the right system, and therefore we define

$$m_i = \frac{R_{g_i}}{R_{L_i} + R_{g_i}}, \quad i \in \{1, 2\}$$

to denote the voltage divider constant in the left and right system. When doing so, following the steps in Appendix section A.1 we find that the extended system can be described by the following differential equation:

$$C_{L_1}\frac{dU_1}{dt} = -\frac{1}{R_{L_1} + R_{g_1}}U_1 - \left(n_1 C_{ind_1} R_{L_2} m_2 + 1\right)\alpha_1 U_1{}^{\beta_1} - n_1 C_{ind_1} m_2 U_2 - m_1\alpha_2(-U_2)^{\beta_2}$$

$$C_{L_2}\frac{dU_2}{dt} = -n_2 C_{ind_2} m_1 U_1 + m_2\alpha_1 U_1{}^{\beta_1} - \frac{1}{R_{L_2} + R_{g_2}}U_2 + \left(n_2 C_{ind_2} R_{L_1} m_1 + 1\right)\alpha_2(-U_2)^{\beta_2}.$$

$$(3.1)$$

It is interesting to see that these differential equations describing the extended system have a strong similarity with those from the induction model (see (2.2)). From the comparison between equation (2.2) and (3.1), one can find that all terms at the right of (2.2) are still present in (3.1). The extra terms can be seen to be related to the loss currents, and represent the stabilizing effect that the loss currents I_{13} and I_{23} have on the system.

3.1.2 Extended system behaviour

The system behaviour can be analysed on the basis of equation (3.1). Let us assume that the system is symmetrical, so that all similar constants are equal (e.g. $R_{L_1} = R_{L_2}$, $R_{g_1} = R_{g_2}$, $m_1 = m_2$, $n_1 = n_2$, etc). Let us furthermore introduce the following constants:

$$A = \frac{1}{C_{L_i}(R_{L_i} + R_{g_i})}$$
$$B = \frac{\left(n_i C_{ind_i} R_{L_j} m_j + 1\right)\alpha_i}{C_{L_i}}$$
$$C = \frac{n_i C_{ind_i} m_j}{C_{L_i}}$$
$$D = \frac{m_i \alpha_j}{C_{L_i}} \tag{3.2}$$

In equation (3.2), i and j are used to explicitly indicate the left or right jet, i.e. $i \neq j$, $i \in \{1, 2\}$, $j \in \{1, 2\}$. Using these constants and the assumption of symmetry between the two jets, we can rewrite equation (3.1) to:

$$\frac{dU_1}{dt} = -AU_1 - BU_1{}^{\beta} - CU_2 - D(-U_2)^{\beta}$$
$$\frac{dU_2}{dt} = -CU_1 + DU_1{}^{\beta} - AU_2 + B(-U_2)^{\beta} \tag{3.3}$$

When we take a closer look at (3.3) we find that the assumption of symmetrical constants also results in a somewhat symmetrical differential equation. In particular, it is easy to see that the following lemma holds:

Lemma 3.1.1. $(U_1, -U_1)$ *satisfies equation (3.3) if and only if* U_1 *satisfies:*

$$\frac{dU_1}{dt} = (C - A)\,U_1 - (B + D)\,U_1^{\beta} \tag{3.4}$$

For the rest of this section we will continue with the symmetrical differential equation description that is described by Lemma 3.1.1. Thereby we will turn our attention to the differential equation of (3.4), and use the fact that its solution U_1 also provides a solution pair $(U_1, -U_1)$ to equation (3.3).

In case of the induction model with symmetrical constants, we have already seen that a symmetrical system description of $U_1 = -U_2$ is reasonable. For this simplified model we have seen that $U_1(t) \approx -U_2(t)$ as $t \to \infty$, and, in particular, in case $U_1(0) = -U_2(0)$ we have that $U_1(t) = -U_2(t)$ for all time. From (2.2) we find that the symmetrical differential equation for the induction model is given by

$$\frac{dU_1}{dt} = (C - A)\,U_1. \tag{3.5}$$

A final result we shall recapitulate from the induction model is that in order to have a charging system it is necessary to have that $C - A > 0$, or equivalently, one would require that $R_g > \frac{1}{nC_{ind}}$. This assumption will also be continued in the rest of this thesis:

Assumption 1 (Charging assumption). *If without further notice, throughout this thesis we shall assume that* $C - A > 0$.

Not only in the induction model the above assumption will ensure a charging system, one can also see from equation (3.4) that in case $C - A < 0$ the system would be non-charging. To see this, it is important to remember that as an arbitrary modelling assumption we have set $U_1 \geq 0$. If we then would have that $C - A < 0$, then it follows that the derivative in (3.4) is always negative. Clearly a non-charging system would not be very interesting to analyze, which is one of the main reasons to stick with assumption 1.
Furthermore, in case $C - A < 0$ we find that the sole equilibrium point of (3.4) is given by $U_1^* = 0$. One may however expect that in the extended model the additional current losses will provide the system with an additional (stable) equilibrium point; if the 'growth' equals the 'loss' the target voltages would come to a halt. This will be the topic of the next subsection

3.1.3   Equilibrium points

In this section we will analyze the equilibrium points from (3.4), which by lemma 3.1.1 also provide equilibrium points to (3.3). Upon combining the modelling assumption $U_1 \geq 0$ with the charging assumption 1, we find that (3.4) contains a 'growth term', i.e. '$(C - A)\,U_1$', and a 'loss term', i.e. '$(B + D)\,U_1^{\beta}$'. Apart from the trivial equilibrium point $U_1^* = 0$, by equating the 'growth' and 'loss term' we find that another (real) equilibrium point of (3.4) is given by

$$U_1^* = \left(\frac{C - A}{B + D}\right)^{\frac{1}{\beta - 1}}. \tag{3.6}$$

One may note that for odd β the equation $(C - A)\,U_1 = (B + D)\,U_1^{\beta}$ would also have a negative solution, since we then get a quadratic expression in solving for U_1. However, this is in

contradiction with our modelling assumption that $U_1 \geq 0$.

Next, it directly follows from lemma 3.1.1 that $(U_1{}^*, -U_1{}^*)$ is also an equilibrium solution to (3.3). In section 3.2 we will furthermore analyze whether these are also the only equilibrium solutions to (3.3).

The nature of the equilibrium points can be studied by means of linearisation. The Jacobian of (3.4) can be calculated to equal:

$$f'(U_1) = (C - A) - (B + D)\beta U_1{}^{\beta-1}. \tag{3.7}$$

By a simple substitution we can now see that, in the equilibrium point of (3.6), the above Jacobian is equal to:

$$f'(U_1{}^*) = (C - A)(1 - \beta). \tag{3.8}$$

As we have that $\beta > 1$ and $C - A > 0$, the eigenvalue of (3.8) is smaller than zero. Thereby we find that $U_1{}^*$ from (3.6) is an asymptotically stable equilibrium of (3.4).
In an analogous fashion, from (3.7) one can find that the trivial equilibrium point $U_1{}^* = 0$ is an unstable equilibrium point of (3.4). At last, note that in the case that the assumption 1 does not hold, the equilibrium point from (3.6) is undefined (for real numbers). In this case the equilibrium point $U_1{}^* = 0$ is stable, which makes sense because under these conditions the system is non-charging.

2-dimensional equilibrium points

For completeness a similar analysis of the equilibrium points can be performed on the full system from (3.3). From lemma 3.1.1 it follows that if $U_1{}^*$ is an equilibrium point of (3.4), then $(U_1{}^*, -U_1{}^*)$ is an equilibrium point of (3.3). Thereby we will show that our previous conclusions on the stability of the equilibrium points from (3.4) also hold in the 2-dimensional case of (3.3). The equilibrium points of interest are given by $(U_1{}^*, -U_1{}^*) = (0, 0)$ and

$$(U_1{}^*, -U_1{}^*) = \left(\left(\frac{C - A}{B + D} \right)^{\frac{1}{\beta-1}}, -\left(\frac{C - A}{B + D} \right)^{\frac{1}{\beta-1}} \right).$$

For the Jacobian of the full system we now find:

$$f'(U_1, U_2) = \begin{bmatrix} -A - B\beta U_1{}^{\beta-1} & -C + D\beta(-U_2)^{\beta-1} \\ -C + D\beta U_1{}^{\beta-1} & -A - B\beta(-U_2)^{\beta-1} \end{bmatrix}.$$

In the non-zero equilibrium point this Jacobian is equal to:

$$f'(U_1{}^*, -U_1{}^*) = \begin{bmatrix} -A - B\beta\frac{C-A}{B+D} & -C + D\beta\frac{C-A}{B+D} \\ -C + D\beta\frac{C-A}{B+D} & -A - B\beta\frac{C-A}{B+D} \end{bmatrix}, \tag{3.9}$$

where the eigenvalues of (3.9) can be found to equal

$$\lambda_{1,2} = -A - B\beta\frac{C - A}{B + D} \pm \left(-C + D\beta\frac{C - A}{B + D} \right). \tag{3.10}$$

Here λ_2 can be simplified to $(C - A)(1 - \beta)$, and as $\beta > 1$ we thus see that this eigenvalue is stable.

The expression for λ_1 is slightly more elaborate, as we obtain:

$$\lambda_1 = -C - A + \beta \frac{C - A}{B + D} (D - B).$$

Also this eigenvalue is stable, which can be shown from the underlying constants of A, B, C, D from the definition of (3.2). As we have that $m_i \in [0, 1]$, it follows directly from (3.2) that $D - B \leq 0$. But this also directly implies that $\lambda_1 < 0$. As both eigenvalues are negative, we have that indeed the non-zero equilibrium point is also stable in the 2-dimensional case.

Similarly we may also investigate the stability of the origin for the full system. We find that the Jacobian in the origin is equal to:

$$f'(0, 0) = \begin{bmatrix} -A & -C \\ -C & -A \end{bmatrix}, \tag{3.11}$$

which has eigenvalues that are given by

$$\lambda_{1,2} = -A \pm C. \tag{3.12}$$

It can easily be verified from (3.12) that $\lambda_1 < 0$ if and only if $C - A < 0$, while λ_2 is always negative. Because of this we thus again see that in the regular case where $C - A > 0$ the origin is unstable, whereas in the non-charging case the origin is stable.

In summary we thus find that indeed our previous conclusion about the stability of the equilibrium points in (3.4) also holds for the full system given by (3.3).

3.1.4 Solving the extended systems differential equation

In this subsection equation (3.4) is solved analytically. This may be done by integration by parts, as is shown in Appendix section A.2. There is however also an easier way, as will be shown in this section.

We start with a bit of a 'trick', and multiply the second line of (3.4) with $(1 - \beta)U_1^{-\beta}$ to obtain:

$$(1 - \beta)U_1^{-\beta}\frac{dU_1}{dt} = (1 - \beta)(C - A)U_1^{1-\beta} - (1 - \beta)(B + D) \qquad \Longleftrightarrow$$
$$\frac{df}{dt} = (1 - \beta)\widetilde{A}f - (1 - \beta)\widetilde{B} \tag{3.13}$$

where $f := U_1^{1-\beta}$, $\widetilde{A} := (C - A)$ and $\widetilde{B} := (B + D)$.

Using this substitution 'trick' we see that the non-linear differential equation of (3.4) can be reduced to an ordinary differential equation. To be complete, we can see that the solution f of (3.13) also gives us a solution to (3.4), since $U_1 = (f)^{\frac{1}{1-\beta}}$.

It is easy to see that the complete solution of (3.13) is given by:

$$f(t) = ce^{(1-\beta)\widetilde{A}t} + \frac{\widetilde{B}}{\widetilde{A}}. \tag{3.14}$$

Given (3.14) we know that the solution of (3.4) is described by:

$$U_1(t) = \left(ce^{(1-\beta)\widetilde{A}t} + \frac{\widetilde{B}}{\widetilde{A}} \right)^{\frac{1}{1-\beta}}. \tag{3.15}$$

The constant c may be solved from a given initial condition $U_1(0)$:

$$c = U_1(0)^{1-\beta} - \frac{\widetilde{B}}{\widetilde{A}}. \tag{3.16}$$

Comparison of (3.15) to the measurements from [18]

Having found a solution to (3.4), next we will check how the equation compares to the measurements from [18]. In this paper measurements are discussed of a ballistic Kelvin dropper with a dual 1 TΩ voltage divider. Furthermore, in this paper we also find that the values $nC_{ind} = 0.05 \cdot 10^{-9}$ and $C_L = 12 \cdot 10^-12$ may be used to model the system. At last, the constants α and β are chosen to obtain a similar target voltage equilibrium as we find in the measurements.

Using these constants we use definition (3.2) to form the combined constants A, B, C, D and from there we can form the final merged constants $\widetilde{A}$ and $\widetilde{B}$. At last, when we plug in the obtained constants in (3.15) and (3.16), we obtain the following figure.

Simulation of the ballistic Kelvin dropper with current losses
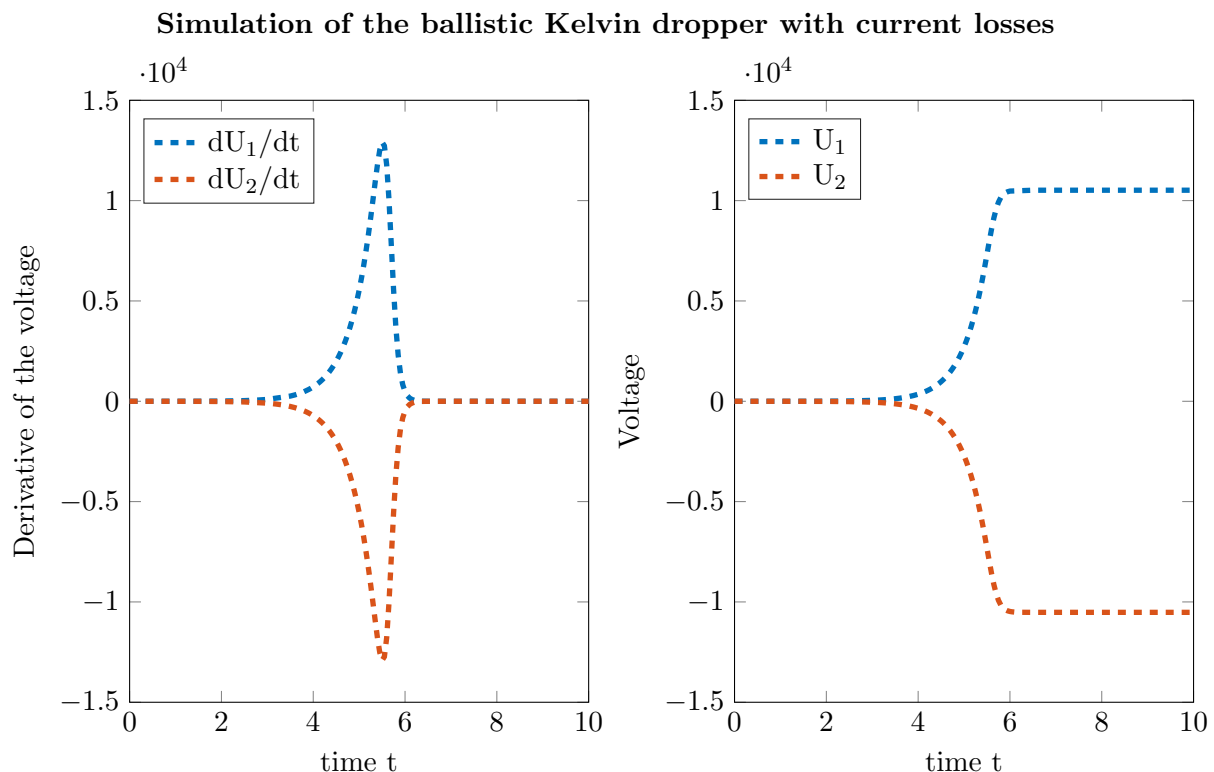
Figure 3.2: Matlab simulation of (3.15). Values for the resistors are chosen according to the resistor voltage divider discussed in [18], see also Figure 2.7. Constants nC_{ind} and C_L were chosen to match the chosen values in [18], and are given by $nC_{ind} = 0.05 \cdot 10^{-9}$ and $C_L = 12 \cdot 10^-12$. At last, the constants α and β that define the amount of current loss are chosen by $\alpha = 7 \cdot 10^{-35}$ and $\beta = 6.5$.

The right of Figure 3.2 may be compared to the induction current measurements as shown in the left of Figure 2.7. This is because the amount of induction current is directly related to the target voltage, see for instance also (A.3) and (A.4) from the Appendix.

When we compare these measurements with the above plot, we remark that a similar behaviour can be observed, i.e. in both cases we find a quick exponential increase which abruptly comes to a halt.

3.2 Other equilibrium solutions?

In subsection 3.1.2 the system behaviour has been analysed at the equilibrium points. Due to the symmetry of the systems it had been assumed that $U_1(t) = -U_2(t)$. Furthermore, by modelling assumptions, it was assumed that $U_1 > 0$ and $U_2 < 0$. In this section we will look at possible other equilibrium points in the U_1, U_2 plane outside the $U_1 = -U_2$ subspace.

In order to find other equilibrium points, we will have a closer look at the extended systems differential equation (3.3). Again we shall use with symmetrical constants A, B, C, D. Furthermore, in this section we will again make use of the charging assumption 1. At last we will use that $B - D \geq 0$ which follows directly from (3.2) and the fact that for the voltage divider constant we have that $m_i \in [0, 1]$. The basic assumptions on the constants in this section are thus given by

Assumption 2 (Standard assumptions on the constants). *If without further notice, throughout this thesis we shall assume that:*

$$C - A \geq 0$$
$$B - D \geq 0.$$

3.2.1 Equation approach

At first we will see whether it is possible to find more equilibrium points by directly solving them from (3.3). For simplicity we write $-U_2 = \widetilde{U_2}$. The equation describing the equilibrium points is now given by:

$$0 = -AU_1 - BU_1^\beta + C\widetilde{U_2} - D\widetilde{U_2}^\beta \tag{3.17}$$

$$0 = -CU_1 + DU_1^\beta + A\widetilde{U_2} + B\widetilde{U_2}^\beta. \tag{3.18}$$

By subtracting $\frac{C}{A}$ times (3.17) from (3.18) we obtain:

$$0 = DU_1^\beta + \frac{C}{A}BU_1^\beta + A\widetilde{U_2} - \frac{C^2}{A}\widetilde{U_2} + B\widetilde{U_2}^\beta + \frac{C}{A}D\widetilde{U_2}^\beta \qquad \Longleftrightarrow$$

$$\left(D + \frac{C}{A}B\right)U_1^\beta = \left(\frac{C^2}{A} - A\right)\widetilde{U_2} - \left(B + \frac{C}{A}D\right)\widetilde{U_2}^\beta \qquad \Longleftrightarrow$$

$$U_1^\beta = \frac{\frac{C^2}{A} - A}{D + \frac{C}{A}B}\widetilde{U_2} - \frac{B + \frac{C}{A}D}{D + \frac{C}{A}B}\widetilde{U_2}^\beta \qquad \Longleftrightarrow \tag{3.19}$$

$$U_1 = \left(\frac{\frac{C^2}{A} - A}{D + \frac{C}{A}B}\widetilde{U_2} - \frac{B + \frac{C}{A}D}{D + \frac{C}{A}B}\widetilde{U_2}^\beta\right)^{\frac{1}{\beta}}. \tag{3.20}$$

Next, equation (3.20) can be plugged into equation (3.17) to obtain an expression from which $\widetilde{U_2}$ may be solved:

$$0 = -A\left(\frac{\frac{C^2}{A} - A}{D + \frac{C}{A}B}\widetilde{U_2} - \frac{B + \frac{C}{A}D}{D + \frac{C}{A}B}\widetilde{U_2}^\beta\right)^{\frac{1}{\beta}} - B\left(\frac{\frac{C^2}{A} - A}{D + \frac{C}{A}B}\widetilde{U_2} - \frac{B + \frac{C}{A}D}{D + \frac{C}{A}B}\widetilde{U_2}^\beta\right) + C\widetilde{U_2} - D\widetilde{U_2}^\beta.$$
$$\tag{3.21}$$

Since equation (3.21) is an implicit equation in the second coordinate ($\widetilde{U_2}$), by equation (3.20) it gives an explicit solution to the first coordinate point U_1.

From equation (3.19) we again see that we need the condition $C - A \geq 0$ from the assumption 2. If this is not the case, there is no real solution where U_1 and $\widetilde{U_2}$ are both strictly positive, e.g. we would have a positive number on the left side and a negative number on the right side.

As an example, in accordance with the assumption 2 we take $A = 1$, $B = 3$, $C = 2$, $D = 1$, $\beta = 3$. For this example equation (3.21) becomes:

$$-\left(\frac{3}{7}\widetilde{U_2} - \frac{5}{7}\widetilde{U_2}^3\right)^{\frac{1}{3}} + \frac{5}{7}\widetilde{U_2} + \frac{8}{7}\widetilde{U_2}^3. \tag{3.22}$$

One may now verify that this equation has 3 real solutions; $\widetilde{U_2} = -\frac{1}{2}$, $\widetilde{U_2} = 0$ and $\widetilde{U_2} = \frac{1}{2}$. Next, from (3.20) one can check that each of these solutions result in equilibrium points on the $U_1 = \widetilde{U_2}$ subspace, i.e. the real solutions of (3.21) and (3.20) are given by $(U_1, \widetilde{U_2}) = (-\frac{1}{2}, -\frac{1}{2})$, $(0, 0)$ and $(\frac{1}{2}, \frac{1}{2})$. That also negative solutions arise is not surprising, as this can be explained by a different initial polarity as opposed to what is assumed. At last, using matlab one may verify that (3.22) also has complex solutions $\widetilde{U_2} = -0.5303 \pm 0.7706i$.

In conclusion we can see that although it is possible to find equilibrium solutions to (3.17) and (3.18), the method does not present a clear overview of whether the equilibrium points are spread only on the $U_1 = \widetilde{U_2}$ subspace or not. By doing several simulations it however seems that there can only be 1 real and strictly positive solution $(U_1{}^*, \widetilde{U_2}{}^*)$ to equation (3.17) and (3.18). In the next subsection we will investigate if this can be shown by using implicit plots.

3.2.2   Implicit plot approach

In this section implicit plots will be used to study the real equilibrium points of equation (3.17) and (3.18). Clearly values for the coefficients A, B, C and D (see equation (3.2)) would need to be chosen to make an implicit plot. In all of the plots in this section, in accordance with the assumption 2, we use the standard example

Assumption 3 (standard example)**.** *The standard constants that will be used in the plots of this section are given by $A = 1$, $B = 2$, $C = 2$ and $D = 1$.*

Furthermore, we will also use $\beta > 1$ as current losses will increase at large operating voltages. Let us assume that $\beta \in \mathbb{N}$ and start with the case that β is even (the case β is odd will be treated later in this section). It is important to realize that, since we have that $\beta > 1$, the terms '$BU_1{}^\beta$' and '$D\widetilde{U_2}^\beta$' will dominate the implicit solutions of equation (3.17) and (3.18) in the case that $|U_1| > 1$ and/or $|\widetilde{U_2}| > 1$. To study this effect, in Figure 3.3 an implicit plot has been made for the relative high value of $\beta = 20$.

In Figure 3.3, we can see that the implicit plot has a strong resemblance to a quadrilateral, where the vertices for this example are located near the coordinates $(-0.9763, 1.029)$, $(0.9321, 0.9675)$, $(-0.8261, -0.3932)$ and $(0.8349, 0.4462)$. This specific shape can be explained on the basis of the limiting behaviour of (3.17), where $\beta \to \infty$ along the even integers, at four points in the $(U_1, \widetilde{U_2})$ plane. These points of interest are $(U_1, \widetilde{U_2}) = (-1, 1), (1, 1), \left(-1, -\frac{A}{C}\right)$ and $\left(1, \frac{A}{C}\right)$. At these points it seems that the 'limit implicit solution' of (3.17) is given by the quadrilateral with the described vertices. In the coming pages we aim to prove this observation.

The limit points of the quadrilateral implicit solution

As previously discussed, when looking at Figure 3.3, one may recognize a more or less quadrilateral shape in the implicit curve of (3.17). From this observation the hypothesis is formed

Implicit plot with $\beta = 20$
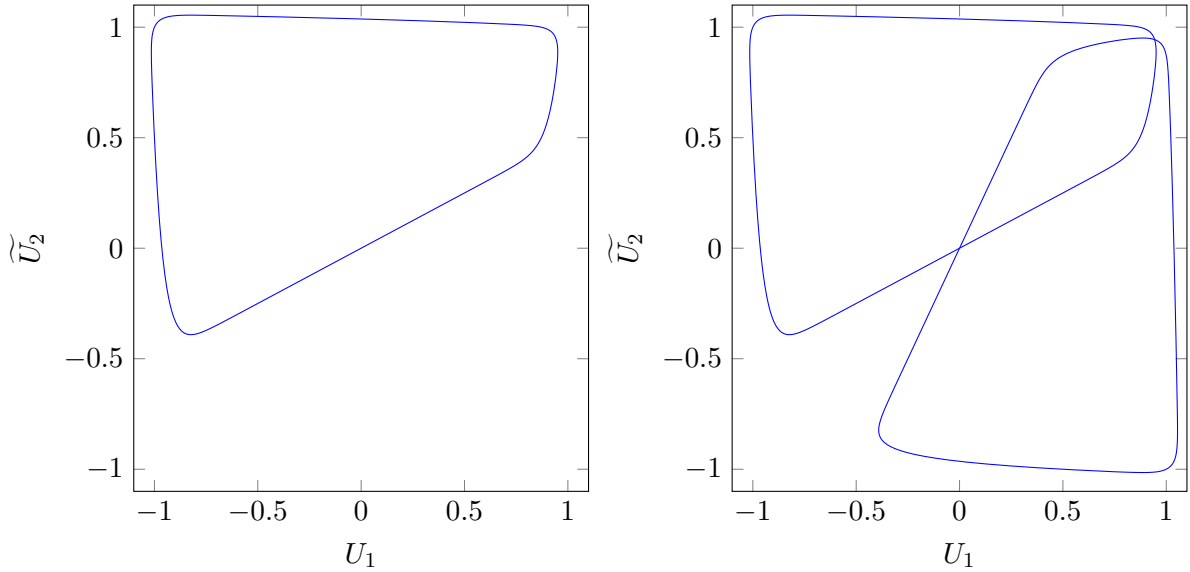
Figure 3.3: Left: a plot of solely equation (3.17). Right: a combined plot of equation (3.17) and (3.18).

that, when $\beta \to \infty$ along the even integers, the implicit solution curve of (3.17) will converge to a quadrilateral with vertices given by $(U_1, \widetilde{U_2}) = (-1, 1), (1, 1), \left(-1, -\frac{A}{C}\right)$ and $\left(1, \frac{A}{C}\right)$. In this subsection we will aim to prove that this hypothesis is correct. We start by proving that the vertices listed above indeed correspond to the 'limiting solution'.

Let us start by looking at the point $(-1, 1)$. As we want to prove that this point is a limiting solution of (3.17), we will consider a tiny shift to this point given by $(-1 + \epsilon_1, 1 + \epsilon_2)$, where $\epsilon_i \in \mathbb{R}$ is considered small (and possibly also negative). Using this shift, we will need to prove that:

$$A(-1 + \epsilon_1) + B(-1 + \epsilon_1)^\beta = C(1 + \epsilon_2) - D(1 + \epsilon_2)^\beta \tag{3.23}$$

holds for arbitrarily small (ϵ_1, ϵ_2), provided that $\beta \to \infty$ along the even integers.
It may be clear that in the strict limit point (where $(\epsilon_1, \epsilon_2) = (0, 0)$), in general equation (3.23) is not correct (for any even value of β), since we would then need that:

$$-A + B = C - D. \tag{3.24}$$

By pure coincidence however, for the main example studied ($A = 1$, $B = 2$, $C = 2$ and $D = 1$) it happens to be that equation (3.24) is met, as can also be verified from Figure 3.3 at $(U_1, \widetilde{U_2}) = (-1, 1)$. However, because the implicit solution curve for $\beta = 20$ is still a bit off to the limiting quadrilateral we expect to get at (even) $\beta = \infty$, the observed 'kink' near $(-1, 1)$ is not yet located in the strict limiting point, but is located at approximately $(-0.9763, 1.029)$.

Returning to (3.23), we are thus interested in its local behaviour near $(\epsilon_1, \epsilon_2) = (0, 0)$ when $\beta \to \infty$ along the even integers. For this purpose let us consider $\epsilon_1 = -\frac{\alpha_1}{\beta}$ and $\epsilon_2 = \frac{\alpha_2}{\beta}$ (where

35

$\alpha_1, \alpha_2 \in \mathbb{R}$, and both may be positive or negative). Using this notation, we can write:

$$A(-1 + \epsilon_1) + B(-1 + \epsilon_1)^\beta = C(1 + \epsilon_2) - D(1 + \epsilon_2)^\beta$$

$$-A\left(1 + \frac{\alpha_1}{\beta}\right) + B\left(1 + \frac{\alpha_1}{\beta}\right)^\beta = C\left(1 + \frac{\alpha_2}{\beta}\right) - D\left(1 + \frac{\alpha_2}{\beta}\right)^\beta. \tag{3.25}$$

Upon inspection of (3.25), given the well known limit $\lim_{n\to\infty}\left(1 + \frac{x}{n}\right)^n = e^x$, one may already recognize the direction we would like to follow. If we take the limit $\beta \to \infty$ on both sides of (3.25) we obtain:

$$-A + Be^{\alpha_1} = C - De^{\alpha_2}$$

$$Be^{\alpha_1} + De^{\alpha_2} = A + C. \tag{3.26}$$

Hereby note that if we choose $\alpha_1 < \ln\left(\frac{A+C}{B}\right)$ in (3.26), we get that $A + C - Be^{\alpha_1} > 0$. This in turn then allows for a real solution to (3.26) that is given by $\alpha_2 = \ln\left(\frac{A+C-Be^{\alpha_1}}{D}\right)$.
It may furthermore be verified that for given constants $A \ldots D$, both α_1 and α_2 may be positive or negative. Therefore it follows that (depending on the constants $A \ldots D$) we may approach (3.23) for any combination of directions (i.e. $(U_1 \uparrow -1, \widetilde{U_2} \uparrow 1)$, $(U_1 \uparrow -1, \widetilde{U_2} \downarrow 1)$, $(U_1 \downarrow -1, \widetilde{U_2} \uparrow 1)$ and $(U_1 \downarrow -1, \widetilde{U_2} \downarrow 1)$).

Unfortunately this does not yet conclude the (sub)proof, as from (3.26) we have only shown that equality holds at the limit $\beta = \infty$. It still remains to be shown that 'the equation (3.25)' is also converging to this 'limit point', i.e. it remains to be shown that we indeed also have an equality in (3.23) for $\beta \gg 2$ (in most cases now necessarily accompanied with values of $(\epsilon_1, \epsilon_2) \neq (0, 0)$).
To further illustrate the issue, as a side-note we may for instance consider the equation $\epsilon^2 = -\frac{1}{\beta}$ with $\epsilon \in \mathbb{R}$. This equation reaches equality in $\beta = \infty$ when $\epsilon = 0$, but will never hold for $\beta \in \mathbb{R}_+$.

Proof. Let us prove that in (3.26) we indeed have equality for small values of $(|\epsilon_1|, |\epsilon_2|)$ when $\beta \gg 2$ (and $\beta \neq \infty$). Like in (3.25), we will define $\epsilon_i := \frac{\alpha_i}{\beta}$, $i \in \{1, 2\}$.

Assume that $0 < \alpha_1 < \ln\left(\frac{A+C}{B}\right)$ and define $\alpha_2 = \ln\left(\frac{A+C-Be^{\alpha_1}}{D}\right)$. We have already shown that in this way, we reach equality in (3.23) for the 'limit solution' (i.e. when $\beta = \infty$, see also (3.26) and the notes below it). This was shown to be the result of the convergence of $\left(1 + \frac{\alpha_i}{\beta}\right)^\beta \to e^{\alpha_i}$ and $\frac{\alpha_i}{\beta} \to 0$ when $\beta \to \infty$ (where we have $i \in \{1, 2\}$).
However, due to the assumption $\alpha_1 > 0$ and these 'neat' convergences, we also know that we have that:
$\exists \beta_N > 2$ such that for $\beta \geq \beta_N$ we have that:

$$-A\left(1 + \frac{\alpha_1}{2\beta}\right) + B\left(1 + \frac{\alpha_1}{2\beta}\right)^\beta < C\left(1 + \frac{\alpha_2}{\beta}\right) - D\left(1 + \frac{\alpha_2}{\beta}\right)^\beta. \tag{3.27}$$

Likewise we have that $\exists \beta_M > 2$ such that for $\beta \geq \beta_M$ we have that:

$$-A\left(1 + \frac{2\alpha_1}{\beta}\right) + B\left(1 + \frac{2\alpha_1}{\beta}\right)^\beta > C\left(1 + \frac{\alpha_2}{\beta}\right) - D\left(1 + \frac{\alpha_2}{\beta}\right)^\beta. \tag{3.28}$$

Note that the reason for the inequality in equations (3.27) and (3.28) lies in the fact that for $\alpha_1 > 0$ we have that $e^{\frac{\alpha_1}{2}} < e^{\alpha_1}$ and $e^{2\alpha_1} > e^{\alpha_1}$.

Now consider a fixed constant $\widehat{\beta} \geq \max(\beta_N, \beta_M)$, such that for $\beta = \widehat{\beta}$ both inequalities (3.27) and (3.28) are met. Let us now define the following function and constant:

$$f(\alpha) := -A\left(1 + \frac{\alpha}{\widehat{\beta}}\right) + B\left(1 + \frac{\alpha}{\widehat{\beta}}\right)^{\widehat{\beta}},$$

$$c := C\left(1 + \frac{\alpha_2}{\widehat{\beta}}\right) - D\left(1 + \frac{\alpha_2}{\widehat{\beta}}\right)^{\widehat{\beta}}.$$

Using this notation we can see from (3.27) and (3.28) that we have that:

$$f\left(\frac{\alpha_1}{2}\right) < c, \tag{3.29}$$

as well as

$$f(2\alpha_1) > c. \tag{3.30}$$

However, it then follows by continuity of $f(\alpha)$ that $\exists \alpha^* \in \left[\frac{\alpha_1}{2}, 2\alpha_1\right]$ such that:

$$f\left(\alpha^*\right) = c, \tag{3.31}$$

which proves our statement under the made assumption that $0 < \alpha_1 < \ln\left(\frac{A+C}{B}\right)$. Furthermore, it may hopefully be clear that the proof is completely analogous under the assumption that $\alpha_1 < 0$. For this case only some inequality signs would need to be 'flipped' (in (3.27), (3.28), (3.29) and (3.30)), as then we have that $e^{\frac{\alpha_1}{2}} > e^{\alpha_1}$ and $e^{2\alpha_1} < e^{\alpha_1}$.

At last, also the proof under the assumption that $\alpha_1 = 0$ can be done using a very similar approach. In this case, we would need to prove that the equation:

$$C\left(1 + \frac{\alpha_2}{\beta}\right) - D\left(1 + \frac{\alpha_2}{\beta}\right)^{\beta} = B - A, \tag{3.32}$$

holds for some combination of α_2 and (even) β other than $\alpha_2 = 0$, $\beta = \infty$.

Without loss of generality, let us first assume that there is a 'limit solution' to (3.32), i.e. let us assume that (3.32) is correct when (even) $\beta = \infty$. One may verify that in this case we have that $De^{\alpha_2} = A + C - B$, which in turn implies that we must have that $A + C - B > 0$ (since $\alpha_2 \in \mathbb{R}$). The 'limit solution' is thus given for $\alpha_2 = \ln\left(\frac{A+C-B}{D}\right)$.

Next, assume that $0 < \alpha_2 = \ln\left(\frac{A+C-B}{D}\right)$. Due to the 'neat' convergences $\left(1 + \frac{\alpha_2}{\beta}\right)^{\beta} \to e^{\alpha_2}$ and $\frac{\alpha_2}{\beta} \to 0$ when $\beta \to \infty$ we then have that:
$\exists \beta_K > 2$ such that for $\beta > \beta_K$:

$$C\left(1 + \frac{\alpha_2}{2\beta}\right) - D\left(1 + \frac{\alpha_2}{2\beta}\right)^{\beta} < B - A. \tag{3.33}$$

Likewise we then have that $\exists \beta_L > 2$ such that for $\beta > \beta_L$:

$$C\left(1 + \frac{2\alpha_2}{\beta}\right) - D\left(1 + \frac{2\alpha_2}{\beta}\right)^{\beta} > B - A. \tag{3.34}$$

Again, the reason for the inequality in (3.33) and (3.34) can be found in the fact that for $\alpha_2 > 0$ we have that $e^{\frac{\alpha_2}{2}} < e^{\alpha_2}$ and $e^{2\alpha_2} > e^{\alpha_2}$.

Now consider a fixed constant $\widetilde{\beta} \geq \max(\beta_K, \beta_L)$, such that for $\beta = \widetilde{\beta}$ both inequalities (3.33) and (3.34) are met. Let us now define the following function:

$$g(\alpha) = C\left(1 + \frac{\alpha}{\widetilde{\beta}}\right) - D\left(1 + \frac{\alpha}{\widetilde{\beta}}\right)^{\widetilde{\beta}}.$$

In this way, it may be clear from (3.33) and (3.34), that we now have that:

$$g\left(\frac{\alpha_2}{2}\right) < B - A, \tag{3.35}$$

as well as

$$g(2\alpha_2) > B - A. \tag{3.36}$$

But then, due to the continuity of $g(\alpha)$ we may conclude that $\exists \alpha^\diamond \in \left[\frac{\alpha_2}{2}, 2\alpha_2\right]$ such that:

$$g\left(\alpha^\diamond\right) = B - A, \tag{3.37}$$

which proves our statement under the made assumption that $0 < \alpha_2 = \ln\left(\frac{A+C-B}{D}\right)$.

Again, it may hopefully be clear that the proof is completely analogous under the assumption that $\ln\left(\frac{A+C-B}{D}\right) = \alpha_2 < 0$. For this case only some inequality signs would have to be 'flipped' (in (3.33), (3.34), (3.35) and (3.36)), as then we have that $e^{\frac{\alpha_2}{2}} > e^{\alpha_2}$ and $e^{2\alpha_2} < e^{\alpha_2}$.

At last it needs to be noted that we do not need to consider the case $(\alpha_1, \alpha_2) = (0,0)$. This would correspond to the case of the 'strict limit point' (i.e. when $(\epsilon_1, \epsilon_2) = (0,0)$, see also (3.24)). Please recall that we are not (just) interested in the strict limit point, but more so in whether the limiting behaviour of (3.23) for $\beta \to \infty$ along the even integers is neatly defined in the neighbourhood of $(\epsilon_1, \epsilon_2) = (0,0)$.

As we have now dealt with all possible cases for $\alpha_1, \alpha_2 \in \mathbb{R}$ it can be concluded that indeed this limiting behaviour is neatly defined. $\square$

Let us also illustrate that the described sequence indeed converges to a solution of (3.23) when even $\beta \to \infty$. For the main example from 2, we find that $\alpha_1 < \ln\left(\frac{3}{2}\right) \approx 0.4$. Let us take $\alpha_1 = 0.1$. From this it follows that we must have $\alpha_2 = \ln\left(3 - 2e^{0.1}\right) \approx -0.236$. Using Matlab to calculate the left and right of (3.25) for some increasing values of even β results in:

Value of β	left of (3.25)	right of (3.25)
2	1.155	0.9861
10	1.1992	1.1653
100	1.2092	1.2058
1000	1.2102	1.2099

Table 3.2: Illustration of the convergence of (3.25) for the described sequence of points. The values for the constants are given by $A = 1$, $B = 2$, $C = 2$, $D = 1$, $\alpha_1 = 0.1$, $\alpha_2 = \ln\left(3 - 2e^{0.1}\right) \approx -0.236$

We will still need to show that also the other vertices of the 'limit implicit solution curve' of (3.17) (given by the quadrilateral), are part of the solution of (3.17) when $\beta \to \infty$ along the

even integers.

Although we will also do this in this subsection, we will be a bit more brief in our proof, as many aspects of the proofs will be very similar to the elaborate proof given for the vertex $(U_1, \widetilde{U_2}) = (-1, 1)$.

Let us continue our extensive proof for the vertex $(1, 1)$. For this point we get:

$$A(1 + \epsilon_1) + B(1 + \epsilon_1)^\beta = C(1 + \epsilon_2) - D(1 + \epsilon_2)^\beta \tag{3.38}$$

$$A\left(1 + \frac{\alpha_1}{\beta}\right) + B\left(1 + \frac{\alpha_1}{\beta}\right)^\beta = C\left(1 + \frac{\alpha_2}{\beta}\right) - D\left(1 + \frac{\alpha_2}{\beta}\right)^\beta$$

$$Be^{\alpha_1} + De^{\alpha_2} = C - A \qquad \text{in the limit } \beta = \infty \tag{3.39}$$

From (3.39) it can now be seen that if we take $\alpha_1 < \ln\left(\frac{C-A}{B}\right)$, we can find a real solution to (3.26) that is given by $\alpha_2 = \ln\left(\frac{C-A-Be^{\alpha_1}}{D}\right)$. Again we have that any combination of α_1, α_2 being positive/negative is possible (depending on constants $A \ldots D$), so also for this point we can approach (3.38) in any combination of directions.

For the studied example we get $\alpha_1 < \ln\left(\frac{1}{2}\right) \approx -0.7$. Choosing $\alpha_1 = -1$ we find $\alpha_2 = \ln\left(1 - 2e^{-1}\right) \approx -1.331$. Similar to table 3.2, using Matlab we can illustrate the convergence in this example for these fixed values of α_i:

Value of β	left of (3.38)	right of (3.38)
2	1	0.5572
10	1.5974	1.4941
100	1.7221	1.7115
1000	1.7344	1.7333
10000	1.7356	1.7355

Table 3.3: Illustration of the convergence of (3.39) for the described sequence of points. The values for the constants are given by $A = 1$, $B = 2$, $C = 2$, $D = 1$, $\alpha_1 = -1$, $\alpha_2 = \ln\left(1 - 2e^{-1}\right) \approx -1.331$

For the limit points $\left(-1, -\frac{A}{C}\right)$ and $\left(1, \frac{A}{C}\right)$ a similar approach as above can be pursued, however in both cases, in the limit $\beta = \infty$, this will result in the expression:

$$Be^{\alpha_1} = 0 \tag{3.40}$$

Clearly equation (3.40) is only met when $\alpha_1 = -\infty$. However, ϵ_1 was chosen to equal $\frac{\alpha_1}{\beta}$. This thus means we would now get $\epsilon_1 = \frac{-\infty}{\infty}$, which is an undefined limit.

We can however also illustrate the limiting behaviour of these points in a different way. Consider the point $\left(-1, -\frac{A}{C}\right)$, we can write:

$$A(-1 + \epsilon_1) + B(-1 + \epsilon_1)^\beta = C\left(-\frac{A}{C} + \epsilon_2\right) - D\left(-\frac{A}{C} + \epsilon_2\right)^\beta \tag{3.41}$$

At first note that in equation (3.41), for the limit $\beta \to \infty$ we can only have that $\epsilon_1 \geq 0 \wedge \epsilon_2 \geq 0$. For example, if $\epsilon_1 < 0$ and $\beta \to \infty$, the left of (3.41) goes to infinity, which cannot be balanced by the right side (this tends to '$-A + \epsilon_2 C$'). Moreover, when $\epsilon_1 > 0$, $\epsilon_2 < 0$ and $\beta \to \infty$, in the limit we get the equality '$\epsilon_1 A = \epsilon_2 C$', which cannot hold for opposite signs of ϵ_i

(since $A > 0$ and $C > 0$). It is thus only possible to approach (3.41) when $\left(U_1 \downarrow -1, \widetilde{U_2} \downarrow -\frac{A}{C} \right)$.
Let us choose $\epsilon_1 = \epsilon_2 = \epsilon > 0$. We can then rewrite (3.41) to the form:

$$B(1 - \epsilon)^\beta + D \left(\frac{A}{C} - \epsilon \right)^\beta = \epsilon(C - A) \tag{3.42}$$

Close inspection of (3.42) shows that for $0 < \epsilon < 1 + \frac{A}{C}$ and increasing β, the left of (3.42) is decreasing, while the right of (3.42) simply equals a (small) positive constant. Decreasing ϵ implies that a larger value of β is required to achieve equality in (3.42). Hereby taking a simultaneous limit $\epsilon \to 0$, $\beta \to \infty$ (along the even integers) can now produce an equality in (3.42).
In order to prove this, note that equation (3.42) consists of three terms, where for the specified ϵ the second term vanishes when $\beta \to \infty$, which follows from the fact that $C > A$ by the assumption of 2. Inspired by this observation, let us equate the first and third term, which results in a solution:

$$\beta = \frac{\ln \left(\epsilon \cdot \frac{C-A}{B} \right)}{\ln(1 - \epsilon)}. \tag{3.43}$$

Without loss of generality, let us assume $0 < \epsilon < \min \left(1, \frac{B}{C-A} \right)$, causing β in (3.43) to be defined and positive. It may be clear that β as a function of ϵ given by (3.43), is a continuous function when $\epsilon \in \left(0, \min \left(1, \frac{B}{C-A} \right) \right)$. Furthermore, this function has an asymptote at $\epsilon = 0$, as we have that $\lim_{\epsilon \downarrow 0} \frac{\ln \left(\epsilon \cdot \frac{C-A}{B} \right)}{\ln(1-\epsilon)} = \infty$.
Next, consider a sequence of points along the curve given by (3.43), for even values of β. For example, for the values of our standard example 3 this would imply a sequence of points $\{(\beta, \epsilon) \colon (2, 0.5), (4, 0.3522), (6, 0.2796), \ldots\}$. Since the second term in (3.42) vanishes for large β, this sequence can be seen to (quickly) converge to a solution of (3.42), as is also illustrated in the table below.

Value of β	left of (3.42)	right of (3.42)
2	0.5	0.5
4	0.3527	0.3522
6	0.2797	0.2796
8	0.2349	0.2349
10	0.2041	0.2041

Table 3.4: Illustration of the convergence of (3.42) for the described sequence of points $\{(\beta, \epsilon) \colon (2, 0.5), (4, 0.3522), (6, 0.2796), \ldots\}$. The values for the constants are given by $A = 1$, $B = 2$, $C = 2$, $D = 1$.

At last we may have a look at the point $\left(1, \frac{A}{C} \right)$. For this point we may write:

$$A(1 + \epsilon_1) + B(1 + \epsilon_1)^\beta = C \left(\frac{A}{C} + \epsilon_2 \right) - D \left(\frac{A}{C} + \epsilon_2 \right)^\beta \tag{3.44}$$

At first note that in equation (3.44), for the limit $\beta \to \infty$ we need that $\epsilon_1 \leq 0$, while ϵ_2 may be either positive or negative. For example, if $\epsilon_1 > 0$ the left of (3.44) will tend to infinity when $\beta \to \infty$, which cannot be balanced by the right of (3.44). Furthermore it may easily be verified that when $\epsilon_1 < 0$, there is no restriction on the sign of ϵ_2 (At least for ϵ_2 sufficiently small). We

can thus approach (3.44) when $\left(U_1 \uparrow 1, \widetilde{U_2} \downarrow \frac{A}{C}\right)$ or $\left(U_1 \uparrow 1, \widetilde{U_2} \uparrow \frac{A}{C}\right)$.

Let us choose $\epsilon_1 = -\epsilon$, $\epsilon_2 = \epsilon$, $\epsilon > 0$. We can then rewrite (3.44) to the form:

$$B(1 - \epsilon)^\beta + D\left(\frac{A}{C} + \epsilon\right)^\beta = \epsilon(A + C) \tag{3.45}$$

Inspection of (3.45) again shows that for small ϵ, i.e. $0 < \epsilon < \frac{C-A}{C}$, and increasing β, the left expression is decreasing, while the right expression simply equals a small positive constant. A proof of a simultaneous limit for $\epsilon \downarrow 0$ and $\beta \to \infty$ can be constructed completely analogous to the case we had in (3.42), as also here the second term vanishes for $\beta \to \infty$. Equating the first and third term of (3.45) gives us:

$$\beta = \frac{\ln\left(\epsilon \cdot \frac{A+C}{B}\right)}{\ln(1 - \epsilon)} \tag{3.46}$$

Let us now assume $0 < \epsilon < \min\left(1, \frac{B}{A+C}\right)$, causing β in (3.46) to be defined and positive.

Note that we again have an asymptote at $\epsilon = 0$, as we have that $\lim_{\epsilon \downarrow 0} \frac{\ln\left(\epsilon \cdot \frac{A+C}{B}\right)}{\ln(1-\epsilon)} = \infty$.

With that in mind, consider a sequence of points along the curve given by (3.46), for even values of β. For constants $A \dots D$ as in the main example, this would imply a sequence of points $\{(\beta, \epsilon): (2, 0.3139), (4, 0.2320), (6, 0.1893), \dots\}$. As the second term vanishes for $\beta \to \infty$, this sequence of points will converge to a solution of (3.45), as is illustrated in the table below.

Value of β	left of (3.45)	right of (3.45)
2	1.6039	0.9416
6	0.6751	0.5679
10	0.4404	0.4284
20	0.2806	0.2806

Table 3.5: Illustration of the convergence of (3.45) for the described sequence of points $\{(\beta, \epsilon): (2, 0.3139), (4, 0.2320), (6, 0.1893), \dots\}$. The values for the constants are given by $A = 1$, $B = 2$, $C = 2$, $D = 1$.

Note that in equation (3.45), by assuming $\epsilon_1 = -\epsilon$, $\epsilon_2 = \epsilon$, $\epsilon > 0$, implicitly the choice was made to approximate the limit while $\left(U_1 \uparrow 1, \widetilde{U_2} \downarrow \frac{A}{C}\right)$. However, it was argued that the limit can also be approximated when $\left(U_1 \uparrow 1, \widetilde{U_2} \uparrow \frac{A}{C}\right)$.

It may be verified that this can be done by, for instance, choosing $\epsilon_1 = -\epsilon$ and $\epsilon_2 = -\frac{A}{2C}\epsilon$, where $\epsilon > 0$. In this way only the (small) positive constant on the right of (3.45) would be altered to '$\frac{A}{2}\epsilon$'. The proof from there on will be completely analogous as already illustrated for (3.42) and (3.45).

Combining the results in this subsection, we have made it credible that the vertices $(U_1, \widetilde{U_2}) = (-1, 1), (1, 1), \left(-1, -\frac{A}{C}\right)$ and $\left(1, \frac{A}{C}\right)$ are a limiting solution of equation (3.17) when $\beta \to \infty$ along the even integers. Hereby feeding the hypothesis that the limiting implicit solution of (3.17) for even $\beta \to \infty$ can be visualised by a quadrilateral with vertices $(U_1, \widetilde{U_2}) = (-1, 1), (1, 1), \left(-1, -\frac{A}{C}\right)$ and $\left(1, \frac{A}{C}\right)$.

The limit lines of the quadrilateral implicit solution

In the previous subsection it is shown that the points $(U_1, \widetilde{U_2}) = (-1, 1), (1, 1), \left(-1, -\frac{A}{C}\right)$ and $\left(1, \frac{A}{C}\right)$ are a solution to (3.17) when $\beta \to \infty$ along the even integers. To show that the limiting solution is a quadrilateral with these points as its vertices, we still need to show that also the line segments $\left\{ \left(U_1, \widetilde{U_2}\right) : U_1 = -1, \widetilde{U_2} \in \left(-\frac{A}{C}, 1\right) \right\}$, $\left\{ \left(U_1, \widetilde{U_2}\right) : U_1 = 1, \widetilde{U_2} \in \left(\frac{A}{C}, 1\right) \right\}$, $\left\{ \left(U_1, \widetilde{U_2}\right) : \widetilde{U_2} = 1, U_1 \in (-1, 1) \right\}$ and $\left\{ \left(U_1, \widetilde{U_2}\right) : \widetilde{U_2} = \frac{A}{C} U_1, U_1 \in (-1, 1) \right\}$ are solutions of (3.17) when $\beta \to \infty$ along the even integers.

That this is the case can be shown rather easily. Consider for instance the first line segment listed above: $U_1 \approx -1$ with $\widetilde{U_2} \in \left(-\frac{A}{C}, 1\right)$. If we write $U_1 = -1 + \epsilon$ (where we will not restrict the sign of ϵ) we can rewrite equation (3.17) to:

$$A(-1 + \epsilon) + B(-1 + \epsilon)^\beta = C\widetilde{U_2} - D\widetilde{U_2}^\beta \qquad \Longrightarrow$$
$$B(1 - \epsilon)^\beta = A(1 - \epsilon) + C\widetilde{U_2} - D\widetilde{U_2}^\beta. \qquad (3.47)$$

Similar to the method used for (3.26) and (3.39), we may now write $\epsilon = \frac{-\alpha}{\beta}$ and obtain:

$$B\left(1 + \frac{\alpha}{\beta}\right)^\beta = A\left(1 + \frac{\alpha}{\beta}\right) + C\widetilde{U_2} - D\widetilde{U_2}^\beta \qquad \Longrightarrow$$
$$Be^\alpha = A + C\widetilde{U_2} \qquad \text{(in the limit } \beta = \infty\text{).} \qquad (3.48)$$

From equation (3.48) one can find a solution for $\alpha = \ln\left(\frac{A + C\widetilde{U_2}}{B}\right)$. Hereby note that this is well defined, since from $\widetilde{U_2} \in \left(-\frac{A}{C}, 1\right)$ it follows that $\frac{A + C\widetilde{U_2}}{B} > 0$. Furthermore it can be seen that, for any given value of $\widetilde{U_2}$, α may be both positive and negative (depending on constants $A \ldots D$). This implies that, at any given value of $\widetilde{U_2} \in \left(-\frac{A}{C}, 1\right)$, the limit of $U_1 \to -1$ may be performed from both the left and right side (again clearly depending on constants $A \ldots D$).

Exactly the same approach may be followed to show that also the line segments $\left\{ \left(U_1, \widetilde{U_2}\right) : U_1 = 1, \widetilde{U_2} \in \left(\frac{A}{C}, 1\right) \right\}$, $\left\{ \left(U_1, \widetilde{U_2}\right) : \widetilde{U_2} = 1, U_1 \in (-1, 1) \right\}$ are part of the 'limit solution curve' when $\beta \to \infty$ along the even integers.
In this way we obtain the limit solution for $U_1 \approx 1$ with $\widetilde{U_2} \in \left(\frac{A}{C}, 1\right)$:

$$Be^\alpha = C\widetilde{U_2} - A, \qquad (3.49)$$

with a solution for α given by $\alpha = \ln\left(\frac{C\widetilde{U_2} - A}{B}\right)$.

Also from the limit solution (3.49) and its solution for α, we can see that, given any $\widetilde{U_2}$, α is well defined and may both be positive and negative (for this line segment only depending on constant A). Thereby again the limit $U_1 \to 1$ may be performed from both the left and right side for any given $\widetilde{U_2} \in \left(\frac{A}{C}, 1\right)$.

Again exploring the same approach, for the case $U_1 \in (-1, 1)$, $\widetilde{U_2} \approx 1$ we can obtain the limit solution:

$$De^\alpha = C - AU_1. \qquad (3.50)$$

From (3.50) we may draw the same conclusions as we already did for (3.48) and (3.49).

At last, for the case $U_1 \in (-1, 1)$ and $\widetilde{U_2} \in \left(-\frac{A}{C}, \frac{A}{C}\right)$, it follows immediately after taking the limit $\beta \to \infty$ (along the even integers) that:

$$AU_1 = C\widetilde{U_2}, \tag{3.51}$$

from which we immediately find the proposed line segment as a limit solution curve.

It has now been shown that all line segments of the proposed limiting quadrilateral are indeed solutions of equation (3.17) when $\beta \to \infty$ along the even integers. When combined with the fact that the points $(U_1, \widetilde{U_2}) = (-1, 1), (1, 1), \left(-1, -\frac{A}{C}\right)$ and $\left(1, \frac{A}{C}\right)$ are also a limiting solutions of (3.17) when $\beta \to \infty$ along the even integers (as proven in subsection 3.2.2), we have thus made it plausible that the indeed the limiting implicit solution curve of (3.17) can be visualised by a quadrilateral with vertices $(U_1, \widetilde{U_2}) = (-1, 1), (1, 1), \left(-1, -\frac{A}{C}\right)$ and $\left(1, \frac{A}{C}\right)$.

Smaller values of even β

With the limiting behaviour studied, the question remains how the implicit solution of (3.17) and (3.18) behaves for smaller, even values of β. The smallest even value to consider is $\beta = 2$. For this value we can prove that the implicit solution curve is given by an elliptical shape. Consider for instance equation (3.17):

$$AU_1 + BU_1{}^2 = C\widetilde{U_2} - D\widetilde{U_2}{}^2$$

$$\left(\sqrt{B}U_1 + \frac{A}{2\sqrt{B}}\right)^2 - \frac{A^2}{4B} = -\left(\sqrt{D}\widetilde{U_2} + \frac{C}{2\sqrt{D}}\right)^2 + \frac{C^2}{4D}$$

$$\left(\sqrt{B}U_1 + \frac{A}{2\sqrt{B}}\right)^2 + \left(\sqrt{D}\widetilde{U_2} + \frac{C}{2\sqrt{D}}\right)^2 = \frac{A^2}{4B} + \frac{C^2}{4D} \tag{3.52}$$

Clearly an analogous result can be obtained for (3.18). By arguments of continuity we can thus conclude that the implicit solution curves of (3.17) and (3.18) converge from the elliptical shape for $\beta = 2$ to the limiting quadrilateral for even $\beta \to \infty$. In Figure 3.4, this is illustrated for the example studied.

From Figure 3.4, one may also note that for every plotted even β one will only have 2 intersection points between the plot of the implicit solution of (3.17) and (3.18).
This can be seen to be the case for each implicit solution curve with even β. Clearly $(U_1, \widetilde{U_2}) = (0, 0)$ is always a solution of equation (3.17) and (3.18). Furthermore, as $\beta > 1$, the implicit solution curves near $(0, 0)$ are 'dominated' by the lines $\widetilde{U_2} = \frac{A}{C}U_1$ (in (3.17)) and $\widetilde{U_2} = \frac{C}{A}U_1$ (in (3.18)). Because of this, the implicit solution curve for (3.17) and (3.18) must move away from each other when $(U_1, \widetilde{U_2}) \in ([0, \epsilon), [0, \epsilon))$. However, as discussed earlier, the implicit solution curves for even β are all part of a closed loop shape, and due to this loop it can be graphically verified that the implicit solution curves for (3.17) and (3.18) must reach one additional intersection.
In the case of the limit quadrilateral that has been extensively discussed in the previous sections the extra intersection may be clear, and will occur at the point $(U_1, \widetilde{U_2}) = (1, 1)$. Furthermore, in the case of $\beta = 2$ we obtain an elliptic shape and the extra intersection can be found at $(U_1, \widetilde{U_2}) = (\frac{1}{3}, \frac{1}{3})$. At last, we also see that when β is further increased, the extra intersection still occurs on the subspace $U_1 = \widetilde{U_2}$ and occurs closer to the limit point $(U_1, \widetilde{U_2})(1, 1)$.

Therefore, for positive β we can conclude that there will only be two real equilibrium points. As we already showed in subsection 3.1.2, two equilibrium solutions can be found using the
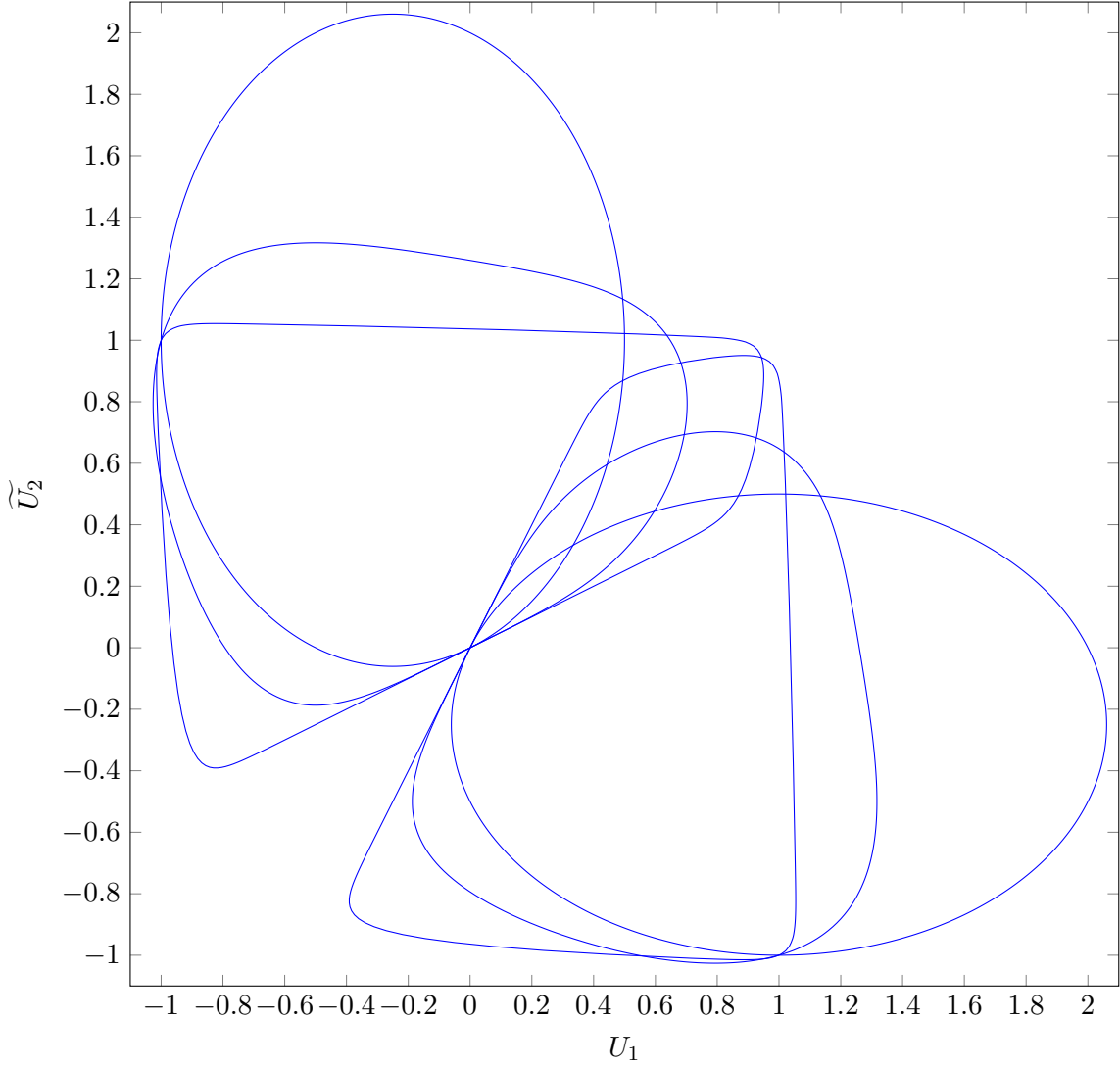
Figure 3.4: A plot of the implicit solutions of (3.17) and (3.18) for $\beta = 2$, $\beta = 4$ and $\beta = 20$.

assumption $U_1(t) = -U_2(t)$. Therefore we have must have that the intersections of the implicit plots are given at the points: $(U_1{}^*, U_2{}^*) = (0, 0)$ and $(U_1{}^*, U_2{}^*) = \left(\left(\frac{C-A}{B+D} \right)^{\frac{1}{\beta - 1}}, -\left(\frac{C-A}{B+D} \right)^{\frac{1}{\beta - 1}} \right)$.

Behaviour for odd β

When we assume β to be odd instead of even, the implicit solutions will become a bit different. Again, since we have that $\beta > 1$, the terms '$BU_1{}^\beta$' and '$D\widetilde{U_2}{}^\beta$' will dominate the implicit solutions of equation (3.17) and (3.18) in the case that $|U_1| > 1$ and/or $|\widetilde{U_2}| > 1$. Different however is that for odd β also an unbounded solution $(B^{\frac{1}{\beta}}U_1)^\beta = -(D^{\frac{1}{\beta}}\widetilde{U_2})^\beta$ can be seen to exist when $|U_1| > 1$ and $|\widetilde{U_2}| > 1$.

For instance, considering the same example as before, we get the following implicit solutions for $\beta = 3$ and $\beta = 21$:

From Figure 3.5, one can again see similar limiting and initial behaviour as we had for the

Implicit plot for odd β
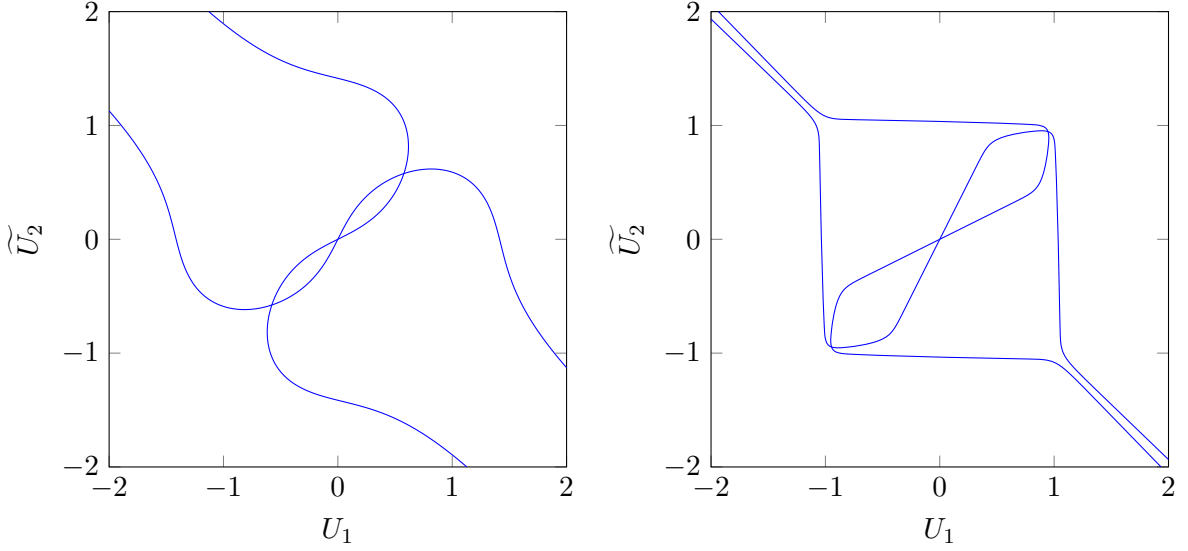
Figure 3.5: A combined implicit plot of equation (3.17) and (3.18). Left: $\beta = 3$, Right: $\beta = 21$. To indicate the distinction between (3.17) and (3.18) in the two figures, in the left figure the solution curve from (3.17) can be traced 'entering' the figure at $(U_1, \widetilde{U_2}) \approx (-1, 2)$ and 'leaving' the figure at $(U_1, \widetilde{U_2}) \approx (1, -2)$.

case where β was even. The behaviour around $(0,0)$ is only different due to the odd power (similar to the difference between the functions $y = x^2$ and $y = x^3$ around $x = 0$). We can for instance still observe the same limiting points of the quadrilateral, with the addition of an extra limiting point $(-1, -1)$ and $(1, -1)$ which are caused by the odd power. That these limiting points are indeed the case may be verified in an analogous fashion as pursued in subsection 3.2.2.

For example, for the points $(-1, -1)$, $(-1, 1)$, $(1, -1)$ and $(1, 1)$ one can take $\epsilon_1 = \pm\frac{\alpha_1}{\beta}$, $\epsilon_2 = \pm\frac{\alpha_2}{\beta}$ (compare this to (3.26) and (3.39)). Moreover for the points $\left(-1, -\frac{A}{C}\right)$ and $\left(1, \frac{A}{C}\right)$ one can use the same approach as used to solve equations (3.42) and (3.45).

To recapitulate this last point, when writing out equation (3.17), it becomes apparent that the term which includes constant 'D' vanishes for $\beta \to \infty$ and may therefore be temporally omitted. With a proper choice for ϵ_1 and ϵ_2 as a function of $\epsilon > 0$, it is possible to solve the reduced equation, leading to solutions similar to (3.43) and (3.46).

$((\epsilon_1, \epsilon_2) = (\epsilon, -\epsilon)$ or $(\epsilon_1, \epsilon_2) = (\epsilon, \frac{A}{2C}\epsilon)$ with $\epsilon > 0$ will do for the point $\left(-1, -\frac{A}{C}\right)$. Likewise $(\epsilon_1, \epsilon_2) = (-\epsilon, \epsilon)$ or $(\epsilon_1, \epsilon_2) = (-\epsilon, \frac{A}{2C}\epsilon)$ with $\epsilon > 0$ will do for the point $\left(1, \frac{A}{C}\right)$).

For both solutions of β one may then verify that $\lim_{\epsilon \downarrow 0} \beta(\epsilon) = \infty$. As β can become arbitrarily large, choosing values of ϵ and β along this curve will then justify the omittance of the vanishing term.

At last, for the case that $\beta \to \infty$ along the odd integers, one can show that the line segments $\left\{ \left(U_1, \widetilde{U_2}\right) : \widetilde{U_2} = -U_1, U_1 < -1, \widetilde{U_2} > 1 \right\}$, $\left\{ \left(U_1, \widetilde{U_2}\right) : \widetilde{U_2} = 1, U_1 \in (-1, 1) \right\}$, $\left\{ \left(U_1, \widetilde{U_2}\right) : U_1 = 1, \widetilde{U_2} \in \left(\frac{A}{C}, 1\right) \right\}$, $\left\{ \left(U_1, \widetilde{U_2}\right) : \widetilde{U_2} = \frac{A}{C}U_1, U_1 \in (-1, 1) \right\}$, $\left\{ \left(U_1, \widetilde{U_2}\right) : U_1 = -1, \widetilde{U_2} \in \left(-1, -\frac{A}{C}\right) \right\}$, $\left\{ \left(U_1, \widetilde{U_2}\right) : \widetilde{U_2} = -1, U_1 \in (-1, 1) \right\}$ and at last

$\left\{ \left(U_1, \widetilde{U_2} \right) : \widetilde{U_2} = -U_1, U_1 > 1, \widetilde{U_2} < 1 \right\}$ are limiting solutions to equation (3.17). A point that can also be seen to be highly plausible from the right sub-figure in Figure 3.5. For an outline of a way to prove that these lines are indeed limit implicit solution curves of (3.17), one may consult subsection 3.2.2.

Comparing the odd β case to the even β case, it is important to note that the implicit solution curves now do not have the same closed loop shape in the figures, which is caused by the fact that when $|U_1| > 1$ and $|\widetilde{U_2}| > 1$, the limiting implicit solutions will tend to the lines $\widetilde{U_2} = - \left(\frac{B}{D} \right)^{\frac{1}{\beta}} U_1$ and $\widetilde{U_2} = - \left(\frac{D}{B} \right)^{\frac{1}{\beta}} U_1$. Note hereby that for $\beta \to \infty$ along the odd integers, both these unbounded 'implicit line solutions' tend to $\widetilde{U_2} = -U_1$.

In the example shown by Figure 3.5 it may be observed that this difference of solutions tending to $\widetilde{U_2} = - \left(\frac{B}{D} \right)^{\frac{1}{\beta}} U_1$ and $\widetilde{U_2} = - \left(\frac{D}{B} \right)^{\frac{1}{\beta}} U_1$ did not initiate extra intersections of the implicit solution curves. This is especially interesting in the right of Figure 3.5, as the implicit solution curves get really close to each other near the points $(-1, 1)$ and $(1, -1)$ (which is not strange as these are limiting solutions for $\beta \to \infty$), and are then seen to diverge from each other when the solution curves tend to the lines $\widetilde{U_2} = - \left(\frac{B}{D} \right)^{\frac{1}{\beta}} U_1$ and $\widetilde{U_2} = - \left(\frac{D}{B} \right)^{\frac{1}{\beta}} U_1$.

That this was not a coincidence for $\beta = 3$ and $\beta = 21$ can be shown to be the result of the constraint $B - D \geq 0$. This can be illustrated nicely by interchanging the value of B and D in the example, as is done in Figure 3.6. By doing so, the limiting solution lines will be the same, but they now correspond to the opposite equation (so where in the example the line $\widetilde{U_2} = - \left(\frac{B}{D} \right)^{\frac{1}{\beta}} U_1$ was a limiting solution of equation (3.17), for swapped B and D it is a limiting solution to equation (3.18)).

The additional intersections between the implicit solution curves that are observed in Figure 3.6 are the result of the transition of the region $|U_1| < 1$ and $|\widetilde{U_2}| < 1$, to the the region $|U_1| > 1$ and/or $|\widetilde{U_2}| > 1$. Because $\beta > 1$, in the first region the linear terms dominate the behaviour for equations (3.17) and (3.18), while for the second region the non-linear terms dominate the behaviour. When $B - D < 0$ this transition can be seen to introduce two extra intersections. When $B - D = 0$ one may verify that only in the limit $|U_1| \to \infty$ and $|\widetilde{U_2}| \to \infty$ there is an additional equality between both implicit solution curves.

Under the assumptions from 2 with $\beta > 1$ we can tell from the from the implicit plots of that for odd β there are 3 equilibrium points, all on the $(U_1, \widetilde{U_2})$ plane. That we now find three equilibrium points instead of two can be explained from the fact that each target starts of with either a positive or a negative charge. In the modelling phase we simply assumed that the left target becomes positive, so that we have $U_1 \geq 0$. Clearly this choice can also be reversed, which would lead to the symmetrical equilibrium point in the third quadrant.

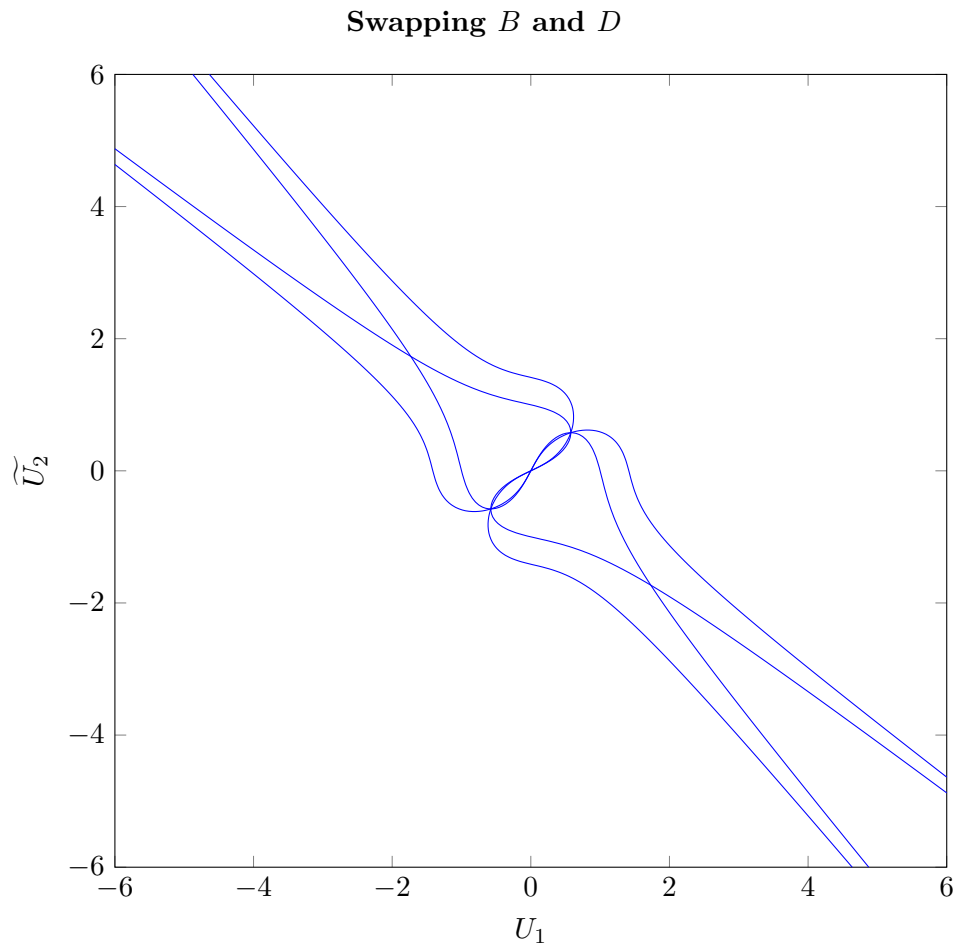Figure 3.6: A combined implicit plot of equation (3.17) and (3.18) where $\beta = 3$. The solution curve for the initially chosen coefficients compared to swapped coefficients B and D.

3.3 Input-Output approach

In this section we investigate whether the Kelvin's water dropper system can be interpreted as an input-output system. Inspired on the external voltage source that is used in the single jet system of [17], we will at first analyze Kelvin's water dropper where consider the induction ring voltage as an input.

3.3.1 Induction ring voltage as input

In this section we shall consider the extended Kelvin system with current losses, however we will now consider the induction ring voltages $U_{R_{g_i}}$, $i = 1, 2$ as an input instead of an autonomous system. Thereby will again use the modelling laws from table 3.1 to derive the differential equation that describes the systems behaviour. Similar to section 3.1.1 we thereby need to eliminate the latent variables, but different from that section we now do not need to write the latent variables solely in terms of the 'state' U_i, but also in terms of the considered 'input' $U_{R_{g_i}}$. From the modelling laws from table 3.1 we can now obtain:

$$I_{16} = \frac{U_{R_{L_1}}}{R_{L_1}} \qquad\qquad I_{26} = -\frac{U_{R_{L_2}}}{R_{L_2}}$$

$$I_{16} = \frac{U_1 - U_{R_{g_1}}}{R_{L_1}} \qquad\qquad I_{26} = -\frac{U_2 - U_{R_{g_2}}}{R_{L_2}} \tag{3.53}$$

$$I_{11} = -n_1 C_{ind_1} U_{R_{g_2}} \qquad\qquad I_{21} = n_2 C_{ind_2} U_{R_{g_1}} \tag{3.54}$$

$$I_{15} = I_{11} - I_{14} \qquad\qquad I_{25} = I_{21} - I_{24}$$

$$I_{15} = I_{11} - I_{13} - I_{16} \qquad\qquad I_{25} = I_{21} - I_{23} - I_{26}. \tag{3.55}$$

Combining the equations (3.53), (3.54) and (3.55) with the capacitor law (see table 3.1) and by defining new, more elaborate current loss assumptions $I_{13} := f_1(U_1, U_{R_{g_2}})$, $I_{23} := f_2(U_2, U_{R_{g_1}})$ we can obtain:

$$C_{L_1} \frac{dU_1}{dt} = -\frac{U_1}{R_{L_1}} - n_1 C_{ind_1} U_{R_{g_2}} + \frac{U_{R_{g_1}}}{R_{L_1}} - f_1(U_1, U_{R_{g_2}}) \tag{3.56}$$

$$C_{L_2} \frac{dU_2}{dt} = -\frac{U_2}{R_{L_2}} - n_2 C_{ind_2} U_{R_{g_1}} + \frac{U_{R_{g_2}}}{R_{L_2}} + f_2(U_2, U_{R_{g_1}}) \tag{3.57}$$

Please note that, by assumption, the left jetting system induced positive current, while the right jetting system induces negative current. A consequence of this is that the voltage drop from target to earth is positive for the left system, where for the right system this is negative. (See also the '+' and '-' signs in Figure 2.1b).
Because of this model assumption we have that U_1, $U_{R_{L_1}}$ and $U_{R_{g_1}}$ are all positive (by assumption), where U_2, $U_{R_{L_2}}$ and $U_{R_{g_2}}$ are all negative. With this in mind it can again be verified from equations (3.56) and (3.57), that for a symmetrical system (i.e. $U_1 = -U_2$, $U_{R_{L_1}} = -U_{R_{L_2}}$, $U_{R_{g_1}} = -U_{R_{g_2}}$, $R_{L_1} = -R_{L_2}$ and $C_{L_1} = C_{L_2}$) the above two differential equation again reveal a symmetrical relationship in the differential equation, i.e. it then directly follows that $\frac{dU_1}{dt} = -\frac{dU_2}{dt}$.

We can see that equations (3.56) and (3.57) form a non-linear system equation. To determine controllability of the system it is therefore not just possible to use the full rank condition

on the regular, controllability matrix. This issue might be overcome by using non-linear control theory, which involves the use of Lie brackets ([8]).

A simple alternative approach is to neglect the current loss terms. As current losses are assumed to increase with the voltage of the induction rings and targets, this may be justified when these voltages remain small. An advantage of neglecting the current losses, is that we can then rewrite equation (3.56) and (3.57) to:

$$
\begin{bmatrix} \dot{U}_1 \\ \dot{U}_2 \end{bmatrix} = \begin{bmatrix} -\frac{1}{C_{L_1}R_{L_1}} & 0 \\ 0 & -\frac{1}{C_{L_2}R_{L_2}} \end{bmatrix} \begin{bmatrix} U_1 \\ U_2 \end{bmatrix} + \begin{bmatrix} \frac{1}{C_{L_1}R_{L_1}} & -\frac{n_1 C_{ind_1}}{C_{L_1}} \\ -\frac{n_2 C_{ind_2}}{C_{L_2}} & \frac{1}{C_{L_2}R_{L_2}} \end{bmatrix} \begin{bmatrix} U_{R_{g_1}} \\ U_{R_{g_2}} \end{bmatrix}.
\tag{3.58}
$$

In equation (3.58) we can recognize a linear input/state space model of the form $\dot{x} = Ax + Bu$. Using this notation, controllability can be verified from the condition $rank([B \mid AB]) = 2$. If we again consider a symmetric system, where we furthermore introduce the notation $a = \frac{1}{R_{L_i}C_{L_i}}$, $b = \frac{n_i C_{ind_i}}{C_{L_i}}$, it is easy to check that the system in not controllable in the case that $a = b$, while otherwise being controllable.

Although we find that the system is not always controllable, we do have that the matrix A is Hurwitz, which in term also guarantees BIBO stability of this input/state space model ([3]). Furthermore for a linear input/state space model it is known that each solution is of the form:

$$
x(t) = e^{At}x(0) + \int_0^t e^{A(t-\tau)}Bu(\tau)\,d\tau.
\tag{3.59}
$$

As we have that matrix A is a diagonal matrix, its matrix exponential is straightforward to compute. For the given case, it is therefore relatively easy to expand equation (3.59) and we obtain:

$$
\begin{aligned}
\begin{bmatrix} U_1(t) \\ U_2(t) \end{bmatrix} &= \begin{bmatrix} e^{-at} & 0 \\ 0 & e^{-at} \end{bmatrix} \begin{bmatrix} U_1(0) \\ U_2(0) \end{bmatrix} + \int_0^t \left(\begin{bmatrix} e^{-a(t-\tau)} & 0 \\ 0 & e^{-a(t-\tau)} \end{bmatrix} \begin{bmatrix} a & -b \\ -b & a \end{bmatrix} \begin{bmatrix} U_{R_{g_1}}(\tau) \\ U_{R_{g_2}}(\tau) \end{bmatrix} \right) d\tau \\
&= e^{-at}\begin{bmatrix} U_1(0) \\ U_2(0) \end{bmatrix} + \int_0^t \left(e^{-a(t-\tau)} \begin{bmatrix} aU_{R_{g_1}}(\tau) - bU_{R_{g_2}}(\tau) \\ -bU_{R_{g_1}}(\tau) + aU_{R_{g_2}}(\tau) \end{bmatrix} \right) d\tau
\end{aligned}
\tag{3.60}
$$

When one would consider a symmetrical input (i.e. $U_{R_{g_1}} = -U_{R_{g_2}}$), equation (3.60) can be simplified further, and can be written as:

$$
\begin{bmatrix} U_1(t) \\ U_2(t) \end{bmatrix} = e^{-at}\begin{bmatrix} U_1(0) \\ U_2(0) \end{bmatrix} + (a+b)e^{-at}\int_0^t \left(\begin{bmatrix} e^{a\tau}U_{R_{g_1}}(\tau) \\ -e^{a\tau}U_{R_{g_1}}(\tau) \end{bmatrix} \right) d\tau
\tag{3.61}
$$

Let us for the moment assume that the input is chosen symmetrical, and set to a constant voltage. Doing so, we can explicitly calculate the integral in (3.61), and obtain:

$$
\begin{bmatrix} U_1(t) \\ U_2(t) \end{bmatrix} = e^{-at}\begin{bmatrix} U_1(0) \\ U_2(0) \end{bmatrix} + \frac{a+b}{a}U_{R_{g_1}}(1 - e^{-at})\begin{bmatrix} 1 \\ -1 \end{bmatrix}
\tag{3.62}
$$

In the above example we can see that when $t \to \infty$, an equilibrium point is reached, which is equal to $U_1 = \frac{a+b}{a}U_{R_{g_1}}$, $U_2 = -\frac{a+b}{a}U_{R_{g_1}}$. This is also in accordance with the equilibrium that can be found from state space equation:

$$
\begin{aligned}
&Ax + Bu = 0 &&\Longleftrightarrow \\
&\begin{bmatrix} -aU_1 \\ -aU_2 \end{bmatrix} = \begin{bmatrix} -(a+b)U_{R_{g_1}} \\ (a+b)U_{R_{g_1}} \end{bmatrix}.
\end{aligned}
$$

Furthermore, when we consider a completely symmetric system $U_2(t) = -U_1(t)$ as also studied in previous sections, we can restrict our view to:

$$\dot{U}_1 = -aU_1 + (a+b)U_{R_{g_1}}. \tag{3.63}$$

In (3.63), the $\dot{x} = Ax + Bu$ structure is still evident. For this (one dimensional) setup the controllability condition becomes $rank([B]) = rank([a+b]) = 1$, which again does imply controllability.

Output power in terms of induction ring voltage

To determine the optimal (constant) voltage on the induction rings one will seek to maximize the output power of the system. Under the assumption that current losses may be omitted (i.e. $I_{i3} = 0$, $i = 1, 2$), one can see from Figure 3.1 that we then have $I_{12} = I_{14} = I_{16}$.
We next investigate the output power in the equilibrium solution $U_1 = \frac{a+b}{a}U_{R_{g_1}}$ in the case of a symmetrical system (i.e. when $U_1 = -U_2$, $U_{R_{g_1}} = -U_{R_{g_2}}$). Using the equations (3.53)-(3.55) we find that in the equilibrium solution the output power is equal to:

$$\begin{aligned} P_{out} &= I_{16}U_1 + I_{26} \cdot -U_2 &\Longleftrightarrow \\ &= 2(1 + R_L n C_{ind})n C_{ind}U_{R_{g_1}}{}^2 \end{aligned} \tag{3.64}$$

From equation (3.64) we observe that the output power increases quadratically with the voltage over the induction rings. Therefore for maximal energy conversion it seems as if one would need a high voltage over the induction rings as an input. However, in the beginning of this chapter it was assumed that current losses could only be omitted when the voltage over the induction rings remains small. When current losses do occur, they will have a double negative effect on the energy conversion efficiency. Therefore it is likely that optimal energy conversion is reached when the voltage over the induction rings is as high as possible, while being just below the point that current losses become significant.
Furthermore, we also see that the output power from (3.64) seems to be dependent on the connected load resistance R_L.

Next, we will investigate the equilibrium output power equations in the case that current losses are not omitted. From the differential equations of (3.56) and (3.57) we find that the target voltages reach an equilibrium that is given by:

$$\widehat{U_1} = U_{R_{g_1}} - R_{L_1}\left(n_1 C_{ind_1}U_{R_{g_2}} + f_1\left(\widehat{U_1}, U_{R_{g_2}}\right)\right) \tag{3.65}$$

$$\widehat{U_2} = U_{R_{g_2}} - R_{L_2}\left(n_2 C_{ind_2}U_{R_{g_1}} - f_2\left(\widehat{U_2}, U_{R_{g_1}}\right)\right). \tag{3.66}$$

Again we note that in the symmetric case we have that $\widehat{U_1} = -\widehat{U_2}$.
From (3.65) and (3.66), we can calculate the analogon of (3.64), where current losses are included. Upon combining the relations from (3.53)-(3.55) with the above two equilibrium solutions, we find that in the equilibrium solution, the output power for a symmetrical setup with current losses is given by

$$\begin{aligned} P_{out} &= I_{16}U_{R_{L_1}} + I_{12}U_{R_{g_1}} + I_{26} \cdot -U_{R_{L_2}} + I_{22} \cdot -U_{R_{g_2}} \\ &= 2\left(nC_{ind}U_{R_{g_1}} - f\left(\widehat{U_1}, U_{R_{g_1}}\right)\right)^2 R_L + 2\left(nC_{ind}U_{R_{g_1}} - 2f\left(\widehat{U_1}, U_{R_{g_1}}\right)\right)U_{R_{g_1}} \end{aligned} \tag{3.67}$$

Again it seems beneficial to use a large load resistor R_L in the setup, as in the above equation there is a linear term in R_L.

To explain that this is not necessarily the case, one needs to keep in mind that the equilibrium solution for U_1 is altered when a resistor R_L is connected (see also (3.65)). From equation (3.65), for fixed values values of the induction ring voltages, we expect that initially the target voltage will increase when larger values of R_L are used. This can also be explained from a physical point of view. In Figure 2.1b, we can see that larger values of R_L, imply that the targets become better insulated, allowing them to reach higher saturated target voltages. However, this increase of target voltage will eventually be put to a stop, due to the current losses that are assumed to increase super-linearly with these target voltages. This saturation of target voltages for larger load resistors can also be observed in the experiments of the single jet system (see also Figure 2c in [17]).

Furthermore, when the target voltages can become larger, it will take longer to reach the equilibrium state (as more droplets will need to be collected to reach the increased target voltage). Therefore, even if the connection of load resistors causes the output power to be larger in the steady state, whether these (extra) resistors are truly beneficial in the system is still dependent on the available time window in which the downstream currents can be harvested. I.e. one needs to keep in mind that the pressurized reservoirs only contain a limited amount of (salty) aqueous solution.

Because of the additional time needed to reach the equilibrium solution of the system, combined with the additional current losses that likely occur for large values of the load resistors, the question remains whether the 'additional' resistors R_L in the system are truly beneficial.

Summary of the output power equations

Summarizing our results, in any case we have that the output power of the ballistic Kelvin's setup equals:

$$P_{out} = \begin{cases} I_{12}U_{R_{g_1}} + I_{22} \cdot -U_{R_{g_2}} & \text{if } R_L = 0 \\ I_{16}U_{R_{L_1}} + I_{12}U_{R_{g_1}} + I_{26} \cdot -U_{R_{L_2}} + I_{22} \cdot -U_{R_{g_2}} & \text{if } R_L \neq 0. \end{cases} \tag{3.68}$$

In the equilibrium solution of a symmetrical setup we have:

$$P_{out} = \begin{cases} 2\left(nC_{ind}U_{R_{g_1}} - 2f\left(U_{R_{g_1}}\right)\right)U_{R_{g_1}} & \text{if } R_L = 0 \\ 2\left(nC_{ind}U_{R_{g_1}} - f\left(\widehat{U_1}, U_{R_{g_1}}\right)\right)^2 R_L + \\ 2\left(nC_{ind}U_{R_{g_1}} - 2f\left(\widehat{U_1}, U_{R_{g_1}}\right)\right)U_{R_{g_1}} & \text{if } R_L \neq 0. \end{cases} \tag{3.69}$$

Note that when $R_L = 0$ we have that $U_1 = U_{R_{g_1}}$, while when $R_L \neq 0$ we reach an equilibrium solution for the target voltage $\widehat{U_1}$ that is implicitly described as a function of $U_{R_{g_1}}$ by equation (3.65).

When current losses are omitted, equation (3.69) may be greatly simplified, and equals:

$$P_{out} = \begin{cases} 2nC_{ind}U_{R_{g_1}}{}^2 & \text{if } R_L = 0 \\ 2(1 + R_L nC_{ind})nC_{ind}U_{R_{g_1}}{}^2 & \text{if } R_L \neq 0. \end{cases} \tag{3.70}$$

3.3.2 Resistors as input

Let us return to the main result obtained in section 2.2.2. Here we concluded that in the absence of current losses the systems behaviour can be described by the following differential equation:

$$\dot{U} = \bar{A}U$$

$$\left[\begin{array}{c} \dot{U}_1 \\ \dot{U}_2 \end{array} \right] = \left[\begin{array}{cc} -A & -C \\ -C & -A \end{array} \right] \left[\begin{array}{c} U_1 \\ U_2 \end{array} \right]$$

$$= \left[\begin{array}{cc} -\frac{1}{C_L(R_L+R_g)} & -\frac{nC_{ind}R_g}{C_L(R_L+R_g)} \\ -\frac{nC_{ind}R_g}{C_L(R_L+R_g)} & -\frac{1}{C_L(R_L+R_g)} \end{array} \right] \left[\begin{array}{c} U_1 \\ U_2 \end{array} \right], \tag{3.71}$$

where U_1 and U_2 are the target voltages. One may note that the constants 'a' and 'b' from section 2.2 have been replaced by 'A' and 'C'. This was done to match the definition of (3.2).

As deduced in section 2.2, the solutions to (3.71) are given by:

$$\left[\begin{array}{c} U_1(t) \\ U_2(t) \end{array} \right] = \left[\begin{array}{c} c_1 e^{\lambda_1 t} + c_2 e^{\lambda_2 t} \\ c_1 e^{\lambda_1 t} - c_2 e^{\lambda_2 t} \end{array} \right], \tag{3.72}$$

where c_1 and c_2 are constants depending on the initial conditions x_0. Moreover λ_1 and λ_2 are the eigenvalues of the system matrix $\bar{A}$. They are given by:

$$\lambda_{1,2} = \mp C - A = \frac{\mp nC_{ind}R_g - 1}{C_L(R_L + R_g)}. \tag{3.73}$$

One thing to note is that in (3.72) the term '$c_1 e^{\lambda_1 t}$' vanishes as $t \to \infty$, since we have that $\lambda_1 < 0$. Furthermore, since we also have that $\lambda_2 > \lambda_1$, for large t the solutions will behave like

$$\left[\begin{array}{c} U_1(t) \\ U_2(t) \end{array} \right] = \left[\begin{array}{c} c_2 e^{\lambda_2 t} \\ -c_2 e^{\lambda_2 t} \end{array} \right]. \tag{3.74}$$

Note that this is exactly the solution that is found when perfectly symmetrical initial conditions are assumed (see (2.4)).

By inspection of the eigenvalues we can also make an important observation on the systems behaviour. Depending on the magnitude of R_g, we end up with either an unstable system in which droplets are overcharged, or a stable system in which no charges are accumulated. That is, we can find for λ_2:

$$\begin{cases} \lambda_2 < 0 & \text{if } R_g < \frac{1}{nC_{ind}} \\ \lambda_2 = 0 & \text{if } R_g = \frac{1}{nC_{ind}} \\ \lambda_2 > 0 & \text{if } R_g > \frac{1}{nC_{ind}} \end{cases} \tag{3.75}$$

Now clearly the differential equation in (3.71) is not completely accurate, as the stabilizing effect of droplet loss has not been incorporated in the model. However, from a physical point of view these losses will cause the systems efficiency to deteriorate. That this is indeed the case can for instance be observed from the results of the single jet system of [17], as is shown in Figure 3.7.

Note that in the left of Figure 3.7 I_1 indicates the upstream current and I_2 indicates the downstream current. The difference between these two currents is therefore equal to the total
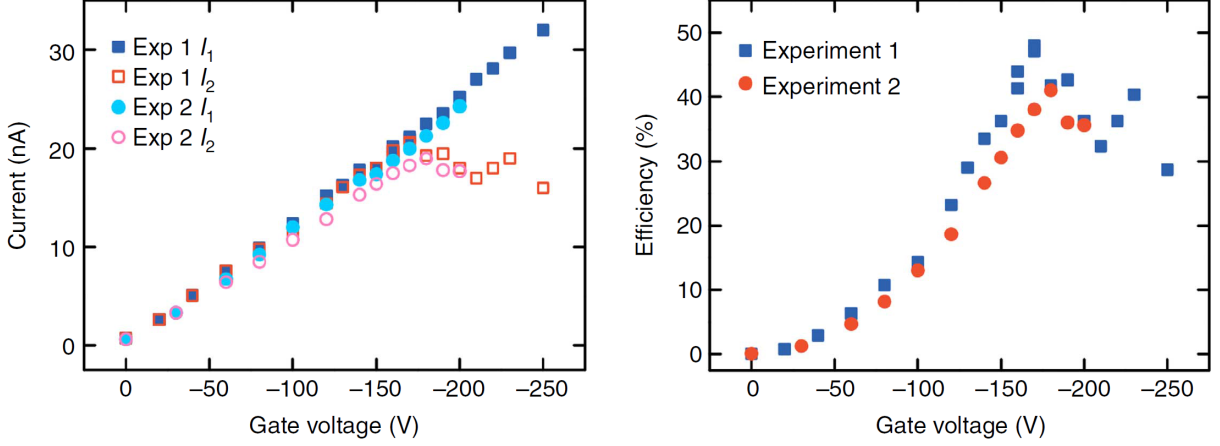
Figure 3.7: Left: induced currents using an external voltage source, Right: Efficiency as a function of the applied voltage. Applied pressure 1.38 bar, average flow rate 6.55 μls^{-1}, pore 30 μm, 10 mM KCl solution, target distance 2.5 cm (experiment 1) and 2.0 cm (experiment 2).

current loss. That is, the amount of droplets that are reflected to the induction rings (I_3) and also the droplets that are lost to the environment (I_{loss}, see also Figure 2.3).

From the comparison between the left and the right of Figure 3.7 we can see that maximal efficiency takes place at/just before the point that current losses become significant. This also matches an earlier statement of [17] that typically about 20% of the droplet charge is lost at maximal efficiency.

As our goal is to maximize the systems efficiency it may thereby be justified to study the system (3.71) with solution (3.72). To ensure that current losses are negligible, so that studying the systems differential equation of (3.71) is justified, we pose restrictions on the target voltages, i.e. $|U_i| \leq U_{max_{target}}$, and on the induction ring voltage, i.e. $|U_{R_{g_i}}| \leq U_{max_{ring}}$. This because we expect that these voltages, especially the latter induction voltage, have a profound effect on the current losses.

Inspired by the observation that the systems charging behaviour is directly related to the gate resistance (see (3.75)), we consider variable resistors as a control input. In this way we may for instance steer the system to an optimal controlled equilibrium point.

From the solution of the system (3.72) and its eigenvalues (3.73), we may conclude that the fastest way to charge the system is to initially choose the gate resistance R_g as high as possible, while simultaneously taking R_L to be as small as possible. Next we likely want to stop the charging process when an optimal controlled equilibrium solution is reached by choosing $R_g = \frac{1}{nC_{ind}}$. From the output power equation of (3.70) it seems however that for an optimal equilibrium point we would like to have R_L to be as high as possible. We would thus initially want to have that $R_g \gg 1 \wedge R_L = 0$, while in a controlled equilibrium we would like $R_g = \frac{1}{nC_{ind}} \wedge R_L \gg 1$. To achieve this one might picture a setup that uses a somewhat classical, variable 'coiled resistor', as the controlling component in an experimental setup. In this way, if the resistance is gradually reduced as the system charges, it seems as if a good trade off between a high charging resistance and a high insulation may be achieved.

A last nice observation is that the intuitive control action described above does not imply the use of a wild 'bang-bang controller', since the restriction $|U_{R_{g_i}}| \leq U_{max_{ring}}$ implies a bound on R_g as the system charges (see also Figure 3.8).

Upon inspection of the measurements shown in Figure 3.7, let us assume that the induction constant of our system is given by $nC_{ind} = 0.12$ nA/V. With this assumption we would have a critical resistance of approximately 8.33 GΩ. Furthermore, let us assume that $R_{max_{gate}} = 200$ GΩ (for illustrative purposes) and that $U_{max_{ring}} = 170$ V (as we also found in Figure 3.7). An intuitive optimal controller for R_g will then have the following R-I curve.
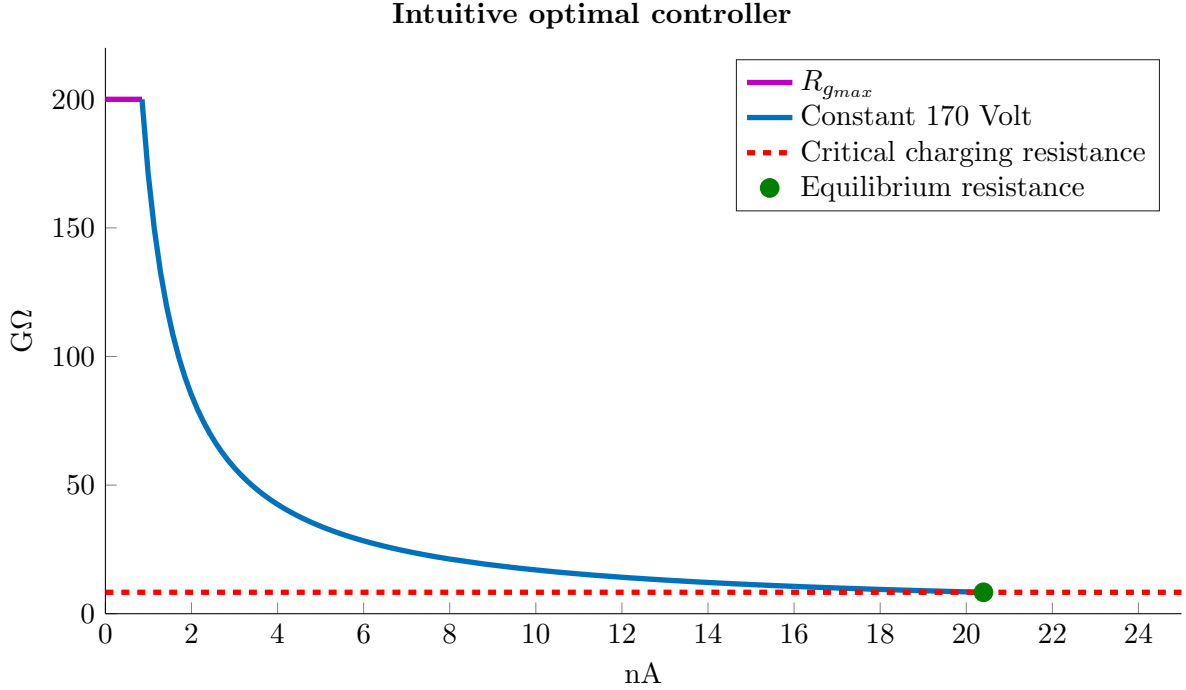
Figure 3.8: Resistance-Current curve for our intuitive optimal R_g controller.

In Figure 3.8 we can see that initially the restriction $R_{max_{gate}}$ is dominant, which is taken over by the restriction $U_{max_{ring}}$ when the induced current grows.

Of course we would also like to investigate how this intuitive optimal controller relates to optimal control theory. Thereby we consider the following cost function:

$$\min_{R_L, R_g} \int_0^T -P_{electric}(t) \ dt, \tag{3.76}$$

where the minus is used to turn our maximization problem into a minimization problem, in order to match the notation of optimization theorems in [12].

Using the notation of the electrical circuit from Figure 3.1, we find that the electrical output power $P_{electric}(t)$ is equal to:

$$
\begin{aligned}
P_{electric}(t) &= U_{R_{L_1}}(t)I_{16}(t) + U_{R_{g_1}}(t)I_{12}(t) + U_{R_{L_2}}(t)I_{26}(t) + U_{R_{g_2}}(t)I_{22}(t) \\
&= I_{16}{}^2(t)R_{L_1} + I_{12}{}^2(t)R_{g_1} + I_{26}{}^2(t)R_{L_2} + I_{22}{}^2(t)R_{g_2} \\
&= 2\left[I_{16}{}^2(t)R_L + I_{12}{}^2(t)R_g\right] \tag{3.77} \\
&= 2\left(R_L + R_g\right)I_{12}{}^2(t). \tag{3.78}
\end{aligned}
$$

Note that in the above equation the equality of (3.77) is due to symmetry, as it may be verified that in a perfect symmetrical setup we have $I_{12} = I_{22}$, $I_{16} = I_{26}$, etc. On the other hand,

equation (3.78) only holds in the absence of current losses, since we then have that $I_{16} = I_{12}$.

It may also be verified that without current losses we have that:

$$I_{12}(t) = \frac{1}{R_L + R_g} U_1(t),$$

so that equation (3.78) can be continued to:

$$P_{electric}(t) = 2(R_L + R_g)\left[\frac{1}{R_L + R_g}U_1(t)\right]^2$$
$$= 2\frac{1}{R_L + R_g}U_1{}^2(t). \tag{3.79}$$

The comparison between output power equations (3.79) and (3.70) shows that both equations contain a quadratic voltage term. The difference being that in the above equation the quadratic relation is given in the target voltage instead of the gate voltage. In particular, (3.79) seems to hint to the need of good target isolation, allowing U_1 to remain large.

There are however some restrictions so that current losses cannot occur. These restrictions are given by:

$$\frac{R_g}{R_L + R_g}U_1(t) \leq U_{max_{ring}}$$
$$U_1(t) \leq U_{max_{target}}.$$

Furthermore, the resistors are assumed to be of finite capacity. Combining the above information brings us to the following optimization goal:

$$\max_{R_L,R_g} \int_0^T \frac{1}{R_L(t) + R_g(t)} U_1{}^2(t)\ dt \tag{3.80}$$

$$\text{subject to:} \quad \frac{R_g(t)}{R_L(t) + R_g(t)}U_1(t) \leq U_{max_{ring}} \tag{3.81}$$

$$U_1(t) \leq U_{max_{target}} \tag{3.82}$$
$$R_g(t) \in [0, R_{max_{gate}}]$$
$$R_L(t) \in [0, R_{max_{load}}]$$
$$\frac{dU_1}{dt} = \frac{nC_{ind}R_g - 1}{C_L(R_L + R_g)}U_1(t)$$
$$U_1(0) = x_0.$$

The above optimal control problem is not straightforward to solve directly. However, if we neglect running constraints, i.e. when we neglect (3.81) and (3.82), we can use Pontryagin's minimization (/maximization) theorem to obtain necessary conditions concerning the solution of the above optimal control problem. This approach is pursued in the following section.

Chapter 4

Optimally controlling the Kelvin water dropper

4.1 Minimization by Pontryagin

Let us first recall the standard optimal control problem. This is the problem of minimizing a cost

$$J(x_0, u(\cdot)) = S(x(T)) + \int_0^T L(x(t), u(t)) \; dt.$$

over all inputs $u : [0, T] \to \mathbb{U}$, subject to

$$\dot{x}(t) = f(x(t), u(t)), \quad x(0) = x_0.$$

Our original optimization problem (3.80) is unfortunately not of the same form, since in this problem we also have mixed state-control constraints. Therefore we first choose to consider a weaker optimization problem, where these constraints are omitted. Moreover we will first take a fixed value for R_L, so that we only need to consider the input $u(t) = R_g(t)$.

Our optimal control problem is then reduced to:

$$\min \int_0^T -\frac{1}{R_L + u(t)} x^2(t) \; dt$$
$$\text{subject to:} \quad u(t) \in [0, M]$$
$$\frac{dx}{dt} = \frac{nC_{ind} \; u(t) - 1}{C_L(R_L + u(t))} x(t)$$
$$x(0) = x_0 > 0. \tag{4.1}$$

which is of the same form as the standard optimal control problem, where:

$$S(x(T)) = 0$$
$$L(x(t), u(t)) = -\frac{1}{R_L + u(t)} x^2(t)$$
$$f(x(t), u(t)) = \frac{nC_{ind} \; u(t) - 1}{C_L(R_L + u(t))} x(t)$$
$$\mathbb{U} = [0, M].$$

The following theorem provides a necessary condition for solutions of the optimal control problem.

Theorem 4.1.1 (Pontryagin's Minimum Principle ([12])). Suppose $u_* : [0, T] \to \mathbb{U}$ is a solution of the optimal control problem, and x_* the resulting optimal state trajectory. Then there exists a function $p_* : [0, T] \to \mathbb{R}^n$ such that:

$$\dot{x}_*(t) = \frac{\partial H\left(x_*(t), p_*(t), u_*(t)\right)}{\partial p}, \qquad\qquad x_*(0) = x_0, \qquad\qquad (4.2)$$

$$\dot{p}_*(t) = -\frac{\partial H\left(x_*(t), p_*(t), u_*(t)\right)}{\partial x}, \qquad\qquad p_*(T) = \frac{\partial S\left(x_*(t)\right)}{\partial x} \qquad\qquad (4.3)$$

and at the solution $x_*(t)$, $p_*(t)$ the input $u_*(t)$ at each moment in time minimizes the Hamiltonian:

$$H\left(x_*(t), p_*(t), u_*(t)\right) = \min_{v \in \mathbb{U}} H\left(x_*(t), p_*(t), v\right) \qquad\qquad (4.4)$$

for every $t \in [0, T]$, where the Hamiltonian $H(x, p, u)$ is defined as

$$H(x, p, u) := p^{\mathrm{T}} f(x, u) + L(x, u). \qquad\qquad (4.5)$$

$\blacksquare$

We can now find that the Hamiltonian for the optimal control problem of (4.1) is given by:

$$H(x, p, u) = p \frac{nC_{ind}\, u - 1}{C_L(R_L + u)} x - \frac{1}{R_L + u} x^2.$$

In pursuit for a solution of (4.4) we first investigate when $0 = \frac{\partial H(x_*, p_*, u)}{\partial u}$:

$$\begin{aligned}
0 &= \frac{\partial H(x_*, p_*, u)}{\partial u} \\
&= p_* x_* \frac{nC_{ind}(C_L(R_L + u)) - (nC_{ind}\, u - 1)C_L}{C_L{}^2 (R_L + u)^2} + x_*{}^2 \frac{1}{(R_L + u)^2} \\
&= \frac{(nC_{ind}R_L + 1)p_* x_* + C_L x_*{}^2}{C_L(R_L + u)^2} \qquad\qquad (4.6)
\end{aligned}$$

From equation (4.6) we see that $\frac{\partial H(x_*(\cdot), p_*(\cdot), u)}{\partial u}$ as a function of u is never zero. Therefore the minimum will always occur at the boundary. That is:

$$u_*(t) = \begin{cases} 0 & \text{if } H\left(x_*(t), p_*(t), 0\right) < H\left(x_*(t), p_*(t), M\right) \\ M & \text{otherwise.} \end{cases} \qquad\qquad (4.7)$$

It may be noted that the first equation in Pontryagin's Minimum Principle, equation (4.2), simply states that the optimal state must be a solution to the prescribed differential equation

$$\begin{aligned}
\dot{x}_*(t) &= \frac{\partial H\left(x_*(t), p_*(t), u_*(t)\right)}{\partial p}, & x_*(0) &= x_0 & \Longrightarrow \\
\dot{x}_*(t) &= f(x_*(t), u_*(t)), & x_*(0) &= x_0 & \Longrightarrow \\
\dot{x}_*(t) &= \frac{nC_{ind}\, u_*(t) - 1}{C_L(R_L + u_*(t))} x_*(t), & x_*(0) &= x_0 & . \qquad (4.8)
\end{aligned}$$

Equation (4.8) can be observed to be a separable differential equation, which can be solved by integration on both sides. That is:

$$\frac{dx_*}{dt} = \frac{nC_{ind}\, u_*(t) - 1}{C_L(R_L + u_*(t))} x_*$$

$$\frac{1}{x_*}\, dx_* = \frac{nC_{ind}\, u_*(t) - 1}{C_L(R_L + u_*(t))}\, dt$$

$$\int_{x_0}^{x_*} \frac{1}{s}\, ds = \int_0^t \frac{nC_{ind}\, u_*(\tau) - 1}{C_L(R_L + u_*(\tau))}\, d\tau$$

$$\ln\left(\frac{|x_*|}{|x_0|}\right) = \int_0^t \frac{nC_{ind}\, u_*(\tau) - 1}{C_L(R_L + u_*(\tau))}\, d\tau$$

$$x_*(t) = x_0 e^{\int_0^t \frac{nC_{ind}\, u_*(\tau) - 1}{C_L(R_L + u_*(\tau))}\, d\tau}. \tag{4.9}$$

where in final step of the derivation the absolute value sign can be dropped since x_0 and x_* both have the same sign. Since by assumption $x_0 > 0$, we can conclude from (4.9) that $x_*(t) > 0 \;\; \forall t \in [0, T]$.

Let us now return to the condition $H\left(x_*(t), p_*(t), 0\right) < H\left(x_*(t), p_*(t), M\right)$ in (4.7). We can deduce that this is equivalent to:

$$H\left(x_*(t), p_*(t), 0\right) < H\left(x_*(t), p_*(t), M\right) \qquad \Longleftrightarrow$$

$$p_*(t) \cdot \frac{-1}{C_L R_L} \cdot x_*(t) - \frac{1}{R_L} x_*^{\,2}(t) < p_*(t) \frac{nC_{ind}M - 1}{C_L(R_L + M)} x_*(t) - \frac{1}{R_L + M} x_*^{\,2}(t) \qquad \Longleftrightarrow$$

$$x_*(t)\left(\frac{C_L}{R_L + M} - \frac{C_L}{R_L}\right) < p_*(t)\left(\frac{nC_{ind}M - 1}{R_L + M} + \frac{1}{R_L}\right) \qquad \Longleftrightarrow$$

$$p_*(t) + \frac{C_L}{1 + nC_{ind}R_L} x_*(t) > 0. \tag{4.10}$$

The last equation from Pontryagin to explore is (4.3). This equation leads to:

$$\dot{p}_*(t) = -\frac{\partial H\left(x_*(t), p_*(t), u_*(t)\right)}{\partial x}, \qquad\qquad p_*(T) = \frac{\partial S\left(x_*(t)\right)}{\partial x} \qquad \Longrightarrow$$

$$\dot{p}_*(t) = -\frac{nC_{ind}\, u_*(t) - 1}{C_L(R_L + u_*(t))} p_*(t) + \frac{2}{R_L + u_*(t)} x_*(t) \qquad p_*(T) = 0. \tag{4.11}$$

Combining all of the above, a solution to Pontryagin's differential equations boils down to finding a solution to:

$$\begin{bmatrix} \dot{x}_* \\ \dot{p}_* \end{bmatrix} = \begin{cases} \begin{bmatrix} -\frac{1}{C_L R_L} & 0 \\ \frac{2}{R_L} & \frac{1}{C_L R_L} \end{bmatrix} \begin{bmatrix} x_* \\ p_* \end{bmatrix} & \text{if } u_*(t) = 0 \\[3mm] \begin{bmatrix} \frac{nC_{ind}M - 1}{C_L(R_L + M)} & 0 \\ \frac{2}{R_L + M} & -\frac{nC_{ind}M - 1}{C_L(R_L + M)} \end{bmatrix} \begin{bmatrix} x_* \\ p_* \end{bmatrix} & \text{if } u_*(t) = M. \end{cases} \tag{4.12}$$

for given conditions $x(0) = x_0 > 0$ and $p(T) = 0$, where $u_*(t) \in \{0, M\}$ according to the 'switching law' defined by (4.7) and (4.10).

4.1.1 Solving (4.12) backwards in time

Since the end condition for $p(t)$ is known, this problem may be solved backwards in time, starting from $t = T$. Thereby we define the switching function; see (4.10)

$$g_*(t) = p_*(t) + q x_*(t), \tag{4.13}$$

where $q = \frac{C_L}{1+nC_{ind}R_L} > 0$, so that the 'switching law' from (4.10) can be redefined to:

$$\begin{cases} u_*(t) \equiv 0 & \text{if } g_*(t) > 0 \\ u_*(t) \equiv M & \text{if } g_*(t) < 0. \end{cases} \tag{4.14}$$

To simplify further calculations, we will also redefine the constant matrices in (4.12). Analogously to (4.12) we will write:

$$\begin{bmatrix} \dot{x}_* \\ \dot{p}_* \end{bmatrix} = \begin{cases} \begin{bmatrix} -a & 0 \\ b & a \end{bmatrix} \begin{bmatrix} x_* \\ p_* \end{bmatrix} & \text{if } g_*(t) > 0 \\ \begin{bmatrix} c & 0 \\ d & -c \end{bmatrix} \begin{bmatrix} x_* \\ p_* \end{bmatrix} & \text{if } g_*(t) < 0. \end{cases} \tag{4.15}$$

Later on in this section, we shall use 'A_1' and 'A_2' to refer to the above two matrices. Furthermore, we have implicitly assumed that $M > \frac{1}{nC_{ind}}$, so that indeed we have that $c > 0$. We remark that this assumption also makes sense, as in the case that $M < \frac{1}{nC_{ind}}$ we are not able to charge the system.

Since we have that $p_*(T) = 0$ and $x_*(t) > 0 \;\forall t$, we can see from (4.13) that $g_*(T) > 0$. The switching law (4.14) then tells us that $u_*(T) \equiv 0$. In turn this allows us to calculate the derivatives $\dot{x}_*(T^-)$, $\dot{p}_*(T^-)$ and $\dot{g}_*(T^-)$:

$$\dot{x}_*(T^-) = -ax_*(T^-) < 0,$$

$$\dot{p}_*(T^-) = bx_*(T^-) + ap_*(T^-) = bx_*(T^-) > 0,$$

$$\dot{g}_*(T^-) = \dot{p}_*(T^-) + q\dot{x}_*(T^-) = (b - qa)\, x_*(T^-).$$

By definition, the constant $b - qa$ can be seen to be positive

$$b - qa = \frac{2}{R_L} - \frac{C_L}{1 + nC_{ind}R_L} \cdot \frac{1}{C_L R_L}$$
$$= \frac{1}{R_L}\left(2 - \frac{1}{1 + nC_{ind}R_L}\right) > 0.$$

So that also $\dot{g}_*(T^-) > 0$.

Since we have that $\dot{g}_*(T^-) > 0$ together with $g_*(T) > 0$, it is reasonable to believe that at some point (backwards in time) the switching function $g_*(t)$ becomes zero. At this time instant t_s the switching law (4.14) tells us we need to switch our input function from $u_*(t) \equiv 0$ to $u_*(t) \equiv M$. It turns out that a switch in input function will indeed occur when the end time T is sufficiently large, as will be shown later in this section (see (4.19)).

Before we look at this switching instant t_s, we first remark that from (4.15) we can see that $p_*(t) < 0$ on $[0, T]$, which follows from the fact that $\dot{p}_*(t) > 0$ whenever $p_*(t) = 0$. As we need to switch from the input function at $t = t_s$, we will have a look at the derivatives $\dot{x}_*(t_s{}^-)$, $\dot{p}_*(t_s{}^-)$

and $\dot{g}_*(t_s{}^-)$:

$$\dot{x}_*(t_s{}^-) = cx_*(t_s{}^-) > 0,$$

$$\dot{p}_*(t_s{}^-) = dx_*(t_s{}^-) - cp_*(t_s{}^-) > 0,$$

$$\begin{aligned}
\dot{g}_*(t_s{}^-) &= \dot{p}_*(t_s{}^-) + q\dot{x}_*(t_s{}^-) \\
&= dx_*(t_s{}^-) - cp_*(t_s{}^-) + qcx_*(t_s{}^-) \\
&= -c\left[p_*(t_s{}^-) + qx_*(t_s{}^-)\right] + (d + 2qc)\,x_*(t_s{}^-) \\
&= (d + 2qc)\,x_*(t_s{}^-) > 0.
\end{aligned}$$

Since we see that $\dot{g}_*(t_s{}^-) > 0$, it follows that the function $g_*(t)$ crosses the time axis at $t = t_s$, i.e. it does not remain constant or 'bounce back' at $t = t_s$. Because of this we have that the switch $u_*(t) \equiv 0$ to $u_*(t) \equiv M$ will be well defined by the switching function.

For now we have only discussed a single switch of the input function. One may wonder whether more of these switches will occur in the time window $[0, t_s)$. This will not be the case, as our previous argument $\dot{g}_*(t_s{}^-) > 0$ in any possible switching instant t_s. Specifically, if at any time t we have that $g_*(t) = 0$, the above calculation shows that this would imply that $\dot{g}_*(t) > 0$. Because of this it is not possible to reach the condition $g_*(t) > 0$ in the time window $[0, t_s)$, which shows that on $[0, T]$ only a single switch of input will occur.

Combining the results obtained so far, a conceptual plot illustrating the optimal control solution of (4.12) is given in Figure 4.1.

An interesting observation is that if the final time T is very small, no switch in input function will occur. The optimal control would then simply be to 'de-charge' the system by letting all the charges escape through a resistor with zero resistance. Although this may seem somewhat counter intuitive, this result can be explained from the output power equation (3.79). As assumed, at $t = 0$ we start with some (random) initial charge x_0. At $t = 0$ the electrical output power thereby equals:

$$P_{electrical}(0) = \begin{cases} \frac{1}{R_L}x_0{}^2 & \text{if } u(0) \equiv 0 \\ \frac{1}{R_L + M}x_0{}^2 & \text{if } u(0) \equiv M. \end{cases} \tag{4.16}$$

We can see from (4.16) that initially the output power is higher for the zero input case. Therefore, if T is small we have that

$$\int_0^T P_{electrical}(t; u(t) \equiv 0)\, dt > \int_0^T P_{electrical}(t; u(t) \equiv M)\, dt.$$

In fact, choosing $u(t) \equiv 0$ will produce a momentarily higher output power at any initial condition x_t. Specifically, this will be the case at the switching time t_s with initial condition x_{t_s}, as is also illustrated in Figure 4.1.

Although we have now explained how momentarily de-charging can be optimal, it may be evident that this will not be an effective long run strategy. When T is sufficiently large, the positive exponential obtained with $u(t) \equiv M$ will serve as a good investment. In this case it turns out to be optimal to first maximally charge the system, whereas close to the end it is optimal to quickly 'harvest' a maximal amount of the accumulated charges. From this point of view it may
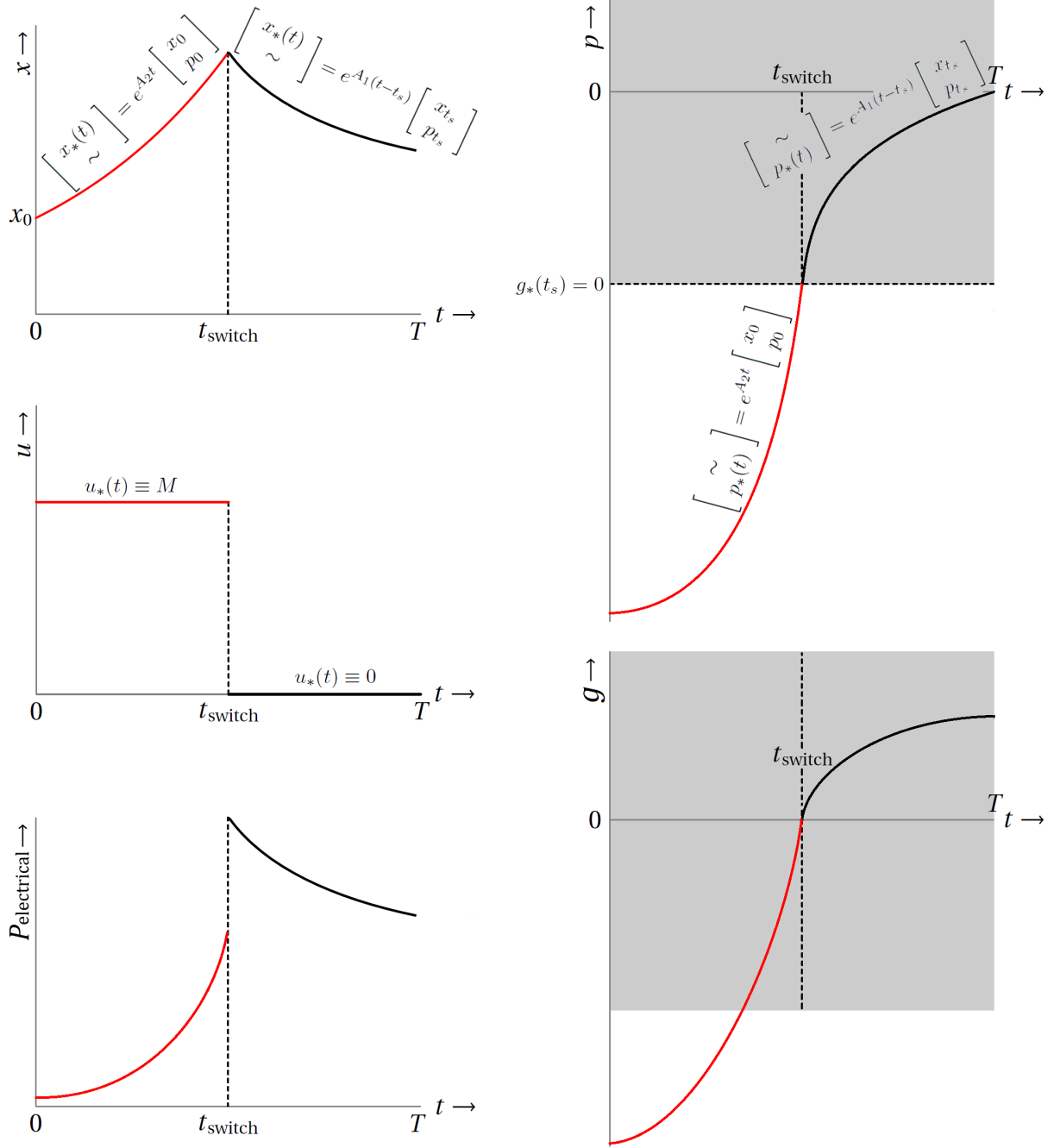
Figure 4.1: Conceptual plots of the optimal state $x_*(t)$, costate $p_*(t)$, input function $u_*(t)$, switching function $g_*(t)$ and output power $P_{electrical}(t)$ corresponding to (4.12)

be expected that the switch time t_s will occur very near the end time T. This is indeed the case, as will be shown next.

Explicit solution to (4.15)

To calculate the switching time t_s, we solve (4.15) backwards in time using end conditions $x_*(T) = x_T$ and $p_*(T) = 0$. Knowing that $u(t) \equiv 0$ on $[t_s, T]$, initially the system will be

represented by the first system matrix of (4.15):

$$\begin{bmatrix} x_*(T-t) \\ p_*(T-t) \end{bmatrix} = e^{(-A_1)t} \begin{bmatrix} x_*(T) \\ p_*(T) \end{bmatrix}$$

$$= \begin{bmatrix} e^{at} & 0 \\ \frac{b}{2a}\left(e^{-at} - e^{at}\right) & e^{-at} \end{bmatrix} \begin{bmatrix} x_T \\ 0 \end{bmatrix}$$

$$= x_T \begin{bmatrix} e^{at} \\ \frac{b}{2a}\left(e^{-at} - e^{at}\right) \end{bmatrix}. \tag{4.17}$$

for a more elaborate calculation of $e^{(-A_1)t}$ one may refer to Appendix A.4.2.

Combining the above equation (4.17) with the switching function $g_*(t)$, we can now calculate when the input needs to be changed to $u(t) \equiv M$. Thereby we find:

$$g_*(T-t) = 0 \qquad\qquad \Longleftrightarrow$$
$$p_*(T-t) + qx_*(T-t) = 0 \qquad\qquad \Longleftrightarrow$$
$$x_T\left(\frac{b}{2a}\left(e^{-at} - e^{at}\right) + qe^{at}\right) = 0, \tag{4.18}$$

which upon solving for t reduces to:

$$t = \frac{\ln\left(\frac{b}{b-2aq}\right)}{2a} \qquad\qquad \Longleftrightarrow$$
$$= \frac{C_L R_L}{2} \ln\left(1 + \frac{1}{nC_{ind}R_L}\right). \tag{4.19}$$

From which we find that the switching time is equal to:

$$t_s = T - \frac{C_L R_L}{2} \ln\left(1 + \frac{1}{nC_{ind}R_L}\right). \tag{4.20}$$

Assuming the values $C_L = 12 \cdot 10^{-12}$, $R_L = 10^{12}$ and $nC_{ind} = 0.05 \cdot 10^{-9}$, as used in [18], equation (4.19) tells us that switch in input function is approximately 0.12 seconds before the final time T.

Although to this point we considered the value of R_L to be fixed, equation (4.20) provides a relation between the switching time t_s and (fixed) R_L. In particular we may consider what happens if we connect a very small load resistor or a very large resistor, i.e. we may take the limit $R_L \downarrow 0$ or $R_L \uparrow \infty$. From (4.20) we can see that this boils down to:

$$\lim_x t_s = \lim_x \left[T - \alpha x \ln\left(1 + \frac{\beta}{x}\right)\right]$$
$$= T - \alpha \lim_x \frac{\ln\left(1 + \frac{\beta}{x}\right)}{\frac{1}{x}}$$

where α and β are constants. Furthermore, it has deliberately not been specified yet which of the two limits we consider. This is because on inspection we can see that either limit will present a 'L'Hôpital case'; $x \downarrow 0$ results in $\frac{\infty}{\infty}$ and $x \uparrow \infty$ results in $\frac{0}{0}$. In either case the limit can therefore be continued to

$$\lim_x \frac{\ln\left(1 + \frac{\beta}{x}\right)}{\frac{1}{x}} = \lim \frac{-\frac{\beta}{x^2} \cdot \frac{1}{1+\frac{\beta}{x}}}{-\frac{1}{x^2}} = \lim \frac{\beta}{1 + \frac{\beta}{x}},$$

so that

$$\lim_{R_L \downarrow 0} t_s = T$$

$$\lim_{R_L \to \infty} t_s = T - \alpha\beta. \tag{4.21}$$

Returning to our example where we used $C_L = 12 \cdot 10^{-12}$ and $nC_{ind} = 0.05 \cdot 10^{-9}$, we can see that the switching obtained with $R_L = 10^{12}$ was already close to limit case $\lim_{R_L \to \infty} t_s$, as we see that in this case

$$\alpha\beta = \frac{C_L}{2} \cdot \frac{1}{nC_{ind}} = 12 \cdot 10^{-2}.$$

As a last comment we intuitively expect that a low value for R_L is optimal, since this will both increase the initial output power (see (4.16)), as well as increase the speed at which the system can be charged (see (4.8)). However, in a later stadium we will also aim to proof this by considering both $R_L(t)$ and $R_g(t)$ as an input.

Knowing the moment that we need to switch the input function, we can see that upon solving

$$\begin{bmatrix} x_*(t_s) \\ p_*(t_s) \end{bmatrix} = e^{A_2 t_s} \begin{bmatrix} x_*(0) \\ p_*(0) \end{bmatrix} \tag{4.22}$$

$$= e^{(-A_1)\cdot(T-t_s)} \begin{bmatrix} x_*(T) \\ p_*(T) \end{bmatrix} \tag{4.23}$$

for unknowns $p_*(0)$ and $x_*(T)$, we have completed the solution to the optimization problem (4.15).

The latter equation in (4.23) is already worked out in (4.17), so that we only need to turn our attention to the first equation. Thereby we will refer the reader to Appendix A.4.3 for the calculation of $e^{A_2 t}$. Thereby we find

$$\begin{bmatrix} x_*(t_s) \\ p_*(t_s) \end{bmatrix} = e^{A_2 t_s} \begin{bmatrix} x_*(0) \\ p_*(0) \end{bmatrix}$$

$$= \begin{bmatrix} e^{ct_s} & 0 \\ \frac{d}{2c}\left(e^{ct_s} - e^{-ct_s}\right) & e^{-ct_s} \end{bmatrix} \begin{bmatrix} x_0 \\ p_0 \end{bmatrix}$$

$$= \begin{bmatrix} x_0 e^{ct_s} \\ x_0 \frac{d}{2c}\left(e^{ct_s} - e^{-ct_s}\right) + p_0 e^{-ct_s} \end{bmatrix}. \tag{4.24}$$

Combining equations (4.17) with (4.24), we may rewrite (4.23) to

$$\begin{bmatrix} x_0 e^{ct_s} \\ x_0 \frac{d}{2c}\left(e^{ct_s} - e^{-ct_s}\right) + p_0 e^{-ct_s} \end{bmatrix} = x_T \begin{bmatrix} e^{a(T-t_s)} \\ \frac{b}{2a}\left(e^{-a(T-t_s)} - e^{a(T-t_s)}\right) \end{bmatrix},$$

which gives us two equations for the two unknowns p_0 and x_T. From these two equations it follows that:

$$x_T = x_0 \, e^{ct_s} \cdot e^{-a(T-t_s)}$$

$$p_0 = x_0 \left(\frac{b}{2a} e^{-2aT + 2(a+c)t_s} - \left(\frac{b}{2a} + \frac{d}{2c} \right) e^{2ct_s} + \frac{d}{2c} \right). \tag{4.25}$$

4.1.2 Both resistors as an input

In the previous section we have solved the optimization problem (4.1). There we considered a fixed load resistor R_L and a variable resistor $R_g(t)$ as an input $u(t)$. In this subsection we will investigate what our optimal control will be when both these resistors are free to choose, i.e. we consider

$$u(t) = \begin{bmatrix} u_1(t) \\ u_2(t) \end{bmatrix} = \begin{bmatrix} R_L(t) \\ R_g(t) \end{bmatrix}.$$

The optimal control problem of (4.1) will then turn into:

$$\min \int_0^T -\frac{1}{u_1(t)+u_2(t)}x^2(t)\ dt$$
$$\text{subject to:}\quad u_1(t) \in [0, M_1]$$
$$u_2(t) \in [0, M_2]$$
$$\frac{dx}{dt} = \frac{nC_{ind}\ u_2(t)-1}{C_L(u_1(t)+u_2(t))}x(t)$$
$$x(0) = x_0 > 0, \tag{4.26}$$

where the Hamiltonian is given by

$$H(x(t), p(t), u(t)) = p(t)\frac{nC_{ind}\ u_2(t)-1}{C_L(u_1(t)+u_2(t))}x(t) - \frac{1}{u_1(t)+u_2(t)}x^2(t).$$

Again we will use Pontryagin's theorem (4.1.1), as it is also valid for the multi-input case. Thereby we will first investigate for which input the Hamiltonian is minimized. Also now we will investigate whether the minimum takes place in the interior of $\mathbb{U}$, so that $0 = \frac{\partial H}{\partial u}$. Simple calculations yield:

$$\begin{bmatrix} \frac{\partial H(x_*(t),p_*(t),u)}{\partial u_1} \\ \frac{\partial H(x_*(t),p_*(t),u)}{\partial u_2} \end{bmatrix} = \begin{bmatrix} \frac{C_L x_*^2(t)-(nC_{ind}\ u_2-1)p_*(t)x_*(t)}{C_L(u_1+u_2)^2} \\ \frac{C_L x_*^2(t)+(nC_{ind}\ u_1+1)p_*(t)x_*(t)}{C_L(u_1+u_2)^2} \end{bmatrix} \tag{4.27}$$

For the moment we assume that $u_1 + u_2 \neq 0$, which can only happen if $u(t) = 0$. From (4.27) we can then see that $\frac{\partial H}{\partial u_1} = 0$ if:

$$nC_{ind}\ u_2 p_*(t)x_*(t) = C_L x_*^2(t) + p_*(t)x_*(t) \qquad \Longleftrightarrow$$
$$u_2 = \frac{C_L x_*(t)}{nC_{ind}\ p_*(t)} + \frac{1}{nC_{ind}}, \tag{4.28}$$

and that $\frac{\partial H}{\partial u_2} = 0$ if

$$nC_{ind}\ u_1 p_*(t)x_*(t) = -\left(C_L x_*^2(t) + p_*(t)x_*(t)\right)$$
$$u_1 = -\left(\frac{C_L x_*(t)}{nC_{ind}\ p_*(t)} + \frac{1}{nC_{ind}}\right). \tag{4.29}$$

From (4.28) and (4.29) we can see that an extremum would take place in the interior of $\mathbb{U}$ when $u_1(t) = -u_2(t)$. Apart from $u(t) = 0$ this can not happen, since both resistors need to have a positive value. Also in this dual input case we thus see that the minimum occurs on the boundary.

Where however previously the boundary of $\mathbb{U}$ was equal to $\{0, M\}$, for the dual input case the boundary is a bit more elaborate. We now have that the boundary consists of 4 edges, i.e. when either input is chosen fixed to its minimum or maximum while the other input is free, as well as 4 vertices, i.e. when both the inputs are chosen equal to its minimum or maximum value. To investigate a minimum on the edges of the boundary, we examine the following partial derivatives:

$$\frac{\partial H\left(x_*(t), p_*(t), \begin{bmatrix} 0 \\ u_2 \end{bmatrix}\right)}{\partial u_2} = \frac{C_L x_*^2(t) + p_*(t)x_*(t)}{C_L u_2^2}$$

$$\frac{\partial H\left(x_*(t), p_*(t), \begin{bmatrix} M_1 \\ u_2 \end{bmatrix}\right)}{\partial u_2} = \frac{C_L x_*^2(t) + (nC_{ind} M_1 + 1) p_*(t)x_*(t)}{C_L (M_1 + u_2)^2}$$

$$\frac{\partial H\left(x_*(t), p_*(t), \begin{bmatrix} u_1 \\ 0 \end{bmatrix}\right)}{\partial u_1} = \frac{C_L x_*^2(t) + p_*(t)x_*(t)}{C_L u_1^2}$$

$$\frac{\partial H\left(x_*(t), p_*(t), \begin{bmatrix} u_1 \\ M_2 \end{bmatrix}\right)}{\partial u_1} = \frac{C_L x_*^2(t) - (nC_{ind} M_2 - 1) p_*(t)x_*(t)}{C_L (u_1 + M_2)^2}. \tag{4.30}$$

For each of the partial derivatives in (4.30) we see that the derivative is never zero as a function of u_1 or u_2. Therefore the minimum will always occur on one of the four vertices, where both the inputs are chosen equal to the minimum or maximum value.

The value of the Hamiltonian in the vertices is given by:

$$H\left(x_*(t), p_*(t), \begin{bmatrix} M_1 \\ 0 \end{bmatrix}\right) = \frac{-p_*(t)x_*(t) - C_L x_*^2(t)}{C_L M_1}$$

$$H\left(x_*(t), p_*(t), \begin{bmatrix} M_1 \\ M_2 \end{bmatrix}\right) = \frac{p_*(t)x_*(t) (nC_{ind}M_2 - 1) - C_L x_*^2(t)}{C_L(M_1 + M_2)}$$

$$H\left(x_*(t), p_*(t), \begin{bmatrix} 0 \\ M_2 \end{bmatrix}\right) = \frac{p_*(t)x_*(t) (nC_{ind}M_2 - 1) - C_L x_*^2(t)}{C_L M_2} \tag{4.31}$$

whereas $H\left(x_*(t), p_*(t), \begin{bmatrix} 0 \\ 0 \end{bmatrix}\right)$ is undefined due to the division by zero. It may however be justified to look at the limit:

$$\lim_{(u_1, u_2) \downarrow (0,0)} H\left(x_*(t), p_*(t), \begin{bmatrix} u_1 \\ u_2 \end{bmatrix}\right) = \lim_{(u_1, u_2) \downarrow (0,0)} \left(\frac{p_*(t)x_*(t) (nC_{ind} u_2 - 1) - C_L x_*^2(t)}{C_L(u_1 + u_2)}\right). \tag{4.32}$$

Also now we aim to find a solution backwards in time, starting from the condition that $p_*(T) = 0$. Similar to the single input case this can be pursued step by step, by choosing the input $u(t)$ such that at each moment in time the Hamiltonian is minimized.

Plugging in $p_*(T) = 0$ in (4.31) and (4.32) it is easy to see that at $t = T$ the Hamiltonian is minimized when $(u_1, u_2) \downarrow (0,0)$, since we then get that:

$$\lim_{(u_1, u_2) \downarrow (0,0)} H\left(x_*(T), 0, \begin{bmatrix} u_1 \\ u_2 \end{bmatrix}\right) = \left(\frac{-x_*^2(T)}{0^+}\right)$$

$$= -\infty.$$

Hereby remember that $x_*(t) > 0 \;\; \forall t$ as previously concluded by (4.9). Since we find that the is minimized when $(u_1, u_2) \downarrow (0,0)$, it seems that again our optimal input at $t = T$ is given by $u(t) = 0$. However, as mentioned we find that for this choice we have that the Hamiltonian is undefined due to a division by zero.

To avoid this problem, in the succeeding calculations we consider the solution for very small, non-zero values of (u_1, u_2). Later on, we shall use the values $(0, \epsilon)$ or (ϵ, ϵ) to describe the solutions.

Completely analogous to (4.8) and (4.11), the Pontryagin equations (4.2) and (4.3) now give us that

$$\dot{x}_*(t) = \frac{nC_{ind}\, u_2 - 1}{C_L(u_1 + u_2)} x_*(t)$$

$$\dot{p}_*(t) = \frac{2}{u_1 + u_2} x_*(t) - \frac{nC_{ind}\, u_2 - 1}{C_L(u_1 + u_2)} p_*(t),$$

where the input (u_1, u_2) will be taken to approach zero. Similar to the notation of (4.15), for convenience we will write:

$$\widetilde{a} = \frac{1 - nC_{ind}\, u_2}{C_L(u_1 + u_2)}$$

$$\widetilde{b} = \frac{2}{u_1 + u_2}.$$

Note that for small u_1 and u_2 these are large positive constants. Furthermore note that at $t = T$ this gives us the same system dynamics as in the first case of (4.15), with the only exception being the tilde. Because of this the solution backwards in time is also similar to (4.17), so that we have

$$\begin{bmatrix} x_*(T - t) \\ p_*(T - t) \end{bmatrix} = e^{(-\widetilde{A_1})t} \begin{bmatrix} x_*(T) \\ p_*(T) \end{bmatrix}$$

$$= x_T \begin{bmatrix} e^{\widetilde{a}t} \\ \frac{\widetilde{b}}{2\widetilde{a}} \left(e^{-\widetilde{a}t} - e^{\widetilde{a}t} \right) \end{bmatrix}. \tag{4.33}$$

In particular we may conclude from (4.33) that in the neighborhood of $t = T$ we have that $x_*(T - t)$ is increasing exponentially whereas $p_*(T - t)$ is decreasing exponentially. From here on we need to investigate how long the vertex $(u_1, u_2) \downarrow (0,0)$ remains the input that minimalizes the Hamiltonian, and especially which vertex will be the new minimalizer of the Hamiltonian when $(u_1, u_2) \downarrow (0,0)$ stops being the minimalizer. Looking back at (4.31) and (4.32), this boils down to determining the minimum from the following four terms

$$\frac{-p_* - C_L x_*}{M_1} \tag{4.34}$$

$$\frac{(nC_{ind} M_2 - 1)p_* - C_L x_*}{M_1 + M_2} \tag{4.35}$$

$$\frac{(nC_{ind} M_2 - 1)p_* - C_L x_*}{M_2} \tag{4.36}$$

$$\lim_{(u_1, u_2) \downarrow (0,0)} \left(\frac{(nC_{ind}\, u_2 - 1)\, p_* - C_L x_*}{u_1 + u_2} \right), \tag{4.37}$$

where for simplicity the common term $\frac{x_*}{C_L}$ has been divided out.

66

Upon closer inspection of the four cases above, we can draw some preliminary conclusions. At first we see that the numerators from (4.35) and (4.36) are equal. Due to the difference in the denominators we can thereby observe that for negative p_* and positive x_* the mutual minimum between (4.35) and (4.36) is given by (4.36).

Furthermore, depending on how we approach the limit $(u_1, u_2) \downarrow (0,0)$, we can see that the numerators between (4.34) and (4.37) are identical or very close to being identical. Assuming that both these numerators are negative we can then see that the difference in denominators will cause the mutual minimum between (4.34) and (4.37) to be given by (4.37). Due to the term $nC_{ind}\, u_2$ in the numerator of (4.37) we furthermore see that initially, when x_* and p_* are described backwards in time by (4.33), the numerator of (4.37) will stay negative for a longer time.

Thereby we can conclude that, in case we need to switch the input function backward in time (which will approximately be the case when $p_* + C_L x_* = 0$), the first switch will be given by $(u_1, u_2) = (0, M_2)$. If, and if so when, we need to switch to $(0, M_2)$ may be determined by equating (4.36) and (4.37), plugging in the backwards solutions for $x_*(t)$ and $p_*(t)$ from (4.33) and solving for t. For instance, in the single input case we solved this in (4.18) and (4.19). However, for the dual input case here it will be convenient to first specify how we approach the limit $(u_1, u_2) \downarrow (0,0)$. Thereby note that if we consider 'the direction of approach' $u_1 = 0$, $u_2 \downarrow 0$, then by (4.21) we can already conclude that in the limit, backwards in time the switch will be immediate, i.e. $t_{switch} = T$.

For completeness we will investigate whether this is also the case for another approach of the limit $(u_1, u_2) \downarrow (0,0)$, let us thereby consider $u_1 = u_2 = \epsilon$, where $\epsilon \downarrow 0$. We then see that

$$\lim_{\epsilon \downarrow 0} H\left(x_*(t), p_*(t), \begin{bmatrix} \epsilon \\ \epsilon \end{bmatrix}\right) < H\left(x_*(t), p_*(t), \begin{bmatrix} 0 \\ M_2 \end{bmatrix}\right)$$

$$\frac{(nC_{ind}\epsilon - 1)\, p_*(t) - C_L x_*(t)}{2\epsilon} < \frac{(nC_{ind}M_2 - 1)p_*(t) - C_L x_*(t)}{M_2}$$

$$\left(\frac{C_L}{M_2} - \frac{C_L}{2\epsilon}\right) x_*(t) < \left(\frac{nC_{ind}M_2 - 1}{M_2} - \frac{nC_{ind}\epsilon - 1}{2\epsilon}\right) p_*(t)$$

$$p_*(t) + \frac{C_L(M_2 - 2\epsilon)}{M_2 + \epsilon(nC_{ind}M_2 - 2)} x_*(t) > 0. \tag{4.38}$$

From equation (4.38) we again recognize a similar switching function before (see (4.13)). Thereby we will now write $\widetilde{q} = \frac{C_L(M_2 - 2\epsilon)}{M_2 + \epsilon(nC_{ind}M_2 - 2)}$, so that our new switching function is given by:

$$\widetilde{g}_*(t) = p_*(t) + \widetilde{q}x_*(t). \tag{4.39}$$

With the new 'tilde notation' we see that the rest of the calculations are analogous to (4.18) and the first of (4.19), the only difference being the tilde above the constants. Thereby we find that the switching time is given by:

$$t_s = T - \frac{\ln\left(\frac{\widetilde{b}}{\widetilde{b} - 2\widetilde{a}\widetilde{q}}\right)}{2\widetilde{a}} \qquad\qquad \Longleftrightarrow$$

$$= T - \frac{\epsilon C_L}{1 - \epsilon nC_{ind}} \ln\left(\frac{M_2 + \epsilon(nC_{ind}M_2 - 2)}{2\epsilon nC_{ind}(M_2 - \epsilon)}\right)$$

Inspection of the above limit shows that in the sub-limit we get a '$0^+ \cdot \infty$ case'. In this sub-limit we have a more or less linear term in ϵ and a more or less logarithmic term in $\frac{1}{\epsilon}$. From

this observation one may argue that the logarithmic term will 'lose' from the linear term, so that the sub-limit is equal to zero. From there we then also see that for the switch time we get $t_s = T$. That this intuitive limit is indeed correct can be shown from tedious calculations relying on L'Hôpital rule, as one can find in Appendix section A.5.

Thereby we have thus shown that in either case of approaching the limit $(u_1, u_2) \downarrow (0,0)$; $u_1 \downarrow 0$, $u_2 = 0$ or $u_1 = u_2 = \epsilon$ where $\epsilon \downarrow 0$, we see that the moment we need to switch the input $u_*(t)$ will approach the end time T.

At last we will show that also after the switch the Pontryagin solution for the dual input case is analogous to the single input case. Instead of constants c and d that were previously introduced when $(u_1, u_2) = (R_L, M)$, when switching to $(u_1, u_2) = (0, M_2)$ we will now write:

$$\widetilde{c} = \frac{nC_{ind}M_2 - 1}{C_L M_2}$$

$$\widetilde{d} = \frac{2}{M_2}.$$

In this way we see that indeed the Pontryagin problem for the dual input case is completely analogous to (4.15), as we now obtain the problem:

$$\begin{bmatrix} \dot{x}_* \\ \dot{p}_* \end{bmatrix} = \begin{cases} \begin{bmatrix} -\widetilde{a} & 0 \\ \widetilde{b} & \widetilde{a} \end{bmatrix} \begin{bmatrix} x_* \\ p_* \end{bmatrix} & \text{if } \widetilde{g}_*(t) > 0 \\[2em] \begin{bmatrix} \widetilde{c} & 0 \\ \widetilde{d} & -\widetilde{c} \end{bmatrix} \begin{bmatrix} x_* \\ p_* \end{bmatrix} & \text{if } \widetilde{g}_*(t) < 0, \end{cases} \tag{4.40}$$

where $\widetilde{g}_*(t)$ is the new switching function as defined by (4.39). One may verify that also here this function is monotonically increasing for $t \in [0, T]$. Because of this all arguments of the previous section still hold for the dual input case.

In particular, as we showed that in the limit $u(t) \downarrow 0$ the switching time equals the end time (i.e. $t_s = T$), maximally charging the system at (almost) all time (i.e. choosing $u * (t) = [0, M]^{\mathrm{T}}, t \in [0, T)$) turns out to be optimal. This is because accumulated charges can instantly be harvested in the ideal case that $u(t) = 0$. From equation (4.24) we then have that

$$\begin{bmatrix} x_*(t) \\ p_*(t) \end{bmatrix} = e^{\widetilde{A}_2 t} \begin{bmatrix} x_*(0) \\ p_*(0) \end{bmatrix}$$

$$= \begin{bmatrix} x_0 e^{\widetilde{c} t_s} \\ x_0 \frac{\widetilde{d}}{2\widetilde{c}} \left(e^{\widetilde{c} t} - e^{-\widetilde{c} t} \right) + p_0 e^{-\widetilde{c} t} \end{bmatrix},$$

Furthermore, we can use (4.25) to show that $p_0 = x_0 \frac{\widetilde{d}}{2\widetilde{c}} \left(1 - e^{2\widetilde{c} T} \right)$ when $t_s = T$.

4.2 Optimal control dealing with State Variable Inequality Constraints (SVICs)

In this section we will investigate whether a solution can be found to the full optimization problem from which we originally started, i.e. problem (3.80). The main challenge in this optimization problem lies in the fact that we now also need to deal with state variable inequality constraints (SVICs), which are not captured in Pontryagin's Minimum principle (Theorem 4.1.1). Over the years various studies have been performed in search of an extension to Pontryagin's principle including SVICs. Recently much of this work was bundled in [7], which contains a survey on the maximal (/minimal) principles for optimal control problems with SVICs. Before we delve deeper into this somewhat 'newly established' theory, we would like to start with a figurative warning sign, which may be given from the following quote from [7]:

> "These problems are not easy to solve, and even the theory is not unambiguous, since there exist various forms of the necessary and sufficient optimality conditions. Because the literature on this subject is not comprehensive and is, at times, incorrect or incomplete, it has been hard to understand, especially for people working in applied areas."

In particular we note that it seems like the theory of optimal control dealing with SVICs has not yet fully crystallized. Two main (*not always solid!*) approaches that are used are those of direct and indirect adjoining ([7]).
In the direct approach the SVICs are directly adjoined to the Lagrangian (i.e. the Hamiltonian) using extra infinite dimensional/time dependent Lagrange multipliers. On the other hand, in the indirect approach a distinction is made between mixed SVICs (SVICs that are also explicitly dependent on the control variables) and pure SVICs (SVICs that only dependent on the state variables and possibly time). In the indirect approach mixed SVICs are still directly adjoined to the Lagrangian, whereas the pure SVICs are adjoined to the Lagrangian by a certain (higher order) time derivative of these pure SVICs.

In either way, the extended Lagrangian may serve as a basis for new necessary conditions that can handle SVICs. In [7] several theorems are proposed for this job. Interestingly these theorems share quite some similarities with Pontryagin's theorem; generally the 'old' Hamiltonian needs to be maximized (/minimized) over all admissible input functions. Furthermore also the state and costate differential equations are similar, even in the way that initial state constraints and final costate constraints arise in the theorems (As may be compared to Theorem 3.3.12 from [12]). The only difference in these latter differential equations is that the partial derivatives need to be performed on the new extended Lagrangian instead of the original Hamiltonian.
Where at the same time the above discussed similar conditions also fully cover Pontryagin's minimum principle, the proposed (mainly 'informal') theorems in [7] are more elaborate/restrictive. The extra conditions hereby mainly being given in terms of the additional multipliers, but also the derivative of the new Lagrangian with respect to the control u now needs to be zero.

However, we would like to stress again that the 'informal' theorems in [7] are only necessary conditions, and at the same time they are not yet rigorously established in their entirety. Furthermore, the only necessary condition that has been proven (at least since the publication of [7]) also requires a fair amount of assumptions. Due to a 'strong constraint qualification' we for instance already have that the theorem is restricted to first order pure state constraints, where the order of the pure state constraints is given by the minimum number of time differentiations

needed to have u appear explicitly in the expression.

As we conclude that the research on optimal control including SVICs is still rather incomplete, we are not surprised that we could not find many references of this particular theory in many lecture notes or books. However, we did stumble upon [2], which presents a rather complete discussion on necessary optimal control theorems, including those with SVICs.

One may also note that in [2] the optimal control theory is gradually extended. This as opposed to [7], where from the start on a very broad class of optimal control problems is allowed. Particularly, in [2] mixed SVICs and pure SVICs are treated separately, from which we see that in general pure SVICs are more difficult to handle, although mixed SVICs are already mentioned to be "notoriously hard to solve."

This is caused by the fact that mixed SVICs depend explicitly on the control u, where pure SVICs only depend implicitly on the control u. When dealing with pure SVICs the state x can thereby only be controlled through the systems differential equation

$$\dot{x}(t) = f(t, x(t), u(t)), \quad x(0) = x_0.$$

Since the problems with just mixed SVICs are already judged to be notoriously hard, we will not consider pure state constraints in this thesis. Therefore we drop the restriction

$$U_1(t) \leq U_{max_{target}}$$

from our originally aimed optimal control problem 3.80. However, since the mixed SVIC

$$\frac{R_g(t)}{R_L(t) + R_g(t)} U_1(t) \leq U_{max_{ring}}$$

seems to be the most significant factor in keeping the current losses at bay, this may partly be justified. For simplicity we will initially again consider $R_L(t)$ to be fixed. The optimal control problem that we will consider in this subsection is as follows:

$$\text{minimize} : S(t_f, x(t_f)) + \int_{t_0}^{t_f} L(t, x(t), u(t)) \, dt$$
$$\text{subject to} : \dot{x}(t) = f(t, x(t), u(t)); \quad x(0) = x_0,$$
$$g_k(t, x(t), u(t)) \leq 0, \quad k = 1 \ldots n_g. \tag{4.41}$$

This leads to a very similar optimal control problem as in (4.1), where we again have that:

$$S(t_f, x(t_f)) = 0$$
$$L(t, x(t), u(t)) = -\frac{1}{R_L + u(t)} x^2(t)$$
$$f(t, x(t), u(t)) = \frac{nC_{ind} \, u(t) - 1}{C_L(R_L + u(t))} x(t), \tag{4.42}$$

now only accompanied with the mixed SVICs:

$$g_1(t, x(t), u(t)) = -u(t)$$
$$g_2(t, x(t), u(t)) = u(t) - M_R$$
$$g_3(t, x(t), u(t)) = \frac{u(t)}{R_L + u(t)} x(t) - M_U. \tag{4.43}$$

70

Note that whereas the input restriction $u(t) \in [0, M_R]$ first only surfaced in the minimization of the Hamiltonian, it is now captured in the state constraints $g_1(\cdot)$ and $g_2(\cdot)$.

Given the above optimization problem we can use Theorem 3.33, accompanied with Remark 3.34 from [2], to provide an extended version of Pontryagin's Minimum Principle (see Theorem 4.1.1).

Theorem 4.2.1 (Minimum Principle with Mixed Inequality Constraints ([2]))**.** Consider the optimal control problem (4.41), with fixed initial time $t_0 = 0$ and fixed final time $t_f = T$, and where $L(\cdot)$, $f(\cdot)$, and $g(\cdot)$ are continuous and have continuous first partial derivatives with respect to (t, x, u) on $[0, T] \times \mathbb{R}^{n_x} \times \mathbb{R}^{n_u}$. Suppose that $u_* \in \hat{\mathcal{C}}[0, T]^{n_u}$ is a minimizer for the problem, and let $x_* \in \hat{\mathcal{C}}^1[0, T]^{n_x}$, continuous at each instant t of continuity of u_*, be the optimal response. Furthermore suppose that the constraint qualification

$$rank \begin{bmatrix} \frac{\partial g(\cdot)}{\partial u} & diag(g(\cdot)) \end{bmatrix} = n_g$$

holds along (t, x_*, u_*) $\forall t \in [0, T]$, i.e. the gradients with respect to u of all the active constraints $g(\cdot) \leq 0$ must be linearly independent.

Define the Hamiltonian and Lagrangian function by

$$\mathcal{H}(t, x, u, \lambda_0, \lambda) = \lambda_0\ L(t, x, u) + \lambda^{\mathrm{T}} f(t, x, u) \tag{4.44}$$

$$\mathcal{L}(t, x, u, \lambda_0, \lambda, \mu) = \mathcal{H}(t, x, u, \lambda) + \mu^{\mathrm{T}} g(t, x, u). \tag{4.45}$$

We then have that:

There exist $(\lambda_0, \lambda_*) \in \hat{\mathcal{C}}^1[0, T]^{n_x+1}$ and $\mu_* \in \hat{\mathcal{C}}[0, T]^{n_g}$, each continuous at each instant t of continuity of u_*, such that:

1. $(\lambda_0, \lambda_*(t), \mu_*(t)) \neq 0, \quad \lambda_0 = \text{constant} \geq 0$

2. $u_*(t) \in \text{argmin}_{v \in \mathbb{R}^{n_u}} \{\mathcal{H}(t, x_*(t), v, \lambda_0, \lambda_*(t)) : g(t, x_*(t), v) \leq 0\}$

3.

$$\begin{cases} \dot{x}_*(t) &= \frac{\partial \mathcal{L}(t, x_*(t), u_*(t), \lambda_0, \lambda_*(t), \mu_*(t))}{\partial \lambda}, & x_*(0) = x_0 \\ \dot{\lambda}_*(t) &= -\frac{\partial \mathcal{L}(t, x_*(t), u_*(t), \lambda_0, \lambda_*(t), \mu_*(t))}{\partial x}, & \lambda_*(T) = \frac{\partial S(T, x_*(T))}{\partial x} \\ 0 &= \frac{\partial \mathcal{L}(t, x_*(t), u_*(t), \lambda_0, \lambda_*(t), \mu_*(t))}{\partial u}. \end{cases}$$

4. $\mu_*(t)^{\mathrm{T}} g(t, x_*(t), u_*(t)) = 0, \quad \mu_*(t) \geq 0$

Furthermore, if t_f is free we have that

$$\mathcal{H}(t, x_*(t), v, \lambda_0, \lambda_*(t)) = -\int_t^{t_{f_*}} \frac{\partial \mathcal{L}(\tau, x_*(\tau), u_*(\tau), \lambda_*(\tau), \mu_*(\tau))}{\partial t}\ d\tau,$$

so that for this case in particular

$$\mathcal{H}(t_{f_*}, x_*(t_{f_*}), u_*(t_{f_*}), \lambda_0, \lambda_*(t_{f_*})) = 0.$$

∎

In the above theorem we have used $\hat{\mathcal{C}}$ to denote piecewise continuous functions, and likewise we used $\hat{\mathcal{C}}^1$ to denote piecewise continuously differentiable functions. Note that the intervals of continuity for all these functions are described by the intervals of continuity of $u_*(t)$. Furthermore, in autonomous systems the Hamiltonian function $\mathcal{H}(\cdot)$ will be constant over time. For these systems, if $\lambda_0 > 0$, the functions $\lambda_{i_*}(t), i = 1 \ldots n_x$ are defined up to a common multiple. This is known as the 'normal case'. In this case it is common practice to normalize the adjoint variables by taking $\lambda_0 \equiv 1$. On the other hand, the 'abnormal case' is given by $\lambda_0 \equiv 0$, which is abnormal in the sense that the necessary conditions of optimality become independent of the cost functional ([2]). We will assume throughout this section that we are dealing with the normal case, and set $\lambda_0 \equiv 1$.

Plugging in the given functions $S(\cdot)$, $L(\cdot)$, $f(\cdot)$ and $g(\cdot)$ into (4.44) and (4.45), we find that the Hamiltonian and Lagrangian are given by

$$\mathcal{H}(x(t), u(t), \lambda(t)) = -\frac{1}{R_L + u(t)}x^2(t) + \lambda(t)\frac{nC_{ind}\ u(t) - 1}{C_L(R_L + u(t))}x(t)$$

$$\mathcal{L}(x(t), u(t), \lambda(t), \mu(t)) = -\frac{1}{R_L + u(t)}x^2(t) + \lambda(t)\frac{nC_{ind}\ u(t) - 1}{C_L(R_L + u(t))}x(t)$$
$$- \mu_1(t)u(t) + \mu_2(t)\left(u(t) - M_R\right) + \mu_3(t)\left(\frac{u(t)}{R_L + u(t)}x(t) - M_U\right),$$

which lead to the following necessary conditions for optimality

$$u_*(t) \in \text{argmin}_{v \in [0, M_R]}\left\{-\frac{1}{R_L + v}x^2(t) + \lambda(t)\frac{nC_{ind}\ v - 1}{C_L(R_L + v)}x(t) : \frac{v}{R_L + v}x(t) \leq M_U\right\},$$
$$\forall t \in [0, T] \tag{4.46}$$

$$\dot{x}_*(t) = \frac{nC_{ind}\ u_*(t) - 1}{C_L(R_L + u_*(t))}x_*(t), \qquad x_*(0) = x_0 \tag{4.47}$$

$$\dot{\lambda}_*(t) = \frac{2}{R_L + u_*(t)}x_*(t) - \lambda_*(t)\frac{nC_{ind}\ u_*(t) - 1}{C_L(R_L + u_*(t))} - \mu_{3_*}(t)\frac{u_*(t)}{R_L + u_*(t)}, \qquad \lambda_*(T) = 0 \tag{4.48}$$

$$0 = \frac{1}{(R_L + u_*(t))^2}{x_*}^2(t) + \lambda_*(t)\frac{nC_{ind}R_L + 1}{C_L\left(R_L + u_*(t)\right)^2}x_*(t)$$
$$- \mu_{1_*}(t) + \mu_{2_*}(t) + \mu_{3_*}(t)\frac{R_L}{(R_L + u_*(t))^2} \tag{4.49}$$

$$0 = -\mu_{1_*}(t)u_*(t) + \mu_{2_*}(t)\left(u_*(t) - M_R\right) + \mu_{3_*}(t)\left(\frac{u_*(t)}{R_L + u_*(t)}x(t) - M_U\right),$$
$$\mu_{1_*}(t) \geq 0,\ \mu_{2_*}(t) \geq 0,\ \mu_{3_*}(t) \geq 0. \tag{4.50}$$

We can see that the necessary optimality conditions (4.46)–(4.50) become rather lengthy, which is also in agreement with [2] that these problems are notoriously hard to solve. This also motivates the fact that in practise some priory assumptions can be made in order to apply Theorem 4.2.1, as described in [2]:

> "In practice, applying Theorem 3.33 (and Remark 3.34) requires that an assumption be made a priori on the sequence of (unconstrained and constrained) arcs in the optimal solution, as well as on the set of active (inequality) terminal constraints. Then, based on the postulated structure of the optimal solution, one shall check whether a pair $(u(\cdot), x(\cdot))$, along with vector functions $\tilde{\lambda}(\cdot)$, $\mu(\cdot)$, and Lagrange multiplier vectors ν^*, ζ^*, can be found such that all of the necessary conditions of

optimality are satisfied. If this is the case, then the corresponding control is a candidate optimal control for the problem; otherwise, one needs to investigate alternative solution structures, i.e., postulate different sequences of arcs and/or sets of active terminal constraints."

we remark that the Lagrange multiplier vectors ν^*, ζ^* in the above quote are part of an extension to general state terminal constraints. In the optimization problem under study in this section these do not play a role.

At first we will also pursue the approach from the above quote. In particular, we will investigate whether the intuitive optimal controller from section 3.3.2 (see also Figure 3.8) holds. Based on this intuitive optimal controller and the results from Pontryagin's classical minimum principle (see subsection 4.1.1), we introduce the candidate optimal controller:

$$u_*(t) = \begin{cases} M_R & \text{if } t \in [0, t_1] \\ \frac{R_L M_U}{x_*(t) - M_U} & \text{if } t \in (t_1, t_2] \\ 0 & \text{if } t \in (t_2, T]. \end{cases} \tag{4.51}$$

Clearly this candidate optimal solution consists of three stages. The underlying idea here is that initially we expect that maximally charging (by choosing $u_*(t) = M_R$) is our best choice. Note that this idea is also supported in the previous subsection by the results of Pontryagin's Minimal Principle without SVICs. If we would continue with this approach however, after some time the induction voltage constraint will be violated. From the moment this tends to happen we therefore shift to our seemingly second best option; maximally charging with respect to the induction voltage constraint, so that $u_*(t)$ moves along $g_3(\cdot) = 0$, which results in the second input case in (4.51). At last, when the end time is approaching, one can make the best of the remaining time by quickly harvesting as much charges/current as possible, i.e. by choosing $u_*(t) = 0$. The latter is also motivated from our previous results, using Pontryagin's Minimal Principle without SVICs.

Upon close inspection of equations (4.46)–(4.50) we find that a solution can be found using this candidate optimal solution, but even more interesting, we can show that the candidate optimal solution is also unique for almost all t.

4.2.1 Solving (4.46)–(4.50)

At first, from the fact that the Hamiltonian is unchanged, we can use our previous argument (i.e. $\frac{\partial H}{\partial u} \neq 0$ for feasible u, see also (4.6)) to show that the input minimizing the Hamiltonian is always a boundary case; i.e. $u_*(t) \in \left\{ 0, \frac{R_L M_U}{x_*(t) - M_U}, M_R \right\}$.

If we then start backwards in time with the condition $\lambda_*(T) = 0$, it follows from the minimization condition (4.46) that we need to start with $u_*(t) = 0$ at the end time $t = T$. Note that this is not in violation with the additional mixed SVIC of $g_3(\cdot)$. For this input the condition (4.50) then gives us

$$0 = -M_R \mu_{2_*}(t) - M_U \mu_{3_*}(t).$$

Since we need that $\mu_{i_*} \geq 0$ where $i \in \{1, 2, 3\}$, the input $u_*(t) = 0$ implies that $\mu_{2_*}(t) = \mu_{3_*}(t) = 0$. In turn, for this input we then obtain from (4.49):

$$\mu_{1_*}(t) = \frac{1}{R_L{}^2} x_*{}^2(T^-) + \lambda_*(t) \frac{n C_{ind} R_L + 1}{C_L R_L{}^2} x_*(t). \tag{4.52}$$

Since we have that $\lambda_*(T) = 0$ and that the state variable $x_*(t)$ is always positive (as shown by (4.9)), we can already see that $\mu_{1_*}(T) > 0$. That we also have that $\mu_{1_*}(t) \geq 0$ when going further back in time can also be shown to follow from (4.52). Due to positive constants and a positive x_*, the condition $\mu_{1_*}(t) \geq 0$ boils down to whether

$$x_*(t) + \lambda_*(t) \frac{nC_{ind}R_L + 1}{C_L} \geq 0. \tag{4.53}$$

Interestingly this is similar to the 'switching law' from (4.10), and from this observation we shall soon show that $\mu_{1_*}(t)$ in (4.52) is indeed positive. At last note that the condition $\mu_{3_*}(t) = 0$ result in the fact that equations (4.47) and (4.48) are equivalent to the regular Pontryagin problem.

Switching from $u_*(t) = 0$

For now we thus see that backwards in time the optimal control problem initially behaves equivalent to the regular Pontryagin problem without mixed SVICs. As a next step we need to check whether, and if so when, the minimization of the Hamiltonian is taken over by another control when going further back in time. In (4.10) we already deduced a switching condition corresponding to

$$\mathcal{H}(x_*(t), 0, \lambda_*(t)) < \mathcal{H}(x_*(t), M_R, \lambda_*(t)), \tag{4.54}$$

however when $x_*(t)$ is sufficiently large the control $u_*(t) = M_R$ may violate the mixed SVIC $g_3(\cdot)$. Since this condition now also gives us a boundary control we will also check when

$$\mathcal{H}(x_*(t), 0, \lambda_*(t)) < \mathcal{H}\left(x_*(t), \frac{R_L M_U}{x_*(t) - M_U}, \lambda_*(t)\right). \tag{4.55}$$

Let us assume that $x_*(t) > M_U$ whenever we consider the control $u_*(t) = \frac{R_L M_U}{x_*(t) - M_U}$. If we then define

$$\widetilde{M}(x_*(t)) := \frac{R_L M_U}{x_*(t) - M_U},$$

we can see that $\widetilde{M}$ as a function of x_* is always positive. Since however in the deduction of (4.10) one can find that the constant M can be divided out, under the made assumption we will obtain the same switching law in (4.54) and (4.55). That is, we need to stick with $u_*(t) = 0$ as long as

$$\lambda_*(t) + \frac{C_L}{1 + nC_{ind}R_L} x_*(t) > 0. \tag{4.56}$$

Interestingly, in the time instant that equality is reached in the switching law, the Hamiltonian becomes independent of the control $u_*(t)$, as one may verify that:

$$\mathcal{H}\left(x_*(t), u_*(t), \left[-\frac{C_L}{1 + nC_{ind}R_L} x_*(t)\right]\right) = -\frac{nC_{ind}}{1 + nC_{ind}R_L} x_*^2(t).$$

Once the sign in (4.56) changes however, the Hamiltonian will again be dependent on the control, since we find that

$$\mathcal{H}\left(x_*(t), u_*(t), \left[-\frac{C_L}{1 + nC_{ind}R_L} x_*(t) - \epsilon\right]\right) = -\frac{nC_{ind}}{1 + nC_{ind}R_L} x_*^2(t) - \epsilon \frac{nC_{ind}\, u_*(t) - 1}{C_L(R_L + u_*(t))} x_*(t). \tag{4.57}$$

From the above expression we can see that minimizing the Hamiltonian then boils down to maximizing

$$\frac{nC_{ind}\, u_*(t) - 1}{C_L(R_L + u_*(t))} x_*(t), \tag{4.58}$$

which curiously enough is precisely the expression defining the differential equation of the state x_*; equation (4.47). For bounded, positive u_* this expression can be seen to be maximized for the upper bound of u_*, maximally reaching $\frac{nC_{ind}}{C_L} x_*(t)$ in the limit $u_* = \infty$. To formally prove this claim one may check that when we take the partial derivative to u_* we obtain:

$$\frac{nC_{ind}R_L + 1}{C_L\left(R_L + u_*(t)\right)^2} x_*(t),$$

which is never zero for positive, bounded u_*. Therefore the maximum will occur at the boundary of u_*. As we furthermore see that the computed partial derivative is always positive, we have that (4.58) as a function of u_* is strictly monotonically increasing, causing the maximum to occur for the upper bound of u_*.

We thus need to choose u_* as large as possible in order to maximize (4.58), and consequently minimize (4.57). This may also be compared to the somewhat previous result where we found that maximal charging is achieved when the gate resistor R_g is as large as possible (e.g. see (3.75)).

Due to the mixed SVIC $g_3(\cdot)$ we can however not always choose $u_* = M_R$, as for large x_* this would violate the constraint. The maximum value of u_* we can take while not violating $g_3(\cdot)$ is thereby on x_* in the following way:

$$u_*(t) = \begin{cases} M_R & \text{if } x_*(t) \in \left(0, M_U \frac{M_R + R_L}{M_R}\right] \\ \frac{R_L M_U}{x_*(t) - M_U} & \text{if } x_*(t) \in \left(M_U \frac{M_R + R_L}{M_R}, M_U(nC_{ind}R_L + 1)\right). \end{cases} \tag{4.59}$$

Note that we did not set the latter upper bound for $x_*(t)$ to ∞, since we have shown in (3.75) that x_* only increases when $u_*(t) = R_g(t) > \frac{1}{nC_{ind}}$. Upon solving

$$\frac{R_L M_U}{x_*(t) - M_U} = \frac{1}{nC_{ind}},$$

for $x_*(t)$ we therefore conclude that the maximum value the target voltage can obtain is $x_*(t) = M_U(nC_{ind}R_L + 1)$. Furthermore one may check that the condition $M_R > \frac{1}{nC_{ind}}$ guarantees that the latter interval in (4.59) is properly defined (in the sense that the lower bound is smaller than the upper bound). Note that the assumption $M_R > \frac{1}{nC_{ind}}$ is also quite natural, as otherwise we would not be able to charge the system.

Inspired on our initial guess for the optimal control (4.51) and assuming that the end time T is sufficiently large, we first consider the case that $x_*(t) \in \left(M_U \frac{M_R + R_L}{M_R}, M_U(nC_{ind}R_L + 1)\right)$ when the discussed switch of control occurs. The idea here being that in the time window $[0, t_s]$, $x_*(t)$ has increased to such an extend that the control $u_* = M_R$ would violate the mixed SVIC $g_3(\cdot)$.

Switching to $u_*(t) = \frac{R_L M_U}{x_*(t) - M_U}$

Given the input $u_*(t) = \frac{R_L M_U}{x_*(t) - M_U}$, equation (4.50) results in

$$0 = -\mu_{1_*}(t)\frac{R_L M_U}{x_*(t) - M_U} + \mu_{2_*}(t)\left(\frac{R_L M_U}{x_*(t) - M_U} - M_R\right) \qquad \Longleftrightarrow$$

$$\mu_{1_*}(t) = \mu_{2_*}(t)\left(1 - \frac{M_R}{R_L M_U}(x_*(t) - M_U)\right),$$

whereas $\mu_{3_*}(t) \geq 0$ remains free with respect to this condition. Due to the constraint $\mu_{1_*}, \mu_{2_*} \geq 0$ it follows that $\mu_{1_*} = \mu_{2_*} = 0$ whenever $\left(1 - \frac{M_R}{R_L M_U}(x - M_U)\right)$ is negative. That this is indeed the case can be verified from the interval condition of $x_*(t)$ in (4.59). Continuing with equation (4.49), we then find that

$$\mu_{3_*}(t) = -\frac{1}{R_L}x_*^2(t) - \lambda_*(t)\frac{nC_{ind}R_L + 1}{C_L R_L}x_*(t). \qquad (4.60)$$

Analogous to the $u_*(t) = 0$ case where we checked whether $\mu_{1_*} \geq 0$ holds in (4.52), we now need to check whether the condition $\mu_{3_*}(t) \geq 0$ still holds in the above equation. Similar to the derivation of (4.53) we thereby find that due to the positive constants and positive x_*, the condition $\mu_{3_*}(t) \geq 0$ now boils down to whether

$$x_*(t) + \lambda_*(t)\frac{nC_{ind}R_L + 1}{C_L} \leq 0. \qquad (4.61)$$

Again the switching law, i.e. (4.56), confirms that will be the case when $u_*(t) = \frac{R_L M_U}{x_*(t) - M_U} \neq 0$. Having established valid multipliers μ_{i_*}, $i = 1\ldots 3$ in the $u_*(t) = \frac{R_L M_U}{x_*(t) - M_U}$ case, we will now turn our attention to the state and costate differential equations, as described by (4.47) and (4.48). Substituting $u_*(t) = \frac{R_L M_U}{x_*(t) - M_U}$ and $\mu_{3_*}(t)$ according to (4.60) in these equations, and a bit of reordering thereby results in:

$$\dot{x}_*(t) = -\frac{1}{C_L R_L}x_*(t) + \frac{M_U(nC_{ind}R_L + 1)}{C_L R_L} \qquad (4.62)$$

$$\dot{\lambda}_*(t) = \frac{M_U + 2}{R_L}x_*(t) + \frac{M_U(nC_{ind}R_L + 1) + 1}{C_L R_L}\lambda_*(t) - \frac{M_U(nC_{ind}R_L + 1)}{C_L R_L}\frac{\lambda_*(t)}{x_*(t)} - 2\frac{M_U}{R_L}. \qquad (4.63)$$

Unfortunately, unlike the regular Pontryagin problem (see (4.15) and (4.40)), we now stumble upon a set of non-linear differential equations. However, (4.62) on itself is just an ordinary differential equation. Also, one may note that the state interval restriction from (4.59) in the $u_*(t) = \frac{R_L M_U}{x_*(t) - M_U}$ case, provides us with the fact that $\dot{x}_*(t)$ is always positive for this optimal control case.

It is not too hard (see Appendix section A.6) to show that the solution of (4.62) is given by

$$x_*(t) = ce^{-\frac{1}{C_L R_L}t} + M_U(nC_{ind}R_L + 1),$$

where constant c needs to be determined from a given initial condition. While solving (4.46)-(4.50) backwards in time, this can for instance be provided by the state value at the switching instant of $u_*(t) = 0$ to $u_*(t) = \frac{R_L M_U}{x_*(t) - M_U}$ or $u_*(t) = M_R$. Let us call this instant t_2, analogous to the notation of our initial optimal control guess (4.51). We then find that

$$x_*(t) = (x_*(t_2) - M_U(nC_{ind}R_L + 1))\,e^{\frac{1}{C_L R_L}(t_2 - t)} + M_U(nC_{ind}R_L + 1). \qquad (4.64)$$

76

Even though we can find a solution for $x_*(t)$ in this optimal control case, finding a solution to $\lambda_*(t)$ satisfying (4.63) is a more challenging task. For this we suggest the use of numeric computational software like Matlab.

Like in the regular Pontryagin problem, we would like to know whether, after the switch from $u_*(t) = 0$, we encounter the switching condition again. Again we will inspect the derivative of the switching function for this purpose. Thereby we find that

$$\dot{g}_*(t) = \dot{\lambda}_*(t) + \frac{C_L}{1 + nC_{ind}R_L}\dot{x}_*(t)$$

which after plugging in (4.62) and (4.63) and some reordering results in:

$$\dot{g}_*(t) = \frac{1}{R_L}\left[\left(2 + M_U - \frac{1}{1 + nC_{ind}R_L}\right)x_*(t) + \frac{1}{C_L}\left(1 + M_U(1 + nC_{ind}R_L)\left(1 - \frac{1}{x}\right)\right)\lambda_*(t) - M_U\right].$$

Furthermore, when we then plug in $\lambda_*(t) = -\frac{C_L}{1+nC_{ind}R_L}x_*(t)$, corresponding to the switching moment, we get:

$$\dot{g}_*(t_s{}^-) = \frac{2nC_{ind}}{1 + nC_{ind}R_L}x_*(t_s{}^-) > 0.$$

This allows us to conclude that the initial switch in input from $u_*(t) = 0$ is properly defined. What we thereby mean to say is that neither $g(t) = 0$ remains constant, nor that we 'bounce back' to $g(t) > 0$ when going further back in time. Furthermore, note that this result holds at each moment we reach $g(t) = 0$, making it impossible to switch back to $u_*(t) = 0$, as for this we would need that $g(t) > 0$.

Having switched to the input $u_*(t) = \frac{R_L M_U}{x_*(t) - M_U}$, we observed that $\dot{x}_*(t) > 0$ for those state values that are possible with this input (see (4.59)). This implies that, when going further back in time, $x_*(t)$ will decrease to the point that $x_*(t) = M_U\frac{M_R + R_L}{M_R}$. As this happens we know from (4.59) that we need to switch to $u_*(t) = M_R$ in order to minimize the Hamiltonian while not violating the constrains $g_i(\cdot)$.

Therefore, in what follows we will investigate the solution to (4.46)-(4.50) in the case that $u_*(t) = M_R$. Note that this optimal control case can also present itself directly after the switch from $u_*(t) = 0$, thereby skipping the $u_*(t) = \frac{R_L M_U}{x_*(t) - M_U}$ case. This would be the case when $x_*(t) \in \left(0, M_U\frac{M_R + R_L}{M_R}\right]$ at the moment of the initial switch from $u_*(t) = 0$.

Switching to $u_*(t) = M_R$

It will turn out that solving the multipliers $\mu_{i_*}(t)$ for the input $u_*(t) = M_R$ will present very similar results as when solving these multipliers for the input $u_*(t) = \frac{R_L M_U}{x_*(t) - M_U}$. Again we start with the condition (4.50), which for the input $u_*(t) = M_R$ reads

$$0 = -\mu_{1_*}(t)M_R + \mu_{3_*}(t)\left(\frac{M_R}{M_R + R_L}x_*(t) - M_U\right) \qquad \Longleftrightarrow$$

$$\mu_{1_*}(t) = \mu_{3_*}(t)\left(\frac{1}{M_R + R_L}x_*(t) - \frac{M_U}{M_R}\right),$$

whereas $\mu_{2_*}(t) \geq 0$ remains free with respect to this condition. Due to the constraint $\mu_{1_*}, \mu_{3_*} \geq 0$ it follows that $\mu_{1_*} = \mu_{3_*} = 0$ whenever $\left(\frac{1}{M_R + R_L}x_*(t) - \frac{M_U}{M_R}\right)$ is negative. That this is indeed

the case can be verified from the interval condition of $x_*(t) \in \left(0, M_U \frac{M_R+R_L}{M_R}\right)$ (see 4.59)). Continuing with equation (4.49), we then find that

$$\mu_{2_*}(t) = -\frac{1}{(R_L + M_R)^2} x_*^2(t) - \lambda_*(t) \frac{nC_{ind}R_L + 1}{C_L (R_L + M_R)^2} x_*(t). \tag{4.65}$$

Also now we need to check whether the condition $\mu_{2_*}(t) \geq 0$ still holds in the above equation. Since the constants and the state x_* are all positive, this question boils down to whether

$$x_*(t) + \lambda_*(t) \frac{nC_{ind}R_L + 1}{C_L} \leq 0.$$

Yet again the switching law, i.e. (4.56), confirms that will be the case when $u_*(t) = M_R \neq 0$. Now only the differential equation for the state x_* and costate λ_* remain, i.e. equations (4.47) and (4.48). However, given the fact that $u_*(t) = M_R$ and $\mu_{3_*}(t) = 0$, these equations are equal to the regular Pontryagin problem, which is discussed in the previous two sections.

Summary of the optimal control results

Combining the results in this section, we have deduced the optimal control strategy for the extended optimal control problem having mixed SVICs, i.e. (4.41)-(4.43). This was done on the basis of Theorem 4.2.1, which resulted in the equations (4.46)-(4.50). Note that the rank condition of the theorem is met, as at each point in time only 1 of the constraints $g_i(\cdot)$ is active. We also remark that we did not always mention the corresponding solution to the optimal state (x_*) and costate (λ_*). However, we found that most of these solutions are equivalent to those discussed in section 4.1. Only the state/co-state differential equations from (4.62) and (4.63) are an exception here. Whereas the solution to the state differential equation is discussed in this section (see (4.64)), we recommend a numeric solver to solve (4.63), since this is a non-linear differential equation.

Similar to the results in the previous two sections we can again see that the optimal control is dependent on the final time T. For example, from (4.19) we find that if $T < \widetilde{t_2} = \frac{C_L R_L}{2} \ln\left(1 + \frac{1}{nC_{ind}R_L}\right)$, it is optimal to only harvest the initial charge x_0 by choosing $u_*(t) = 0$. In this case the state and costate are described by (4.17). Here x_T can be solved from the initial condition $x_*(0) = x_0$, from which we find that $x_T = x_0 e^{-\frac{1}{C_L R_L}T}$.

In case the end time T is larger it pays of to initially charge the system maximally, choosing $u_*(t) = M_R$. However, taking $u_*(t) = M_R$ can only be done for a limited amount of time, as otherwise the maximal voltage on the induction rings are exceeded. From the state and costate equation of (4.24), this maximal time may be calculated from:

$$x_0 e^{\frac{nC_{ind}M_R-1}{C_L(R_L+M_R)}t_1} = M_U \frac{M_R + R_L}{M_R} \qquad \Longleftrightarrow$$

$$t_1 = \frac{C_L(R_L + M_R)}{nC_{ind}M_R - 1} \ln\left(\frac{M_U(M_R + R_L)}{x_0 M_R}\right).$$

Thereby we find that if $T \in [\widetilde{t_2}, t_1 + \widetilde{t_2}]$ the optimal strategy is to choose $u_*(t) = M_R$ for $t \in [0, T - \widetilde{t_2})$ and to choose $u_*(t) = 0$ for $t \in [T - \widetilde{t_2}, T]$. The state and costate equations for this case are described by (4.24) for the first part, and by (4.17) for the latter part. In these equations the constants p_0 $(:=\lambda_0)$ and x_T can again be determined from the initial conditions x_0 and $p_T = 0$ $(:=\lambda_T = 0)$. If we adopt the notation $t_2 = T - \widetilde{t_2}$, so that the final switch to

$u_*(t) = 0$ occurs at $t = t_2$, this solution is given by (4.25), with only the notational difference $t_2 := t_s$.

At last we consider the case that $T > t_1 + \widetilde{t_2}$. In this case we have more time to charge the system, but at $t = t_1$ we need to 'throttle back' the input $u_*(t)$ to $\frac{R_L M_U}{x_*(t) - M_U}$ so that we do not exceed the maximal voltage on the induction rings. Given this input, the state and costate differential equations are given by (4.62) and (4.63). Whereas the solution to the state differential equation can be solved in an exact manner (see (4.64)), we recommend the use of a numeric solver like matlab to solve (4.63).

To sum up our results, let us illustrate the solution to the necessary conditions of (4.46)-(4.50) for the case that T is sufficiently large, i.e. $T > t_1 + \widetilde{t_2}$. The optimal control is then consists of 3 segments, as illustrated in table 4.1.

Interval t	Optimal Control $u_*(t)$	Optimal State $x_*(t)$	Optimal Co-state $\lambda_*(t)$
$[0, t_1)$	M_R	$x_0 e^{ct}$	$x_0 \frac{d}{2c}\left(e^{ct} - e^{-ct}\right) + \lambda_0 e^{-ct}$
$[t_1, t_2)$	$\frac{R_L M_U}{x_*(t) - M_U}$	$(x_*(t_2) - \beta) e^{a(t_2 - t)} + \beta$	solution of (4.63)
$[t_2, T]$	0	$x_T e^{a(T-t)}$	$x_T \frac{b}{2a}\left(e^{-a(T-t)} - e^{a(T-t)}\right)$

Table 4.1: The optimal control strategy when $T > t_1 + \widetilde{t_2}$. Note that we adopted the a, b, c, d notation of (4.15). Furthermore we introduced the constant $\beta := M_U(1 + nC_{ind}R_L)$.

Working our way backwards we may solve the unknown constants x_T and λ_0. We will illustrate this for x_T, whereas we would need to know the explicit solution of (4.63) to solve λ_0. When we plug in $x_*(t_2)$ from the third row into the second row, we obtain

$$x_*(t) = \left(x_T e^{aT} - \beta e^{at_2}\right) e^{-at} + \beta.$$

for $t \in [t_1, t_2)$, i.e. when $u_*(t) = \frac{R_L M_U}{x_*(t) - M_U}$. At $t = t_1$ this must be equal to $x_*(t_1^-)$ from the first row. Thereby we find that

$$x_0 e^{ct_1} = \left(x_T e^{aT} - \beta e^{at_2}\right) e^{-at_1} + \beta \qquad \Longleftrightarrow$$

$$x_T = e^{-aT}\left(x_0 e^{(a+c)t_1} + \beta\left(e^{at_2} - e^{at_1}\right)\right).$$

The multipliers that correspond to the solution from table 4.1 are shown in the table below.

Interval t	Multipliers $\mu_{1_*}(t)$	$\mu_{2_*}(t)$	$\mu_{3_*}(t)$
$[0, t_1)$	0	$-\alpha_1 x_*^2(t) - \alpha_2 x_*(t)\lambda_*(t)$	0
$[t_1, t_2)$	0	0	$-\alpha_3 x_*^2(t) - \alpha_4 x_*(t)\lambda_*(t)$
$[t_2, T]$	$\alpha_5 x_*^2(t) + \alpha_6 x_*(t)\lambda_*(t)$	0	0

Table 4.2: Multipliers $\mu_{i_*}, i = 1 \ldots 3$ corresponding to solution from table 4.1.

Where the constants $\alpha_i, i = 1 \ldots 6$ from table 4.2 are given by

$$\alpha_1 = \frac{1}{(R_L + M_R)^2} \qquad \alpha_3 = \frac{1}{R_L} \qquad \alpha_5 = \frac{1}{R_L{}^2}$$

$$\alpha_2 = \frac{nC_{ind}R_L + 1}{C_L(R_L + M_R)^2} \qquad \alpha_4 = \frac{nC_{ind}R_L + 1}{C_L R_L} \qquad \alpha_6 = \frac{nC_{ind}R_L + 1}{C_L R_L{}^2}.$$

To conclude we have shown that the optimal control for the problem (4.41)-(4.43) is dependent on the end time T. If T is very small it is optimal to only harvest the initial charge x_0. For a slightly larger value of T it is optimal to first maximally charge the system, only to maximally harvest the accumulated charges at the end. At last, if T is sufficiently large the situation is similar to the last, only at $t = t_1$ the control needs to be 'throttled back' so that the constraint concerning the maximal induction ring voltage is not violated.

At last we would like to mention how the optimal control problem could benefit when we consider a variable load resistor R_L. As we have seen in the previous section, initially choosing $R_L = 0$ will be the best choice in order to maximally charge the system. This may also be evident from the state differential equation, as the derivative is maximized when $R_L = 0$ while R_g needs to be as large as possible.

Also in the second stage of the optimal control solution, i.e. when $u_*(t)$ needs to be 'throttled back' (see the interval $[t_1, t_2)$ from table 4.1), a variable load resistor R_L may be put to good use. At first, from (4.59) we find that increasing R_L can delay the moment that we need to 'throttle back' our input. Furthermore, from (3.65) and (3.65) one can find that under the assumed symmetrical conditions the equilibrium for the target voltage is given by:

$$\widehat{U_1} = (1 + nC_{ind}R_L)\, U_{R_g}.$$

Thereby we see that increasing R_L allows for a higher equilibrium of the target voltage U_1, while keeping the induction voltage U_{R_g} at its maximum. On its turn a higher target voltage will cause the output power to increase, as we have shown in (3.79).

Chapter 5

Conclusions and recommendations

5.1 Conclusions

The main topic of this thesis is Kelvins water dropper. A ballistic version of this system has previously been presented in [18]. There it is shown from a practical setup that the system can be used to harvest electrical energy, as the kinetic energy from the droplets is converted into electrical energy, with measured efficiencies of up to 18 %. Article [18] also describes that the behaviour of the system can be analyzed on the basis of an equivalent electrical network.

On the basis of this observation, the Kelvin system has been further analyzed from a mathematical background. Thereby the inductive model from [18] is extended so that charge losses to the induction rings are also included in the model. These losses occur when the induced charge of the droplets becomes too high, causing droplets to deflect in their trajectory to the target. We find that by incorporating these losses an extra stable equilibrium solution arises in the system, which occurs when the amount of charge losses is equal to the amount of charge induction. Furthermore, we show that the differential equation that is obtained for a symmetrical system can be solved explicitly.

Besides analyzing the Kelvin system, we have also investigated whether the Kelvin system can be controlled, and if so how this can be done in an optimal way. For this purpose we have investigated the system where the induction voltages provide the input, as well as the system in which the resistors are variable and form the input. Especially this last choice of input we found promising, since we found that the resistors have a direct impact on the charging behaviour of the system. Therefore the choice of variable resistors has been explored in our quest of finding an optimal control for the system.

For the above optimal control problem we have mainly considered the well-known Minimum Principle from Pontryagin. As cost criterion we hereby choose to the output power over a fixed time window, which will be maximized.
We have shown that the necessary conditions that are obtained from the Minimum Principle can be solved. Thereby the necessary conditions indicate that the optimal way of controlling the system is dependent on the total amount of time. If we consider the end time to be sufficiently large, it turns out that we initially need to charge the system as much as is possible. That is, in case we do not consider a maximal induction voltage restriction to keep current losses at bay, the maximal way of doing so is simply given by the maximal value of R_g. In the case that we do consider a maximal induction voltage restriction, the maximal way of charging the system is to maximize R_g with respect to this additional restriction.

At last, in all cases it turns out that close to the end time, it is optimal to de-charge the system by choosing $R_g = 0$, so that in this last time window most of the (accumulated) charges can be harvested.

5.2   Recommendations

The work that is presented in this thesis has many opportunities for further study. At first, the assumptions that were made to analyze the Kelvin system may be investigated. For instance, one may check whether similar results can be obtained if we would have considered a slightly different electrical network to model the systems behaviour.

As in most of the studied examples from this thesis, we assumed that we are dealing with a symmetrical setup. Thereby one may still investigate the implications of a non-symmetrical setup. As a part of this, one may for instance investigate whether small deviations in internal constants of the model, also result in only slight deviations of the model behaviour.
The assumption of a symmetrical setup has, in some sections of this thesis, also served as a motivation to consider the study of 1-dimensional systems instead of 2-dimensional systems. For further research, one may for instance also look for a solution to the 2-dimensional non-linear system equation from (3.3) instead of its one dimensional counterpart. This 2-dimensional system equation may also be used in the optimal control problem we considered.

Furthermore, the optimal control problem that is discussed in chapter 4 can also be continued in many ways. For instance, the Pontryagin equations for the 2 resistor input case with mixed State Variable Inequality Constraints (SVICs) still needs to be investigated. Also one may pursue a broader optimal control problem that includes pure SVICs besides only mixed SVICs. In this way, the proposed optimal control problem in which we also restrict the target voltage to some maximum can be investigated. Furthermore it is easy to see that this constraint is a first order pure SVIC, so that the theory from section 7 of [7] can be used, as well as Theorem 3.36 from [2].
At last we remark that one may investigate sufficient conditions in the optimal control problem, which are for instance described in section 8 of [7]. Another example of a sufficient condition is given by the Hamilton-Jacobi-Bellman equation, and is discussed [12].

Finally, it would also be interesting to verify the results from this thesis in a practical (ballistic) setup of Kelvins water dropper. In an actual setup, it would furthermore also be possible to see whether the maximal induction voltage restriction we posed to minimize current losses can also be relaxed. One could for instance investigate whether a control action that is based on actual measurements of the current losses is achievable.

Bibliography

[1] Alexander Barnaveli. Problem no 17 (2010). "Kelvin's dropper". In *International Young Physicists' Tournament (IYPT)*, volume 23, July 2010. Location conference: Vienna, Austria.

[2] Benoît C. Chachuat. Nonlinear and dynamic optimization: from theory to practice. Lecture notes, Laboratoire d'Automatique, École Polytechnique Fédérale de Lausanne, 2007. Chapter 3.

[3] Mohammed Dahleh, Munther A Dahleh, and George Verghese. Lectures on dynamic systems and control. Technical report, Massachuasetts Institute of Technology, Department of Electrical Engineering and Computer Science, 2011. Chapter 15.

[4] S Desmet, F Orban, and F Grandjean. On the Kelvin electrostatic generator. *European Journal of Physics*, 10(2):118, 1989.

[5] Andrew M Duffin and Richard J Saykally. Electrokinetic power generation from liquid water microjets. *The Journal of Physical Chemistry C*, 112(43):17018–17022, 2008.

[6] Lester Evans and J Truman Stevens. Kelvin water dropper revisited. *The Physics Teacher*, 15(9):548–549, 1977.

[7] Richard F Hartl, Suresh P Sethi, and Raymond G Vickson. A survey of the maximum principles for optimal control problems with state constraints. *SIAM review*, 37(2):181–218, 1995.

[8] J. K. Hedrick and A Girard. Control of nonlinear dynamic systems: Theory and applications. Technical report, University of California, Berkeley, Department of Mechanical Engineering, 2005. Chapter 6.

[9] Hsin-Fu Huang. Voltage build-up time responses of Kelvin's water droplet generator: Variations due to different geometric configurations. *Journal of Electrostatics*, 72(6):447–456, August 2014.

[10] Hassan K Khalil. *Nonlinear systems*. Prentice hall New Jersey, 1996. Theorem 2.2.

[11] Se-yuen Mak. The Kelvin water-drop electrostatic generator - an improved design. *The Physics Teacher*, 35(9):549–551, 1997.

[12] Gjerrit Meinsma. Optimal control. Lecture notes, University of Twente, January 2014. Course code: 156162.

[13] Jan Willem Polderman and Jan C. Willems. *Introduction to the Mathematical Theory of Systems and Control*. Online download, September 2013. Original book (Doi: "10.1007/978-1-4757-2953-5"), book available from "http://wwwhome.math.utwente.nl/∼ poldermanjw/onderwijs/DISC/mathmod/book.pdf". Date is of last update.

[14] W Thomson. On a self-acting apparatus for multiplying and maintaining electric charges, with applications to illustrate the voltaic theory. *Proceedings of the Royal Society of London*, 16:67–72, 1867.

[15] Herbert H Woodson and James R Melcher. *Electromechanical Dynamics*, volume 2. New York, NY: John Wiley and Sons, Inc., 1968. Page 388-392. Published online: "http://ocw.mit.edu/resources/res-6-003-electromechanical-dynamics-spring-2009/", (Accessed 5 May, 2015), License: Creative Commons Attribution-NonCommercial-Share Alike.

[16] Yanbo Xie. *Microfluidic energy conversion by application of two phase flow.* PhD thesis, University of Twente, Enschede, September 2013.

[17] Yanbo Xie, Diederik Bos, Lennart J de Vreede, Hans L de Boer, Mark-Jan van der Meulen, Michel Versluis, Ad J Sprenkels, Albert van den Berg, and Jan C. T. Eijkel. High-efficiency ballistic electrostatic generator using microdroplets. *Nature communications*, 5, April 2014. doi: http://dx.doi.org/10.1038/ncomms4575, ESI available from: "http://www.nature.com/ncomms/2014/140407/ncomms4575/full/ncomms4575.html".

[18] Yanbo Xie, Hans L. de Boer, Ad J. Sprenkels, Albert van den Berg, and Jan C. T. Eijkel. Pressure-driven ballistic Kelvin's water dropper for energy harvesting. *Lab on a Chip*, 14:4171–4177, July 2014. doi: 10.1039/C4LC00740A, ESI available from: "http://pubs.rsc.org/en/content/articlelanding/2014/lc/c4lc00740a#!divAbstract".

[19] Markus Zahn. Self-excited ac high voltage generation using water droplets. *American Journal of Physics*, 41(2):196–202, 1973.

[20] Marko Zigart and Marko Marhl. Curiosity: The Kelvin water-drop generator. *Physics Education*, 37(2):155, 2002.

Appendix A

Appendix

A.1 Deriving the manifest behaviour

We start by writing the latent variables I_{16} and I_{26} in terms the manifest variables U_1 and U_2 and the loss currents. Note that the loss currents are directly given in terms of U_1 and U_2. Since we will encounter these latent variables more often when rewriting other latent variables, we choose to stick with these variables for now, where we will substitute them together at once in the end.

$$
\begin{aligned}
I_{16} &= I_{12} + I_{23} \\
&= \frac{U_{R_{g_1}}}{R_{g_1}} + I_{23} \\
&= \frac{U_1 - U_{R_{L_1}}}{R_{g_1}} + I_{23} \\
&= \frac{U_1 - I_{16}R_{L_1}}{R_{g_1}} + I_{23} \\
R_{g_1}I_{16} &= U_1 - I_{16}R_{L_1} + R_{g_1}I_{23} \\
(R_{g_1} + R_{L_1})I_{16} &= U_1 + R_{g_1}I_{23} \\
I_{16} &= \frac{U_1}{R_{g_1} + R_{L_1}} + m_1 I_{23}.
\end{aligned}
\tag{A.1}
$$

Note that in Figure 3.1 we do allow non-symmetrical resistors (the resistors for the left and right jetting system are hereby indicated with a 1 or 2). Simultaneously we will therefore also need to incorporate the index 1 or 2 for the voltage divider constant m (e.g. in equation (A.1) we have $m_1 = \frac{R_{g_1}}{R_{g_1} + R_{L_1}}$).

A similar result to (A.1) can be obtained for I_{26}:

$$I_{26} = I_{22} + I_{13}$$
$$= -\frac{U_{R_{g_2}}}{R_{g_2}} + I_{13}$$
$$= -\frac{U_2 - U_{R_{L_2}}}{R_{g_2}} + I_{13}$$
$$= -\frac{U_2 + I_{26}R_{L_2}}{R_{g_2}} + I_{13}$$
$$R_{g_2}I_{26} = -(U_2 + I_{26}R_{L_2}) + R_{g_2}I_{13}$$
$$(R_{g_2} + R_{L_2})I_{26} = -U_2 + R_{g_2}I_{13}$$
$$I_{26} = -\frac{U_2}{R_{g_2} + R_{L_2}} + m_2 I_{13}. \tag{A.2}$$

Using the result of (A.1) and (A.2), also variables I_{11} and I_{21} can relatively easy be computed in terms of U_1 and U_2 as shown below.

$$I_{11} = -n_1 C_{ind_1} U_{R_{g_2}}$$
$$= -n_1 C_{ind_1}(U_2 - U_{R_{L_2}})$$
$$= -n_1 C_{ind_1}(U_2 + I_{26}R_{L_2})$$
$$= -n_1 C_{ind_1}\left(U_2 + \left[-\frac{U_2}{R_{g_2} + R_{L_2}} + m_2 I_{13}\right] R_{L_2}\right)$$
$$= -n_1 C_{ind_1}\left(1 - \frac{R_{L_2}}{R_{g_2} + R_{L_2}}\right) U_2 - n_1 C_{ind_1} m_2 I_{13} R_{L_2}$$
$$= -n_1 C_{ind_1} m_2 U_2 - n_1 C_{ind_1} m_2 I_{13} R_{L_2}. \tag{A.3}$$

And similarly for I_{21}:

$$I_{21} = n_2 C_{ind_2} U_{R_{g_1}}$$
$$= n_2 C_{ind_2}(U_1 - U_{R_{L_1}})$$
$$= n_2 C_{ind_2}(U_1 - I_{16}R_{L_1})$$
$$= n_2 C_{ind_2}\left(U_1 - \left[\frac{U_1}{R_{g_1} + R_{L_1}} + m_1 I_{23}\right] R_{L_1}\right)$$
$$= n_2 C_{ind_2}\left(1 - \frac{R_{L_1}}{R_{g_1} + R_{L_1}}\right) U_1 - n_2 C_{ind_2} m_1 I_{23} R_{L_1}$$
$$= n_2 C_{ind_2} m_1 U_1 - n_2 C_{ind_2} m_1 I_{23} R_{L_1}. \tag{A.4}$$

Now the remainder is easy. At first we have that:

$$I_{15} = I_{11} - I_{14}$$
$$= I_{11} - I_{13} - I_{16} \tag{A.5}$$

And completely analogous for I_{25}:

$$I_{25} = I_{21} - I_{24}$$
$$= I_{21} - I_{23} - I_{26} \tag{A.6}$$

The manifest behaviour of the system with current losses can now be found by plugging in equations (A.1), (A.2), (A.3) and (A.4), together with the condensator and loss current equations (as shown in table (3.1)) into equations (A.5) and (A.6). This (and a bit of reordering) results in:

$$C_{L_1}\frac{dU_1}{dt} = -\frac{1}{R_{L_1} + R_{g_1}}U_1 - \left(n_1 C_{ind_1} R_{L_2} m_2 + 1\right)\alpha_1 U_1^{\beta_1} - n_1 C_{ind_1} m_2 U_2 - m_1 \alpha_2 (-U_2)^{\beta_2}$$

$$C_{L_2}\frac{dU_2}{dt} = -n_2 C_{ind_2} m_1 U_1 + m_2 \alpha_1 U_1^{\beta_1} - \frac{1}{R_{L_2} + R_{g_2}}U_2 + \left(n_2 C_{ind_2} R_{L_1} m_1 + 1\right)\alpha_2 (-U_2)^{\beta_2}.$$

A.2 Solving equation (3.4) using integration by parts

In this section we will show how the separable differential equation from subsection 3.1.4 can be solved using integration by parts. As a first approach, we see that the equation can be rewritten to separable differential equation:

$$\begin{aligned}
\frac{dU_1}{dt} &= (C - A)\,U_1 - (B + D)\,U_1^{\beta} \\
&= \widetilde{A}U_1 - \widetilde{B}U_1^{\beta} \\
&= U_1\left(\widetilde{A} - \widetilde{B}U_1^{\beta-1}\right)
\end{aligned}$$

$$\frac{1}{U_1\left(\widetilde{A} - \widetilde{B}U_1^{\beta-1}\right)}dU_1 = 1\ dt, \tag{A.7}$$

where $\widetilde{A} := (C - A)$ and $\widetilde{B} := (B + D)$.

In order to solve (A.7), we first expand its left side to a from similar to a partial fraction expansion:

$$\frac{1}{U_1\left(\widetilde{A} - \widetilde{B}U_1^{\beta-1}\right)} = \frac{a}{U_1} + \frac{b}{\widetilde{A} - \widetilde{B}U_1^{\beta-1}}$$

$$\Leftrightarrow$$

$$1 = \left(\widetilde{A} - \widetilde{B}U_1^{\beta-1}\right)a + U_1 b \tag{A.8}$$

Separating the constant terms from terms which contain U_1 in (A.8), it follows that $a = \frac{1}{\widetilde{A}}$ and $b = \frac{\widetilde{B}}{\widetilde{A}}U_1^{\beta-2}$. We thus have:

$$\frac{1}{U_1\left(\widetilde{A} - \widetilde{B}U_1^{\beta-1}\right)} = \frac{\frac{1}{\widetilde{A}}}{U_1} + \frac{\frac{\widetilde{B}}{\widetilde{A}}U_1^{\beta-2}}{\widetilde{A} - \widetilde{B}U_1^{\beta-1}} \tag{A.9}$$

Equation (A.9) can now be integrated as part of solving the separable differential equation

given by (A.7):

$$\int \left(\frac{\frac{1}{\widetilde{A}}}{U_1} + \frac{\frac{\widetilde{B}}{\widetilde{A}} U_1{}^{\beta-2}}{\widetilde{A} - \widetilde{B} U_1{}^{\beta-1}} \right) dU_1 = \int \left(\frac{\frac{1}{\widetilde{A}}}{U_1} \right) dU_1 + \int \left(\frac{\frac{\widetilde{B}}{\widetilde{A}} U_1{}^{\beta-2}}{\widetilde{A} - \widetilde{B} U_1{}^{\beta-1}} \right) dU_1$$

$$= \frac{1}{\widetilde{A}} \ln |U_1| + \int \left(\frac{-\frac{1}{(\beta-1)\widetilde{A}}}{x} \right) dx \quad \text{where } x = \widetilde{A} - \widetilde{B} U_1{}^{\beta-1}$$

$$= \frac{1}{\widetilde{A}} \ln |U_1| - \frac{1}{(\beta-1)\widetilde{A}} \ln \left| \widetilde{A} - \widetilde{B} U_1{}^{\beta-1} \right|$$

$$= \frac{1}{(\beta-1)\widetilde{A}} \left(\ln |U_1|^{\beta-1} - \ln \left| \widetilde{A} - \widetilde{B} U_1{}^{\beta-1} \right| \right)$$

$$= \frac{1}{(\beta-1)\widetilde{A}} \ln \left(\frac{|U_1|^{\beta-1}}{\left| \widetilde{A} - \widetilde{B} U_1{}^{\beta-1} \right|} \right)$$

$$= \frac{1}{(\beta-1)\widetilde{A}} \ln \left(\left| \frac{U_1{}^{\beta}}{\widetilde{A} U_1 - \widetilde{B} U_1{}^{\beta}} \right| \right) \tag{A.10}$$

For now constants have been omitted. However, these can be combined with a constant we get for integrating the right side of (A.7). With the indefinite integral of the left side of the separable differential equation (A.7) established and given by (A.10), this equation may be further solved as:

$$\int \left(\frac{\frac{1}{\widetilde{A}}}{U_1} + \frac{\frac{\widetilde{B}}{\widetilde{A}} U_1{}^{\beta-2}}{\widetilde{A} - \widetilde{B} U_1{}^{\beta-1}} \right) dU_1 = \int 1 dt$$

$$\frac{1}{(\beta-1)\widetilde{A}} \ln \left(\left| \frac{U_1{}^{\beta}}{\widetilde{A} U_1 - \widetilde{B} U_1{}^{\beta}} \right| \right) = t + c$$

$$\ln \left(\left| \frac{U_1{}^{\beta}}{\widetilde{A} U_1 - \widetilde{B} U_1{}^{\beta}} \right| \right) = (\beta-1)\widetilde{A}(t+c)$$

$$\frac{U_1{}^{\beta}}{\widetilde{A} U_1 - \widetilde{B} U_1{}^{\beta}} = c_2 e^{(\beta-1)\widetilde{A}t} \quad \text{where } c_2 = \pm e^{(\beta-1)c\widetilde{A}}$$

$$U_1{}^{\beta} = c_2 e^{(\beta-1)\widetilde{A}t} \left(\widetilde{A} U_1 - \widetilde{B} U_1{}^{\beta} \right)$$

$$\left(1 + c_2 \widetilde{B} e^{(\beta-1)\widetilde{A}t} \right) U_1{}^{\beta-1} = c_2 \widetilde{A} e^{(\beta-1)\widetilde{A}t}$$

$$U_1{}^{\beta-1} = \frac{c_2 \widetilde{A} e^{(\beta-1)\widetilde{A}t}}{1 + c_2 \widetilde{B} e^{(\beta-1)\widetilde{A}t}}$$

$$U_1(t) = \left(\frac{c_2 \widetilde{A} e^{(\beta-1)\widetilde{A}t}}{1 + c_2 \widetilde{B} e^{(\beta-1)\widetilde{A}t}} \right)^{\frac{1}{\beta-1}}$$

$$U_1(t) = \left(\frac{\frac{1}{c_2} e^{(1-\beta)\widetilde{A}t} + \widetilde{B}}{\widetilde{A}} \right)^{\frac{1}{1-\beta}}. \tag{A.11}$$

The constant c_2 may be determined from a given initial condition $U_1(0)$:

$$U_1(0) = \left(\frac{\frac{1}{c_2} \widetilde{B}}{\widetilde{A}} \right)^{\frac{1}{1-\beta}}. \tag{A.12}$$

Straightforward calculations hereby yield:

$$c_2 = \frac{1}{\widetilde{A}U_1(0)^{1-\beta} - \widetilde{B}},$$

as a solution of (A.12).

A.3   Unique solution of (3.4) for $t \in [0, \infty)$

Consider that we are given a system of the form:

$$\dot{x}(t) = f(x(t)), \qquad x(t_0) = x_0 \in \mathbb{R}^n, \quad t \geq t_0. \tag{A.13}$$

When we are given a differential equation with initial conditions in the form (A.13), there are some technical irregularities that may occur. At first we can not be sure whether a solution exists at all, but it may also happen that the system has multiple solutions (i.e. that there is not a unique solution). As an example of the latter case we consider the system:

$$\dot{x}(t) = [x(t)]^{\frac{1}{3}}, \qquad \text{with initial condition } x(0) = 0, \tag{A.14}$$

where it may be verified that both $x(t) \equiv 0$ and $x(t) = \left(\frac{2}{3}t\right)^{\frac{3}{2}}$ are valid solutions to (A.14).

Fortunately uniqueness of solutions can be guaranteed when the function $f(x)$ from (A.13) does not increase nor decrease too quickly ([12]). A measure for the rate of increase is the Lipschitz constant.

Definition A.3.1 (Lipschitz continuity, ([12])). *A function $f : \mathbb{R}^m \to \mathbb{R}^n$ is Lipschitz continuous on $\Omega \subset \mathbb{R}^m$ if a Lipschitz constant $K \geq 0$ exists such that*

$$\|f(x) - f(z)\| \leq K\|x - z\|$$

for all $x, z \in \Omega$. It is Lipschitz continuous at $x_0 \in \mathbb{R}^m$ if it is Lipschitz continuous on some neighborhood Ω of x_0.

If the function $f(x)$ in (A.13) is Lipschitz continuous at x_0, then uniqueness of a (maximal) solution to (A.13) is ensured by the following theorem:

Theorem A.3.1 (Lipschitz condition, ([12], originally by [10])). *Let $t_0 \in \mathbb{R}$ and $x_0 \in \mathbb{R}^n$. If f is Lipschitz continuous at x_0 then, for some $\delta > 0$, the differential equation (A.13) has a unique solution $x(t; x_0)$ on time interval $t \in [t_0, t_0 + \delta)$.*
Furthermore, for any fixed $t \in [t_0, t_0 + \delta)$ the $x(t)$ depends continuously on x_0.

We say that a function is locally Lipschitz if it is Lipschitz continuous at every x_0. By the above theorem, solutions $x(t)$ can be uniquely continued at any t if f is locally Lipschitz ([12]). However, Theorem A.3.1 is a local theorem, since it only guarantees existence and uniqueness over an interval $[t_0, t_0 + \delta]$, where δ may be very small. By repeated application of the above theorem one may try to extend this interval. However, in general, the interval of existence of the solution cannot be extended indefinitely ([10]). This explains the necessity for the notion of a maximal solution. An interesting phenomenon is that solutions $x(t; x_0)$ may 'escape' in a finite time, so that they are only defined on a bounded time interval. A more precise notion of (finite) escape time and maximal solutions is given by Lemma 1.1.4 from [12].

That the system function $f(x)$ from (3.4) is locally Lipschitz for $x_0 > 0$, will be shown next. The function $f(x)$ here is given by:

$$f(x) = \widetilde{A}x - \widetilde{B}x^\beta, \qquad \text{where } \widetilde{A}, \widetilde{B} > 0 \text{ and } \beta > 1$$

with derivative:

$$f'(x) = \widetilde{A} - \widetilde{B}\beta x^{\beta-1}. \tag{A.15}$$

Now if a scalar function $f(x)$ is differentiable on $[a, b]$ then we know from the Mean Value Theorem that $\forall x_1, x_2 \in [a, b]$ we have that:

$$f(x_1) - f(x_2) = f'(\xi)(x_1 - x_2)$$

for some ξ between x_1 and x_2. A direct consequence is that $\forall x_1, x_2 \in [a, b]$:

$$\begin{aligned}
|f(x_1) - f(x_2)| &= |f'(\xi)| \cdot |x_1 - x_2| \\
&\leq \max_{\xi \in [a,b]} |f'(\xi)| \cdot |x_1 - x_2|. \tag{A.16}
\end{aligned}$$

On the basis of (A.15) and (A.16) we are now ready to make the proof. For any $\xi \in (0, M]$, with $M \in \mathbb{R}_+$ we have:

$$\begin{aligned}
|f'(\xi)| &= |\widetilde{A} - \widetilde{B}\beta\xi^{\beta-1}| \\
&\leq |\widetilde{A} + \widetilde{B}\beta\xi^{\beta-1}| \\
&\leq \widetilde{A} + \bar{K}\widetilde{B}\beta, \tag{A.17}
\end{aligned}$$

where $\bar{K} = \max\{1, M, M^{\beta-1}\}$.
For the sake of completeness; $\bar{K} = 1$ when $M \in (0, 1) \wedge \beta \in (1, 2)$, $\bar{K} = M$ when $M \geq 1 \wedge \beta \in (1, 2)$ or when $M \in (0, 1) \wedge \beta \in [2, \infty)$ and at last $\bar{K} = M^{\beta-1}$ when $M \geq 1 \wedge \beta \in [2, \infty)$.

On the basis of (A.17) it may be concluded that $f(x) = \widetilde{A}x - \widetilde{B}x^\beta$ is locally Lipschitz, where we can choose the Lipschitz constant in Theorem A.3.1 equal to:

$$K = \widetilde{A} + \bar{K}\widetilde{B}\beta,$$

from which we can conclude that (3.4) has a unique maximal solution for $t_0 \in \mathbb{R}$ and $x_0 \in (0, M]$.

As mentioned previously, this does not guarantee that (3.4) has a solution $\forall t \in [t_0, \infty)$, as in theory it can still happen that the system has a 'finite escape time'. That is, it may happen that the solution $x(t)$ tends to $\pm\infty$ in a finite amount of time. That this is not the case may be verified from the analytical solution of (3.4), as was deduced in Subsection 3.1.4 (as well as Appendix Section A.2).

For $t_0 = 0$ and $x_0 = U_1(0)$, the solution to (3.4) is given by (see also (3.15) and (3.16)):

$$U_1(t) = \left[ce^{(1-\beta)\widetilde{A}t} + \frac{\widetilde{B}}{\widetilde{A}}\right]^{\frac{1}{1-\beta}}, \tag{A.18}$$

with constant c given by:

$$c = U_1(0)^{1-\beta} - \frac{\widetilde{B}}{\widetilde{A}}.$$

Note that the exponent $\frac{1}{1-\beta}$ in (A.18) is negative. Therefore we can see that solutions 'blow up' when:

$$0 = ce^{(1-\beta)\widetilde{A}t} + \frac{\widetilde{B}}{\widetilde{A}}.$$

Some simple calculus shows us that this is equivalent to:

$$0 = \left(U_1(0)^{1-\beta} - \frac{\widetilde{B}}{\widetilde{A}} \right) e^{(1-\beta)\widetilde{A}t} + \frac{\widetilde{B}}{\widetilde{A}} \qquad\qquad \Longleftrightarrow$$

$$e^{(1-\beta)\widetilde{A}t} = \frac{\widetilde{B}}{\widetilde{B} - \widetilde{A}U_1(0)^{1-\beta}} \qquad\qquad \Longleftrightarrow \qquad\qquad (A.19)$$

$$t^* = -\frac{1}{(\beta - 1)\widetilde{A}} \cdot \ln\left(\frac{\widetilde{B}}{\widetilde{B} - \widetilde{A}U_1(0)^{1-\beta}} \right), \qquad\qquad (A.20)$$

where t^* indicates the 'blow-up time'.

Note that the above derivation is only valid when the right of (A.19) is positive and when the denominator does not equal zero. Recall from subsection 1.1.1 in the introduction that the system starts due to some random imbalance, so that we know that

$$U_1(0) = \epsilon,$$

where ϵ is some small positive constant. We will hereby assume that ϵ is sufficiently small, specifically that $\epsilon < \left(\frac{\widetilde{B}}{\widetilde{A}} \right)^{\frac{1}{1-\beta}}$, so that the above derivation can indeed be made.

Furthermore, given that $U_1(0)$ is particularly small, it is easy to see that the 'blow-up time' t^* in (A.20) is negative. However, since we consider time being positive and started from $t_0 = 0$ in (A.18), we can conclude that the system will never blow up.

Thereby we have thus proven that equation (3.4) has a unique solution for $U_1(0) = \epsilon > 0$ for $t \in [0, \infty)$. $\qquad\qquad\qquad\qquad\qquad\qquad\qquad\qquad\qquad\qquad\qquad\qquad\qquad\qquad$ $\square$

A.4 Matrix exponentials

A.4.1 $\quad e^{At}$ from (2.2)

The matrix we consider is given by:

$$A = \begin{bmatrix} -a & -b \\ -b & -a \end{bmatrix}.$$

At first one may note that:

$$\begin{bmatrix} -a & -b \\ -b & -a \end{bmatrix} = \begin{bmatrix} -a & 0 \\ 0 & -a \end{bmatrix} + \begin{bmatrix} 0 & -b \\ -b & 0 \end{bmatrix},$$

and we also have that

$$\begin{bmatrix} -a & 0 \\ 0 & -a \end{bmatrix} \begin{bmatrix} 0 & -b \\ -b & 0 \end{bmatrix} = \begin{bmatrix} 0 & -b \\ -b & 0 \end{bmatrix} \begin{bmatrix} -a & 0 \\ 0 & -a \end{bmatrix} \qquad \left(= \begin{bmatrix} 0 & ab \\ ab & 0 \end{bmatrix} \right).$$

Based on this observation we can use the rule $e^{(M_1+M_2)t} = e^{M_1 t} e^{M_2 t}$, since M_1 and M_2 commute.

Calculation of $e^{M_1 t}$ is straightforward, and we have

$$e^{M_1 t} = \begin{bmatrix} e^{-at} & 0 \\ 0 & e^{-at} \end{bmatrix}.$$

For the calculation of $e^{M_2 t}$, we calculate the eigenvalues, given by $\lambda_{1,2} = \pm b$, with corresponding eigenvectors $v_{1,2} = \begin{bmatrix} \mp 1 \\ 1 \end{bmatrix}$. From this it follows that:

$$
\begin{aligned}
e^{M_2 t} &= \begin{bmatrix} -1 & 1 \\ 1 & 1 \end{bmatrix} \begin{bmatrix} e^{bt} & 0 \\ 0 & e^{-bt} \end{bmatrix} \begin{bmatrix} -1 & 1 \\ 1 & 1 \end{bmatrix}^{-1} \\
&= \frac{1}{2} \begin{bmatrix} e^{-bt} + e^{bt} & e^{-bt} - e^{bt} \\ e^{-bt} - e^{bt} & e^{-bt} + e^{bt} \end{bmatrix}
\end{aligned}
$$

Thus we have:

$$
\begin{aligned}
e^{At} &= e^{M_1 t} e^{M_2 t} \\
&= \begin{bmatrix} e^{-at} & 0 \\ 0 & e^{-at} \end{bmatrix} \frac{1}{2} \begin{bmatrix} e^{-bt} + e^{bt} & e^{-bt} - e^{bt} \\ e^{-bt} - e^{bt} & e^{-bt} + e^{bt} \end{bmatrix} \\
&= \frac{1}{2} \begin{bmatrix} e^{(-a-b)t} + e^{(-a+b)t} & e^{(-a-b)t} - e^{(-a+b)t} \\ e^{(-a-b)t} - e^{(-a+b)t} & e^{(-a-b)t} + e^{(-a+b)t} \end{bmatrix}.
\end{aligned}
$$

A.4.2 $e^{(-A_1)t}$ from (4.17)

Utilizing the 'a, b, c, d notation' from (4.15), the matrix at hand here is given by

$$-A_1 = \begin{bmatrix} a & 0 \\ -b & -a \end{bmatrix}. \tag{A.21}$$

It is easy to see that the eigenvalues of $(-A_1)$ are given by:

$$\lambda_{1,2} = \pm a.$$

The corresponding eigenvectors are given by:

$$v_1 = \begin{bmatrix} -\frac{2a}{b} \\ 1 \end{bmatrix}, \quad v_2 = \begin{bmatrix} 0 \\ 1 \end{bmatrix}.$$

Thereby we find that:

$$
\begin{aligned}
e^{(-A_1)t} &= \begin{bmatrix} -\frac{2a}{b} & 0 \\ 1 & 1 \end{bmatrix} \begin{bmatrix} e^{at} & 0 \\ 0 & e^{-at} \end{bmatrix} \begin{bmatrix} -\frac{2a}{b} & 0 \\ 1 & 1 \end{bmatrix}^{-1} \\
&= \begin{bmatrix} -\frac{2a}{b} & 0 \\ 1 & 1 \end{bmatrix} \begin{bmatrix} e^{at} & 0 \\ 0 & e^{-at} \end{bmatrix} \begin{bmatrix} -\frac{b}{2a} & 0 \\ \frac{b}{2a} & 1 \end{bmatrix} \\
&= \begin{bmatrix} e^{at} & 0 \\ \frac{b}{2a} \left(e^{-at} - e^{at} \right) & e^{-at} \end{bmatrix}. \tag{A.22}
\end{aligned}
$$

A.4.3 $e^{A_2 t}$ from (4.23)

Also here we will use the simplified 'a, b, c, d notation' from (4.15). The matrix at hand is:

$$A_2 = \begin{bmatrix} c & 0 \\ d & -c \end{bmatrix}.$$

Note that A_2 is very similar to $(-A_1)$ from (A.21). Thereby the calculation of the matrix exponential will be very similar. In fact, the matrices are even identical when making the substitution $c = a$, $d = -b$. In this way the matrix exponential $e^{A_2 t}$ can also be deduced by performing this substitution in (A.22). However, as the computation of the eigenvalues and eigenvectors is quite easy, we will calculate the matrix exponential using the conventional approach.

It is easy to see that the eigenvalues of A_2 are given by

$$\lambda_{1,2} = \pm c,$$

with corresponding eigenvectors:

$$v_1 = \begin{bmatrix} \frac{2c}{d} \\ 1 \end{bmatrix}, \quad v_2 = \begin{bmatrix} 0 \\ 1 \end{bmatrix}.$$

Thereby we find that:

$$
\begin{aligned}
e^{A_2 t} &= \begin{bmatrix} \frac{2c}{d} & 0 \\ 1 & 1 \end{bmatrix} \begin{bmatrix} e^{ct} & 0 \\ 0 & e^{-ct} \end{bmatrix} \begin{bmatrix} \frac{2c}{d} & 0 \\ 1 & 1 \end{bmatrix}^{-1} \\
&= \begin{bmatrix} \frac{2c}{d} & 0 \\ 1 & 1 \end{bmatrix} \begin{bmatrix} e^{ct} & 0 \\ 0 & e^{-ct} \end{bmatrix} \begin{bmatrix} \frac{d}{2c} & 0 \\ -\frac{d}{2c} & 1 \end{bmatrix} \\
&= \begin{bmatrix} e^{ct} & 0 \\ \frac{d}{2c}\left(e^{ct} - e^{-ct}\right) & e^{-ct} \end{bmatrix}.
\end{aligned}
\tag{A.23}
$$

A.5 Limit t_s

$$
\begin{aligned}
\lim_{\epsilon \downarrow 0} t_s &= \lim_{\epsilon \downarrow 0} \left(T - \frac{\epsilon C_L}{1 - \epsilon n C_{ind}} \ln\left(\frac{M_2 + \epsilon(n C_{ind} M_2 - 2)}{2\epsilon n C_{ind}(M_2 - \epsilon)} \right) \right) \\
&= T - \lim_{\epsilon \downarrow 0} \left(\frac{\ln\left(\frac{M_2 + \epsilon(n C_{ind} M_2 - 2)}{2\epsilon n C_{ind}(M_2 - \epsilon)} \right)}{\frac{1 - \epsilon n C_{ind}}{\epsilon C_L}} \right).
\end{aligned}
\tag{A.24}
$$

This sub-limit presents us with the L'Hôpital case $\frac{\infty}{\infty}$. Therefore we look at the limit of the

derivatives:

$$\lim_{\epsilon \downarrow 0} \left(\frac{\ln\left(\frac{M_2 + \epsilon(nC_{ind}M_2 - 2)}{2\epsilon nC_{ind}(M_2 - \epsilon)}\right)}{\frac{1 - \epsilon nC_{ind}}{\epsilon C_L}} \right)$$

$$= \lim_{\epsilon \downarrow 0} \left(\frac{\frac{(nC_{ind}M_2 - 2)\cdot 2\epsilon nC_{ind}(M_2 - \epsilon) - (M_2 + \epsilon(nC_{ind}M_2 - 2))\cdot(2nC_{ind}(M_2 - 2\epsilon))}{(2\epsilon nC_{ind}(M_2 - \epsilon))^2} \cdot \frac{2\epsilon nC_{ind}(M_2 - \epsilon)}{M_2 + \epsilon(nC_{ind}M_2 - 2)}}{\frac{-nC_{ind}\cdot \epsilon C_L - (1 - \epsilon nC_{ind})\cdot C_L}{(\epsilon C_L)^2}} \right)$$

$$= \lim_{\epsilon \downarrow 0} \left(\frac{\frac{2\epsilon^2(nC_{ind})^2 M_2 - 4\epsilon^2 nC_{ind} - 2nC_{ind}M_2{}^2 + 4\epsilon nC_{ind}M_2}{2\epsilon nC_{ind}(M_2 - \epsilon)} \cdot \frac{1}{M_2 + \epsilon(nC_{ind}M_2 - 2)}}{\frac{-1}{\epsilon^2 C_L}} \right)$$

$$= \lim_{\epsilon \downarrow 0} \left(\epsilon C_L \cdot \frac{M_2{}^2 - \epsilon^2 nC_{ind}M_2 - 2\epsilon M_2 + 2\epsilon^2}{(M_2 - \epsilon)[M_2 + \epsilon(nC_{ind}M_2 - 2)]} \right)$$

$$= 0.$$

Using the above derivation we may conclude that

$$\lim_{\epsilon \downarrow 0} t_s = T.$$

A.6   Solution to the ODE from (4.62)

For convenience in notation, let us introduce the constants

$$\alpha = \frac{1}{C_L R_L}$$

$$\beta = \frac{M_U(nC_{ind}R_L + 1)}{C_L R_L}$$

Utilizing this notation, we rewrite (4.62) to classical ODE form

$$\dot{x} + \alpha x = \beta. \tag{A.25}$$

For the homogeneous solution of this equation we use $x_h(t) = ce^{\lambda t}$. This results in

$$\lambda ce^{\lambda t} + \alpha ce^{\lambda t} = 0 \qquad \Longleftrightarrow$$

$$\lambda = -\alpha.$$

Thereby note that the function $ce^{\lambda t}$ is never zero for $c \neq 0$, so that the division is allowed. From here it follows that the homogeneous solution is given by

$$x_h(t) = ce^{-\alpha t}.$$

For the particular solution we set $x_p(t) = K$, with K being a constant. Plugging this in into (A.25) gives us

$$\alpha K = \beta \qquad \Longleftrightarrow$$

$$K = \frac{\beta}{\alpha}.$$

Having found the homogeneous and particular solution of (A.25), we know that it's solution is given by

$$x(t) = x_p(t) + x_h(t)$$

$$= ce^{\lambda t} + \frac{\beta}{\alpha}.$$